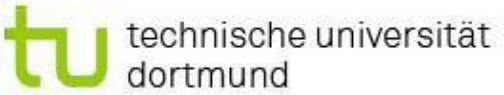

Interference with the spatial organization of Ras in cancer cells

Dissertation

zur Erlangung des Grades
Dr. rer. nat. in Chemie/Chemischer Biologie
der Fakultät für Chemie und Chemische Biologie
der Technischen Universität Dortmund
vorgelegt von

M. Sc. Dina Carolin Truxius
Geboren in Herne

Dortmund, Oktober 2015

Die vorliegende Arbeit wurde im Zeitraum vom 01.01.2011 bis zum 20.10.2015 am Max-Planck-Institut für molekulare Physiologie in Dortmund, Abteilung Systemic Cell Biology, unter der Leitung von Herrn Prof. Dr. Philippe I. H. Bastiaens, durchgeführt.

Abteilung II: Systemic Cell Biology
Prof. Dr. Philippe I. H. Bastiaens

1. Gutachter: Prof. Dr. Philippe I. H. Bastiaens
2. Gutachter: Prof. Dr. Frank Wehner

Eidesstattliche Versicherung

Ich erkläre hiermit an Eides Statt, dass ich die vorliegende Doktorarbeit mit dem Titel „Interference with the spatial organization of Ras in cancer cells“ selbständig und ohne Benutzung anderer als der angegebenen Hilfsmittel angefertigt habe; die aus fremden Quellen direkt oder indirekt übernommenen Gedanken sind als solche kenntlich gemacht. Die Arbeit wurde bisher in gleicher oder ähnlicher Form keiner anderen Prüfungskommission vorgelegt und auch nicht veröffentlicht.

Ort, Datum

Unterschrift

Das Beginnen wird nicht belohnt, einzig das Durchhalten (K. von Siena)

Index

1. Zusammenfassung

Onkogenes KRas wird mit einer Vielzahl von Krebserkrankungen wie Bauchspeicheldrüsen-, Dickdarm- und Lungenkarzinomen assoziiert, die mit einer schlechten Prognose und Überlebenschance für den Patienten einhergehen. Durch onkogene Mutationen wird Ras in einem dauerhaft aktiven Zustand gehalten und nachgeschaltete Signalkaskaden werden so permanent aktiviert. Die Folgen sind unkontrolliertes Wachstum und Überleben entarteter Zellen. Deshalb stellen alle Ras-Proteine interessante Angriffspunkte für zielgerichtete Krebs-Therapien dar. Trotz bekannter Struktur und Funktionen ist Ras bis heute ein „undruggable“ Protein, bei dem eine zielgerichtete Therapie sehr schwierig ist.

In dieser Arbeit wurde der Krebsphänotyp in verschiedenen KRas-abhängigen Modellsystemen untersucht. Zuerst wurde in humanen Krebszelllinien, die aus verschiedenen Tumorgeweben stammten, der Phänotyp nach chemischer Inhibition und genetischer Herabregulation von PDEδ untersucht. Alle Zelllinien wiesen unterschiedliche Abhängigkeiten von onkogenem KRas auf, wobei ein starker Einfluss auf das Wachstum nur bei KRas-abhängigen Pankreas- und Lungenkarzinomzellen, aber nicht bei KRas-abhängigen Dickdarmkarzinomzellen beobachtet werden konnte. Die jeweiligen Wildtyp-Zellen zeigten zumeist kein vermindertes Wachstum. Die genetische Manipulation zeigte exakt die gleichen Effekte auf das Zellwachstum wie der neue PDEδ Inhibitor Deltazinone 1, was bedeutet, dass PDEδ ein geeignetes Zielprotein für die gerichtete pharmakologische Therapie KRas-abhängiger Tumore ist.

Als nächstes wurden zwei Zelllinien aus dem Pankreas von transgenen Mäusen, die entweder eine („oncogene addiciton“) oder zwei onkogene Mutationen („synthetic sickness“) tragen, für einen genetischen Screen in Gegenwart von chemischen PDEδ-Inhibitoren, verwendet. Die Zelllinien exprimieren entweder onkogenes KRas oder onkogenes KRas in Kombination mit mutiertem p53 unter endogener Promoterkontrolle. Wie zu erwarten war die Zelllinie mit der zusätzlichen p53-Mutation resistenter gegenüber dem PDEδ-Inhibitor Deltarasin.

Diese Arbeit verdeutlicht, dass die Verfügbarkeit von freiem PDEδ unabdingbar für das Überleben von KRas-abhängigen Zellen ist. Die Auswirkungen der PDEδ-Inhibition auf das Zellwachstum in humanen KRas-abhängigen Zellen und die Unterschiede im Verhalten der beiden Mauszelllinien verdeutlichen,

dass der Mutationsstatus einen kritischer Faktor für die Empfindlichkeit gegenüber PDEδ-Inhibitoren und der daraus resultierenden gestörten räumlichen Organisation von KRas darstellt. Der Erwerb zusätzlicher onkogener Mutationen erlaubt es Zellen alternative Signalwege zu nutzen, um auf äußere Einflüsse reagieren und so ihr Überleben sichern zu können.

2. Abstract

Oncogenic KRas is associated with a multitude of human cancers, like pancreatic, colorectal, and lung carcinomas, concomitant with poor prognosis and survival. Oncogenic mutations retain Ras in a constitutively active conformation, causing sustained activation of downstream signaling cascades, which leads to uncontrolled proliferation and survival. Hence, all Ras proteins are interesting molecules for targeted cancer therapies. Although the structure and functions of Ras proteins are known, it still remains an “undruggable” protein so far.

In this work, the cancer phenotype upon RNAi and pharmacological inhibition in several KRas addiction model systems was elaborated. First, in a panel of human cancer cell lines, from various tumor origins, the interference with the cancer phenotype after PDEδ inhibitor treatment and inducible shRNA-mediated downmodulation of PDEδ was studied. These cell lines exhibited different degrees of oncogenic KRas dependencies and a strong effect on cell survival could only be observed in KRas-dependent pancreatic and lung tumor cells, whereas colorectal carcinoma cells with an oncogenic KRas background were only slightly affected. Cells with wildtype KRas remained mostly unaffected. The new class PDEδ inhibitor Deltazinone 1 and the genetic manipulation of PDEδ showed identical effects on cell growth, demonstrating that PDEδ is a valid target for the pharmacological therapy of KRas-dependent tumors.

Second, murine pancreatic cancer cells, derived from transgenic mice, with either one (oncogene addiction) or two oncogenic mutations (synthetic sickness) were used for a synthetic lethal screen in the presence of small molecule PDEδ inhibitors. Both cell lines either express oncogenic KRas or oncogenic KRas in combination with mutant p53 under the control of endogenous promoters. Here, the cell line with the additional loss of p53 fuction seemed to be more resistant to PDEδ inhibition by Deltarasin.

This work demonstrates that the availability of PDEδ is inevitable to ensure survival of oncogenic KRas-dependent cancer cells. The effects on growth in human KRas-dependent cell lines and the different behaviors observed in the murine systems prove that the mutation status is critical for the susceptibility towards PDEδ inhibition and the resulting interference with the spatial organization of KRas. The acquisition of additional oncogenic mutations allows for better adaptation to changes in the environment and ensures cellular survival.

3. Introduction

Cells interpret extracellular stimulation by growth factors or hormones. In order to generate an appropriate output, they integrate these signals with intracellular information and the subsequent transmission is mediated via complex protein signaling networks. It is already known that different stimuli lead to various outcomes, despite sharing the same network components (Santos, 2007). Such structures are highly intertwined, regulated by the directionality of informational flow and the connectivity between modules, which create a causal network in time and space.

Signal transduction requires interaction or stimulation, which first causes a certain signal strength and duration that has to overcome a specific threshold for downstream activation of the signaling cascade. The output is dependent on the input signal, the transmission into certain signaling pathways, and the spatial organization of the network components. To maintain output reproducibility and to provide the ability to specifically and rapidly react to a changing environment, each module is highly controlled in a dynamic context-sensitive way (Kholodenko, 2006). Further, every signal needs to be either terminated at a defined point in time to prevent over-activation and misregulation or it has to be maintained for sustained or constant activation as with survival information. Usually, the programmed cell death (apoptosis) is initiated if the transmission of survival signals stops.

For fine-tuning of transmitted information and the possibility to take alternative routes upon activation, non-linear signaling features and a dynamic interplay of interaction partners, catalyzing opposing reactions, are neccessary. In this way, the existence of negative and positive feedback loops is required to generate a robust system (Kitano, 2004). By regulating the directionality of signal propagation in time and space, according to the input and signal strength, they are inevitable for cellular homeostasis.

Although these networks are robust structures, they are susceptible to external and internal perturbations on fragile signaling hubs (Amit, 2007). In this way, overexpression of crucial components and the acquisition of oncogenic mutations are highly probable to permanently change the state of a given network. As a result, misregulated proliferative information is mediated, which can lead to cancer initiation. If the acquisition of an oncogenic mutation provides survival

advantages in cells, like higher proliferation rates, increased cellular fitness, or lower susceptibility to chemotherapeutics, a tumor becomes more and more dependent on this particular mutation (oncogene addiction) with time. Oncogene addiction is described as such: the inhibition of a particular oncogene is sufficient to halt the neoplastic phenotype in tumors, which rely on a single dominant oncogene for growth and survival (Weinstein, 2006). There are three biological models for oncogene addiction (figure 1), known as genetic streamlining, oncogenic shock, and synthetic lethality (Torti, 2011).

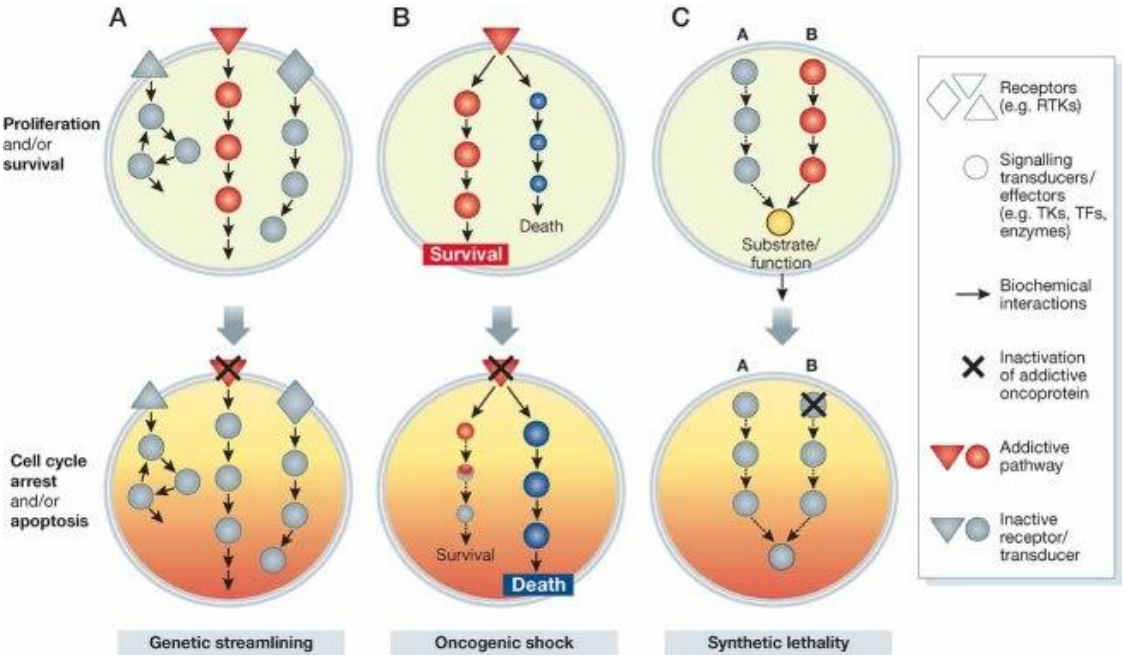

Figure 1: Schematic representation of the three models of oncogene addiction. (A) Genetic streamlining, (B) Oncogenic shock and (C) Synthetic lethality are shown. Figure adapted from Torti, 2011.

In genetic streamlining, the constant genetic drift filters non-essential pathways out which do not contribute to an increase in cellular fitness. As a result, the cell becomes more susceptible to acute perturbations; thus sudden changes rapidly reduce the cellular fitness, causing a collapse. The genetic shock model describes a single oncogene (e.g. a RTK), which simultaneously triggers survival and pro-apoptotic signals. Under normal conditions, the survival signal output is dominating. Upon inhibition of the oncogene, an imbalance of the basal signal and pro-apoptotic information emerges, which can lead to apoptosis. The model of synthetic lethality postulates that two genes are in a synthetic lethal relationship when the loss of one or the other still exerts survival signal but the loss of

both leads to death. The concept of synthetic lethality can be extended to the situation of mutation acquisition in two oncogenes, which causes increased cellular fitness (synthetic sickness). Isogenic cell lines are therefore compared in terms of their response to certain inhibitors in a pairwise manner to determine specific target effects (Kaelin 2005).

3.1 Ras proteins are signaling hubs

This work aims to exploit differences in the cancer phenotype in the context of oncogenic KRas addiction between RNAi and small molecule inhibiton in several *in vitro* models systems. As the Ras proteins are the biological background of this work, one need to first understand their major role in signal mediation under normal and pathological conditions.

Originally, Ras proteins were discovered in 1980 as peripheral membrane proteins localized at the inner leaflet of the plasma membrane (Willingham, 1980). In 1982, the RAS (rat sarcoma) gene product was found to be the first oncogene (Parada, 1982) and a part of the Harvey virus (Harvey, 1964) with the ability to cause tumor formation in rats. Later, Ras was identified as a GTP-binding protein (McCormick, 1989), which localizes to the plasma membrane (Willumsen, 1984) and harbors lipid modifications (Hancock,1989). It belongs to a protein superfamily (Ras superfamily) of 150 related proteins, including Rho, Rab, Arf, Rac, and Ran (Wennerberg, 2005). The three well-studied forms of Ras, Harvey-Ras (HRas), neuroblastoma-Ras (NRas) (Ulsh, 1984; Ireland, 1989), and the two splice variants of KRas are members of the Ras subfamily (Norton, 1984).

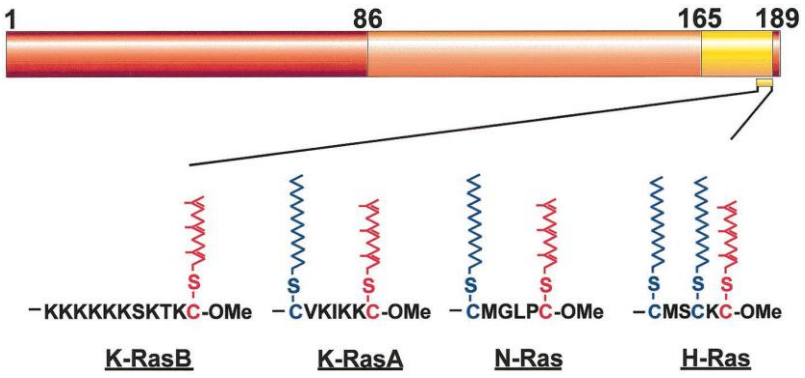

Figure 2: The sequence conservation or Ras proteins is shown by a color gradient, ranging from red (100% similarity) to yellow (low similarity) on top. The membrane anchor region of the respective isoforms is depicted below. Farnesylation is shown in red, as it is a permanent modification and palmitoylation is represented in blue. Figure apapted from (Bar-Sagi, 2001)

All three Ras proteins are structurally similar (figure 2) and belong to the class of guanine nucleotide binding proteins (GNBBs), possessing a catalytic G-domain (Paduch, 2001; Wennerberg, 2005), which binds GTP or GDP with similar affinities (Vetter, 2001). Ras proteins are 188/189 amino acids in length with a molecular weight of 21 kDa. Starting from the N-terminus, the first domain is identical in all three isoforms of Ras (KRas, NRas, and HRas) and includes 85 amino acids. The second domain is built of 80 amino acids, with lower sequence identity (90 %). Both regions form the catalytic G-domain (amino acids 1–165), which includes the guanine nucleotide-binding pocket, the characteristic feature of small GTPases. The third domain is named hypervariable region (HVR) and terminated by the CAAX box motif (Cox, 2002), bearing the lowest sequence identity among all three Ras forms (Valencia, 1991). Where C is a cysteine, A stands for aliphatic amino acid and X can be any amino acid. This region plays an important role in regulating the biological activity (Rocks, 2005) and spatial organization of Ras (Hancock, 1989; Hancock, 1990; Lorentzen, 2010; Schmick, 2014).

A common feature of GTP-binding proteins is their switch-like behavior, controlled by GDP/GTP cycling. The transition between GTP-loaded and GDP-loaded states of Ras is known as the GTPase cycle (figure 3), and occurs in response to activation of GEFs (Guanine-nucleotide exchange factors) and GAPs (GTPase-activating proteins) from upstream signaling events. In the GDP-bound state, GNBBs are inactive. Upon GTP-binding, they undergo conformational changes in the G-domain, resulting in an active state.

In a cell, the cytoplasmic GTP concentration has a tenfold higher affinity to be bound when compared to GDP (Antonarakis, 1998; Zhang, 2005). GDP is interchangeable with GTP by GEFs. The exchange from GDP to GTP causes a conformational change in the switch 1 and switch 2 region (loaded-spring mechanism), forming an effector loop and the γ-phosphate of GTP interacts with Thr 35 and Gly 60 of the respective region (Vetter, 2001). The P-loop (GXXXXGKS/T, aa 10–16) forms a polyanion hole (Dreusicke, 1986), neutralizing the negative charge of the γ-phosphate of GTP. To counteract activation, GTPase-activating proteins (GAPs) amplify the GTPase activity 100,000 fold, resulting in a fast hydrolysis of GTP to GDP (Gideon, 1992), promoting the formation of the inactive form (Bernards 2004). The hydrolysis reaction is Mg^{2+}-

dependent and requires the formation of a stabilized transition state where the nucleophilic attack of a water molecule on the γ-phosphate of GTP is possible (Vetter, 2001).

This core effector region of Ras (aa 32 and 40) is essential for the interactions between GAPs and downstream effectors as the changes in the tertiary structure allow to distinguish between the “off” (GDP-bound) and “on” (GTP-bound) state. As a side effect of effector binding, the dissociation of GTP is diminished because the GTP-bound form of the GTPase is stabilized. GEFs and GAPs not only exhibit different expression patterns and localizations, but also differ in their regulations and activation by a multitude of cellular receptors and proteins.

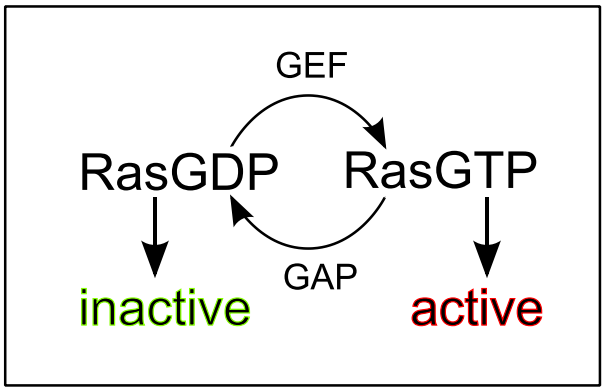

Figure 3: The GTPase Cycle. Ras is a molecular switch and transitions between a GTP-bound and GDP-bound state. GEFs catalyze the nucleotide exchange reaction, whereas GAPs perform the opposed reaction. Ras becomes active in the GTP-bound state and can bind to downstream effectors of the signaling cascade

In summary, Ras can exist in two states, the active GTP-bound and the inactive GDP-bound state, caused by the dynamics of the GTPase cycle (figure 2). In the active conformation, Ras functions as a trigger to activate downstream signaling proteins. Ras proteins connect a multitude of upstream signals to an even larger variety of downstream effectors, thereby functioning as signaling hubs (figure 4). The cellular outcome ranges from cell proliferation, cell cycle progression, migration, cytoskeletal remodeling, senescence, and apoptosis (Vojtek, 1998; Shields, 2000; Adjei, 2001; Downward, 2003; Karnoub, 2008; Fedorenko, 2013). Consequently, the acquisiton of an oncogenic mutation in the Ras proteins is concomitant with aberrant downstream signaling and associated with a multitude of cancers. Oncogenic mutations in all isoforms frequently occur close to the active site, either in the P-loop at position 12 (G12V/D) or 13 or in the switch 2 region (Q61L), where it blocks the GAP-mediated hydroly-

sis reaction from GTP to GDP (Seeburg, 1984; Trahey, 1987; John, 1988; Tong, 1989; Prior, 2012). Such mutations abolish the formation of a transition state for GTP-hydrolysis and lead to an accumulation of GTP-bound Ras. For sterical reasons, in case of Ras G12V/D, no other residue is possible and this mutation interferes with the formation of the transition state and the intrinsic GTPase activity (Privé, 1992).

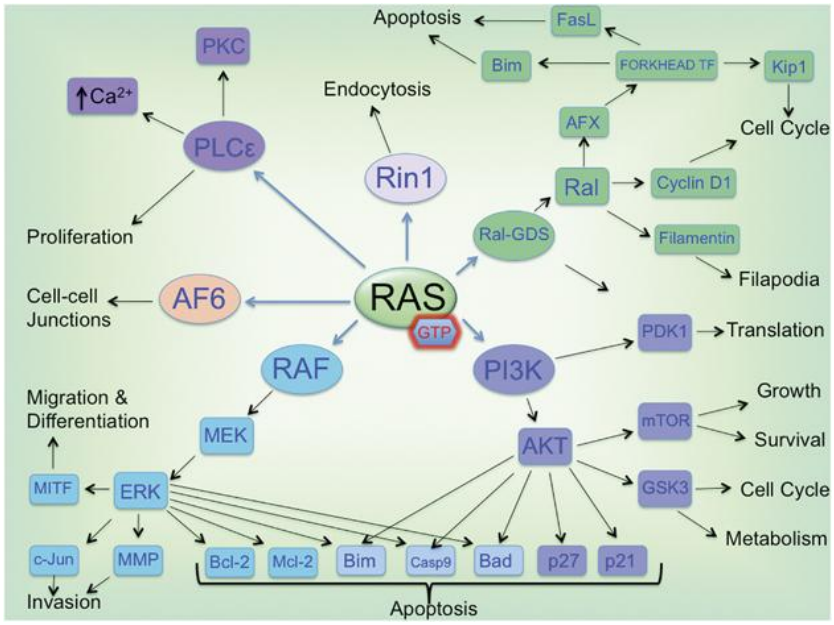

Figure 4: Ras as the central node converges signaling information from upstream receptor activation and transmits it via different pathways, including MAPK and PI3K/Akt. The outcome ranges from growth and survival to invasion and apoptosis. Figure adapted from (Fedorenko, 2013)

Ras is activated at the plasma membrane by upstream growth factor stimulation and mediates proliferative information through the Ras-Raf-MAPK (Mitogen-activated protein kinase) pathway (Pearson, 2001) and survival or death signaling via the PI3K/Akt (Phosphatidylinositol 3-kinase) pathway (Marte, 1997). A plethora of other downstream effectors like the stress-response pathway via MEKK1, cell-cycle regulation via Ral, Raf, and PI3K (Gille, 1999), actin cytoskeleton remodeling via Ral and Rac, and PLCε regulation (Wing, 2003) have been reported to be activated (figure 4). In general, the recruitment of cytosolic factors to the plasma membrane is one possibility to potentiate the signaling outcome as it causes a dimensionality reduction in their diffusional space, which makes the subsequent reaction more probable (Schmick, 2014).

There are three classes of Ras effectors, which either harbor a Ras-binding domain (RBD) or the structurally similar Ras-associating domain that allows for interaction with the Ras effector loop.

The first class contains proteins with a RBD-motif, including Raf family members and scaffold proteins like CNK (connector enhancer of kinase suppressor of Ras 1) and KSR (kinase suppressor of Ras 1). Briefly, these proteins activate Mek, the dual-specificity MAPK. Mek phosphorylates and thereby activates Erk1 and Erk2, resulting in transcriptional activity for cell growth and cell cycle entry. Another interaction partner of Erk is MNK (MAPK-interacting ser/thr kinase), which contributes to cell growth control. Erk also phosphorylates and activates RSK (ribosomal protein S6 kinase) a downstream target of mTor (mammalian target of rapamycin), thereby connecting the mTor pathway to Ras/MAPK signaling. (Sengupta, Peterson, and Sabatini 2010)

The serine/threonine kinase mTor is an integrator of mitogenic and nutrient inputs and senses nutrient, oxygen and energy levels of the cell (Hay, 2004; Sarbassov, 2005; Jewell, 2013). The downstream regulators for protein synthesis of mTor are the eukaryotic initiation factor 4E-binding protein (4E-BP1) (Poulin, 1998) and S6 kinase (RSK). Upon growth factor stimulation, mTor-activating signals are mediated via the PI3K/ pathway and act both downstream and upstream of Akt, thereby connecting Ras/MAPK, mTor and PI3K/Akt signaling. Akt phosphorylates and thereby inactivates Tuberin (TSC2, Tuberous Sclerosis Complex 2), a negative regulator of mTor (Inoki, 2002). Akt phosphorylation of TSC2 releases TSC inhibition of the Ras family member RheB (Ras homolog enriched in brain), which then accumulates in its GTP-bound state and activates mTor (Sengupta, 2010). This double negative feedback loop from Akt to mTor via TSC2 and RheB causes mTor activation. With regard to other signaling pathways, TSC2 is also a direct substrate of Erk and RSK.

The second protein family, known to directly interact with Ras is PI3K. The catalytic subunit p110 can directly bind to Ras (Samuels, 2005). PI3K pathway mutations occur in 30 % of all cancers (Luo, 2003). Among the PI3K pathway proteins, PTEN (PI3K-phosphatase with tensin homology) is the second most commonly tumor suppressor, after p53, which is lost during tumorigenesis (Bonneau, 2000). The third group of Ras effectors consists of RalGDS and PLCε, which harbor RA domains (Ras-associating domains).

All the above mentioned pathways can be simultaneously activated, as they are tightly controlled by the high degree of connections between individual signaling components and globally by the existence of feedback loops to maintain cellular homeostasis under normal conditions. As shown for mTor, upstream signals from Ras and PI3K are integrated to only allow for cell proliferation under environmentally favorable conditions (Wullschleger, 2006). Instead, cancer cells promote growth and survival under inappropriate conditions. In case of Ras, any mutation that leads to constitutively active conformation causes a hyperactivation of downstream effectors, resulting in abnormal growth or enhanced survival. In this way, the uncontrolled Ras activity can lead to pathophysiological consequences, including cancer. The activation signals generated by oncogenic Ras could be inhibited by targeting the GTPase cycle with specific drugs, making it an attractive target for pharmaceutical research. Until now, Ras proteins remain an “undruggable” target, as any drug design failed because of toxicity and pleiotropic effects (Cox , 2002; Carón, 2005).

Apart from oncogenic Ras, several other components like PI3K or EGFR are also frequently found to be misregulated in cancers. The complexity of all these networks has to be understood in order to spot pathological alterations and to drive the cell to a senescent or apoptotic state. Interestingly, oncogenic Ras mutations and mutations in other components of the MAPK signaling pathway, like mutant B-Raf, have been shown to be mutually exclusive in malignant melanoma (Davies, 2002). Oncogenic KRas mutations are frequently found in early stages of tumor progression. Hence, the deregulation of Ras-mediated signaling is essential for tumorigenesis. Similar to oncogenic B-Raf, mutations in Ras family members and loss of PTEN are mutually exclusive in mice and human (To, 2005). Nonetheless, simultaneous alterations in more than one signaling component have been demonstrated for solid tumors where the overexpression of EGFR-related genes in combination with oncogenic KRas are good prediction markers whether a certain chemotherapeutical strategy can be applied (Amado, 2008).

To focus on relevant signaling output with regard to this work, two opposing signaling pathways, namely MAPK and p53, will be discussed further in the following sections.

3.1.1 Ras activates the MAPK pathway

The MAPK (mitogen-activated protein kinase) pathway, a downstream signaling cascade of Ras, translates extracellular input into gene expression. The diverse output can result in cell growth, migration, division, and survival (Raman, 2007). The MAPK pathway can be activated by several extracellular stimuli (growth factors, hormones) each binding to a different receptor (Wolf, 2002).

One such ligand is Epidermal Growth Factor (EGF), which specifically activates the receptor tyrosine kinase (RTK) EGFR (epidermal Growth Factor Receptor). Upon EGF-stimulation, EGFR undergoes dimerization and subsequent trans-phosphorylation on specific tyrosine residues in its C-terminal domain by its intrinsic kinase activity. These phosphorylated tyrosine residues serve as recognition sites (Ullrich, 1990; J. Schlessinger, 1992; Schlessinger, 2000) for various adaptor proteins, like Grb2 (Schlessinger, 2003; Batzer, 1994). Following recruitment of Grb2, SOS (Son of Sevenless, a guanine nucleotide exchange factor (GEF)) is activated to exchange GTP for GDP on Ras (Jorissen, 2003). The MAPK module is activated by GTP-bound Ras and composed of the kinases Raf (MAPKKK), Mek (MAPKK), and Erk (MAPK). Proliferative signals are transmitted in a stepwise manner by phosphorylation and activation of the following kinase (figure 5).

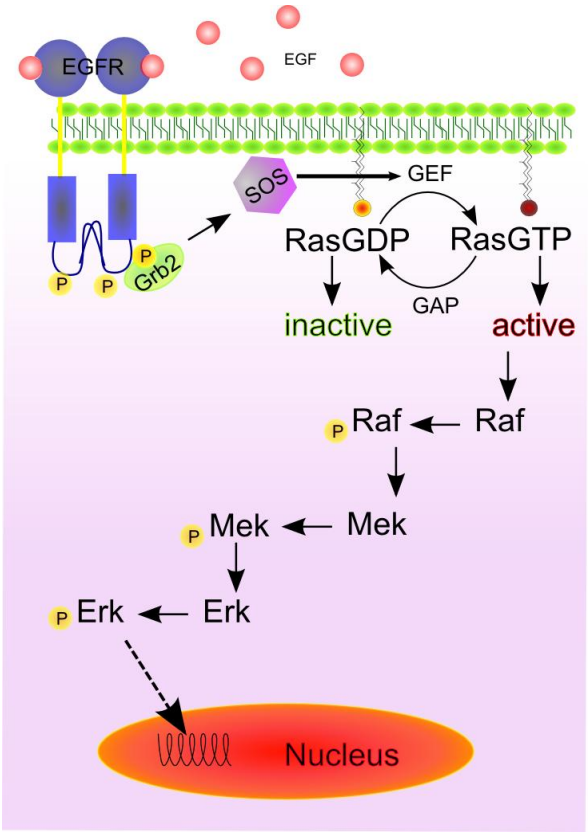

Figure 5: Schematic representation of the EGF-mediated EGFR activation and signal transmission to the Raf-Mek-Erk signaling cascade via active Ras. After growth factor stimulation, Ras is activated and consecutively each kinase activates the downstream kinase by phosphorylation in a cascade manner. Phosphorylated Erk1/2 can either translocate to the nucleus to activate the transcription machinery or phosphorylate cytosolic substrates.

More precisely, Ras alters its conformation from an inactive (GDP-bound) to an active state (GTP-loaded). The GTP-bound state favors the binding of effector proteins like the cytosolic serine/threonine kinase Raf (Kolch, 2000). The Ras-binding domain (RBD) of Raf interacts with Ras-GTP thereby recruiting Raf to the plasma membrane. For Raf-1 it was shown to require membrane-bound Ras for its activation (Morrison, 1997). The Ras-mediated concentration of Raf on the plasma membrane facilitates dimerization and subsequent Raf activation (Hu, 2013; Nan, 2013).

Phosphorylated Raf activates Mek, a dual specificity tyrosine/threonine kinase, by phosphorylation (Seger, 1995). Mek then activates another downstream serine/threonine kinase Erk by phosphorylation. Erk is the terminal protein in the MAPK pathway. ERK1 and ERK2 (extracellular-signal-regulated kinase) are serine/threonine kinases, with a molecular weight of 44 and 42 kDa, respectively. For full Erk2 activity, a conserved Thr(183)-Xxx-Tyr(185) motif in the activation loop has to be phosphorylated on both residues by active Mek (Kolch,

2000), causing Mek-Erk dissociation and Erk homodimerization (Wolf, 2002; Seger, 1995).

Erk has a broad spectrum of cytosolic and nuclear substrates, such as transcription factors, protein kinases and phosphatases, as well as cytoskeletal and scaffold proteins (Yoon, 2006). Erk dimers translocate from the cytosol into the nucleus (Fukuda, 1997). This nuclear accumulation happens within 5-15 minutes and induces transcription (Adachi, 1999). How the translocation functions in detail is still not fully understood. Regarding the existence of a nuclear translocation signal (NTS), which facilitates nuclear import of Erk, contrary opinions exist in literature (Chuderland, 2008; Lidke, 2010). Although this process is phosphorylation-dependent, kinase activity is not required because kinase-dead mutants of Erk2 also accumulate in the nucleus (Khokhlatchev, 1998). Nonetheless, the nuclear translocation is a requirement in terms of transcription induction and proliferation (Brunet, 1999). Erk phosphorylates S6-kinase (RSK) and the ternary complex factors (TCFs), Elk-1, Net-1, and Sap (Yoon, 2006). Elk initiates the expression of several genes required for proliferation. ERK1/2 activation and its localization are dynamically controlled by continuous phosphorylation and dephosphorylation cycles, which can be differentially regulated upon stimulation (Costa, 2006; Santos, 2007). A variety of substrate genes is under the control of a serum-response-element (SRE). RSK phosphorylates the serum response factor (SRF), which first binds to one of the TCF proteins and then to the SRE in the promoter of immediate early genes, like Fos and Myc (Anjum, 2008; Buchwalter, 2004). Active Erk and Erk-mediated signaling can be inactivated by serine/threonine phosphatases, tyrosine phosphatases and dual specificity phosphatases DUSP, (5, 6, 7 and 9) (Owens, 2007).

The MAPK pathway is a robust and conserved network and homeostasis is maintained by the dynamic interplay of positive and negative feedback loops, which account for the variety of output signals. Using the interaction between Ras and its upstream GEF as an example, SOS not only activates Ras, but exhibits an allosterically elevated activity when active Ras is present (Waters, 1995), asserting a positive feedback on itself. Hence, SOS functions as a GEF as well as an effector for Ras proteins. Another example is the interplay between Raf, Mek and Erk. Erk as the terminal node mediates on one hand a positive feedback loop on Mek, thereby activating itself (signal amplification). On

the other hand, there is the negative feedback on Raf, to silence the upstream activation signal, promoting stability of the system (Santos, 2007).

As may be imagined, the presence of oncogenic Ras triggers MAPK-mediated proliferative signals, causing uncontrolled cell growth and migration, essential features of tumorigenesis. As Erk is downstream of Ras, Raf, and Mek, several inhibitors and sensors (Murphy, 2002; Harvey, 2008; Toettcher, 2013) have been developed. Moreover, commercially available kinase activity-based read-out kits are available to monitor Erk activation as a proof of upstream activation.

3.1.2 The p53 protein functions as a tumor suppressor

Aside from the MAPK pathway, several other signaling routes are affected by active Ras, like the p53 pathway. In contrast to the oncogenic nature of Ras, p53 is a tumor suppressor, which functions as a checkpoint for abnormal signaling and is frequently mutated in a large number of cancers.

The p53 gene was first discovered in 1979 (Lane, 1979) and 10 years later it was confirmed that the p53 protein plays a key role in several human cancers (Harris, 1993), functioning as the “Guardian of the genome” (Sigal, 2000). The p53 gene is a tumor suppressor, encoding for a 393 aa protein, whose signaling pathway integrates important checkpoints to regulate cell growth and apoptosis after intrinsic or extrinsic stresses (Jin, 2001; Vogelstein, 2000; Vousden, 2002). Regardless of the type of stress, p53 activation either results in cell cycle arrest, cellular senescence (Hayflick, 1965), DNA repair or apoptosis (Jin, 2001; Vousden, 2002).

In response to stress, p53 is posttranslationally modified by phosphorylation, acetylation, methylation, ubiquitination or sumoylation (Appella, 2001). These PTMs raise the half-life of p53 from 6-20 min to hours and cause a 3-10-fold increased protein concentration. Moreover, the binding to specific DNA sequences, which regulates the transcription of genes, is enhanced. Besides the single-cell level, direct communication with neighboring cells by secretion of proteins that alter the cellular environment is also facilitated by p53 (Harris, 2005).

The p53 pathway can be divided into five steps. First, input is generated by activating stress signals, which are integrated by mediators. Several proteins are

activated that interact with p53 thereby modulating its stability (Jin, 2001). This either leads to transcriptional activation or protein-protein interactions resulting in growth arrest, senescence, apoptosis or DNA repair (figure 6).

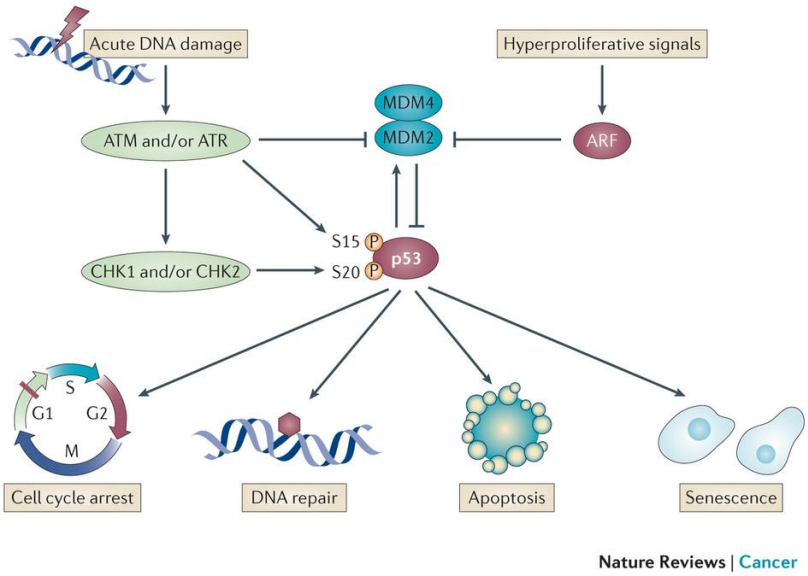

Figure 6: Upon DNA damage, dsDNA breaks and triggers the activation of ataxia-telangiectasia mutated (ATM), a kinase, which phosphorylates CHK2 kinase via ATR and CHK2. CHK1 and 2 phosphorylate p53 thereby stabilizing it. Serine 15 and 20 are important for its stabilization. MDM-2 and MDM-4 bind to the transcriptional activation domain, thereby inhibiting p53 transactivation, MDM also functions as E3 ubiquitin ligase, targeting for proteasome-mediated degradation. Phosphorylation allows interaction with downstream targets to initiate apoptosis, cell cycle arrest, DNA repair or senescence (Figure adapted from Bieging, 2014)

The p53 network is tightly controlled by 10 feedback loops (positive or negative). Under normal conditions, p53 levels are downregulated by MDM-2, Cop-1, Pirh-2 or JNK (negative regulators) that promote constant degradation (ubiquitin/proteasome pathway). These genes are upregulated by p53 itself, keeping the p53 protein level low (negative feedback) (figure 6). Further negative regulators are p73 delta N, cyclin G, Wip-1 and Siah-1. Upon stress, p53 protein levels are elevated by inhibition of the interaction with MDM-2. Second, a series of modulators (kinases, acetylases) will activate the transcriptional activity. Positive feedback loops are transmitted via PTEN-Akt, p14/19 Arf, and Rb.

The specific DNA-binding activity of p53 is mediated via the carboxy terminal tetramerization domain and was also shown to be triggered by phosphorylation (Hupp, 1992), ss DNA, deletion/truncation (30 aa), and interaction with cellular proteins (Hupp, 1992; Jayaraman, 1995). The protein binding occurs through a p53-responsive element (p53 RE), which is found either in the promoter or in the intron of target genes. The p53 RE monomer unit is composed of

RCWWGYYY, where R is a purine, W is either A or T, and Y is a pyrimidine. Thus, two 10 bp sequences with a spacer of 0-13 nucleotides form the regulatory sequence for p53-responsive genes (Riley, 2008). Subsequent to p53 tetramer binding, transcription of target genes is initiated and results in activation of multiple proteins, acting in different pathways to promote tumor suppression (figure 7).

The loss of p53 function by mutation or deletion is a common feature of tumorigenesis. As such, these mutations mostly result in the expression of p53, which has lost its wild-type functions. In almost 90 % of all human tumors, it commonly exhibits missense mutations, resulting in a stable mutant p53 protein, which lacks its specific DNA binding function and accumulates in the nucleus (Soussi, 2001). Such missense mutations occur in <50 % of PDAC cases (Rozenblum, 1997). Cells with a dominant-negative regulation of mutant p53 acquire oncogenic properties (gain-of-function), independent of the status of wild-type p53 (Petitjean, 2007; Brosh, 2009). Such gain-of function mutants actively promote cancer (Blandino, 1999; de Vries, 2002; Brosh, 2009; Dittmer, 1993). They exhibit an enhanced tumorigenic potential, enhanced drug/chemotherapy resistance, and altered transcriptional activities, compared to cells that lack p53.

Patients with Li-Fraumeni syndrome have a mutant TP53 allele and are more susceptible to cancer (Vousden, 2009). As shown in animal models, the presence of one mutant allele leads to enhanced chemo-resistance and a broader tumor spectrum. Among the different tumor types, carcinomas, sarcomas, and lymphomas are predominant, concomitant with increased metastasis and genomic instability (Lavigueur, 1989; Olive, 2004; Liu, 2010). In general, mutant p53 drives invasion, migration, scattering, angiogenesis, stem cell expansion, survival, proliferation, and tissue remodeling by signal transmission through different pathways. The resulting alterations in the DNA-binding ability change the regulation of gene expression or the interactions with different proteins and transcription factors.

As shown in figure 7, p53 mutants can be divided into structural mutants, which cause unfolding of the protein, and DNA-contact mutants, which change the amino acid composition critical for DNA binding (Sigal, 2000).

Point mutation R172H (structural mutant) and R270H (contact mutant) (codons 175 and 273 in humans) engineered in mice under endogenous locus are model systems of Li-Fraumeni Syndrome (p53 $^{R270H/+}$). With time, they evolve allele-specific tumors like osteosarcomas, breast cancer, soft tissue sarcoma and leukemia. In combination with oncogenic KRas, they reflect late-stage pancreatic cancer with metastatic properties (Olive, 2004).

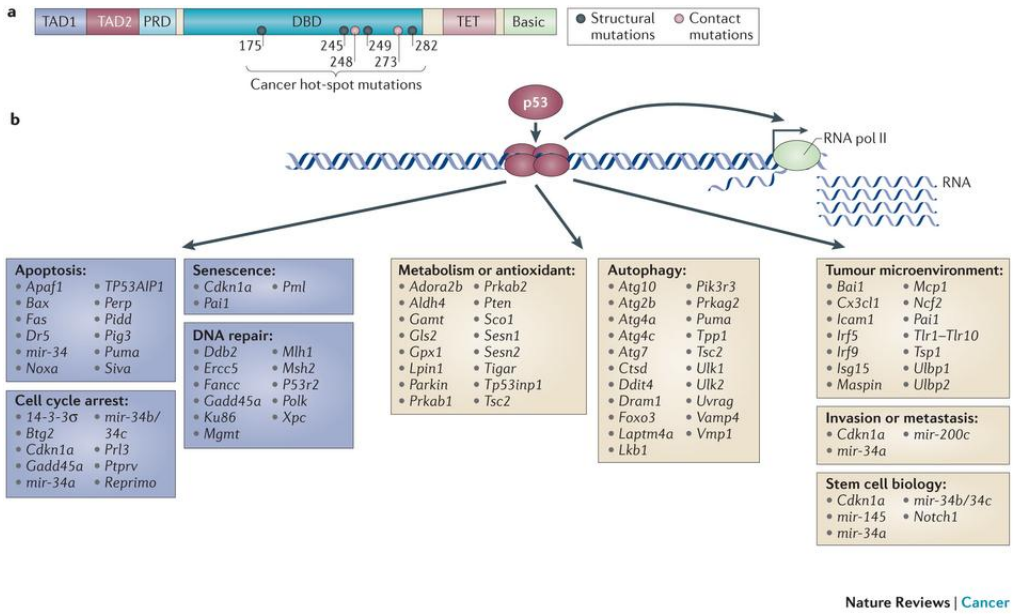

Figure 7: Structure of p53. The p53 protein has two N-terminal transcriptional activation domains (TADs), followed by a proline-rich domain (PRD), a DNA-binding domain (DBD) and a tetramerization domain (TET) and the C-terminal region, rich in basic residues (Basic). The most frequent mutations are shown as either structural or contact mutants. After tetramer formation and binding to DNA, several genes are regulated, grouped into functional groups as depicted in the boxes. (Figure adapted from Bieging, 2014)

Due to the complex topology of the network, p53 was found to share signaling routes of the Ras/MAPK pathway. There is evidence, that structural mutant p53 can interact with the cell cycle regulator BTG2, preventing it from deactivating HRas (Solomon, 2012). Upon phosphorylation of p53 at serine 33 and 46 by p38 MAPK, p38 MAK is itself phosphorylated, regulated by the MAPK pathway. Wip-1 phosphatase inactivates p38 MAPK and is a p53-regulated gene, which forms a negative feedback loop by connecting p53 and Ras (Takekawa, 2000). Heat-shock proteins, activated Ras and PTEN have been shown to stabilize p53 (Suh, 2011). Additionally, the introduction of oncogenic Ras into primary cells was shown to cause p53-dependent senescence (Bates, 1998; Eliyahu, 1984; Parada, 1984). Nonetheless, oncogenes like Ras and Myc are usually detected by the p53 checkpoint and such transformed cells are subsequently

killed, demonstrating its tumor suppressor function. The dual role of p53 is reflected by the ability to detect mutations in cell cycle regulators and by blocking the progression of cell cycle, affecting a broad range of outcomes.

3.2 The KRas oncogene

During tumor progression, KRas is the most frequently mutated isoform among the Ras proteins (Allegra, 2009; Aguirre, 2003) and present in 30 % of all cancers (Forbes, 2011).

Discovered in 1983, the human KRAS gene was detected in the genomic DNA of human LX-1 lung carcinoma cells and found to be a homologue of two retroviral oncogenes (Kirsten Rat Sarcoma Virus and Murine Sarcoma Virus), related to rodent sarcoma virus genes (Shimizu, 1983). One year later, it was shown that the gene product can also result in an abnormal form of the p21 protein, which is able to transform NIH3T3 cells. This aberrant gene product predominantly occurred in carcinoma tissue and was therefore linked to an abnormal state of activation (Norton,1984). Following these first observations, KRas was found to initiate signaling cascades and mediate information from the cell periphery to the nucleus, resulting in cell differentiation, proliferation, apoptosis, and cell migration/chemotaxis (Rajalingam, 2007; Zuber, 2000; Campbell, 1998). Moreover, it induces changes in the cytoskeleton and consequently affects cell shape, adhesion, and migration (Esser, 1998). KRas consists of 188 amino acid residues, divided into four domains with a molecular mass of 21.6 kDa. Moreover, it was shown to be the only isoform, which is essential in mouse embryogenesis. Neither HRas nor NRas knockouts have detectable side effects on the development of mouse embryos, whereas a KRas knockout is embryonic lethal at 12-14 days, concomitant with late-onset growth and hemopoietic defects (Johnson, 1997; Koera, 1997).

The human genome has two copies of the KRAS gene, KRAS1 and KRAS2, (McGrath, 1983), which are localized at chromosomes 6p11-12 and 12p11.1-12.1 (Popescu, 1985). The splice variant KRas4A undergoes additional palmitoylation by palmitoyltransferase upstream of the CAAX motif. KRas4B is the predominant splice variant of KRAS2 (Pan, 1990) and there is no detectable palmitoylation of this splice variant (Hancock, 1989). The KRAS4B gene product was exclusively used in the present work and will be further named KRas.

It has been demonstrated that the wild-type KRAS gene is frequently replaced by mutant KRAS during tumor progression in many types of cancer (Allegra, 2009; Aguirre, 2003). Once the KRAS gene mutates, it acquires oncogenic properties and seems to be involved in the development of various human cancers (Kranenburg, 2005; Barbacid, 1987; Malumbres, 2003).

Such oncogenic transformations are widely present in pancreatic cancer (90 %), colorectal carcinomas (40-50 %), and lung carcinomas (30-50 %) (Bos, 1989; Schubbert, 2007a; Schubbert, 2007b). The acquisition of a mutant KRAS allele has been observed in both, human and mouse tumors, indicating that the absence of normal alleles may facilitate transformation by one copy of the oncogenic KRAS allele (Hingorani, 2003). Like the other Ras proteins, KRas needs to be in the active GTP-bound state to be able to interact with downstream effectors. As mentioned before, oncogenic KRas (KRasG12V) has an impaired GTPase activity. The G12V mutation causes a sterical clash in the active site and locks the protein in a permanent GTP-bound state, as the GAP-mediated GTP hydrolysis reaction is prevented (Vetter, 2001). As a consequence, the protein is constitutively active and permanently transmits proliferative and survival signals. Since KRas functions as the signal integration point for proliferative and survival information, this leads to hyper-activation of important cellular pathways, like MAPK activation. Such mechanisms are regularly found in cancer. Regarding the constitutively active mutant G12V, recent research shows that KRas is not constitutively active, rather readily activated by upstream stimuli (Huang, 2014), leading to a prolonged strong KRas activity.

In more than 90 % of reported pancreatic adenocarcinomas, constitutively active mutations in the KRAS gene were found (KRasG12D/V). At the time of diagnosis, pancreatic adenocarcinomas harbor oncogenic KRas mutations (>80 %) with an average survival rate of the patients below 6 months (American Cancer Society). Tobacco exposure (Hruban, 1993), as well as coffee drinking (Porta, 1999) and milk, butter, and alcohol consumption (Morales, 2007) were reported to correlate with pancreatic cancer bearing oncogenic KRas. The growth and survival in several pancreatic cell lines were shown to be KRas-dependent (Singh, 2009; Collisson, 2011). KRas mutations are frequent in early cancer stages and play an important role in PanIN (pancreatic intraepithelial neoplasia) formation, whereas an additional mutation in the tumor suppressor

p53 characterizes late stage cancer (Hingorani, 2003; Aguirre, 2003; Hingorani, 2005; Hezel, 2006). Mouse models with inducible KRas G12D demonstrate that fibrotic stroma is formed and maintained after induction. Inactivation of mutant KRas, accompanied with p53-/+ results in tumor regression, pointing towards the adaption and subsequent addiction of oncogenic KRas signaling (Collins, 2012).

The second highest occurrence of KRas mutations, around 50 % of all cases, is found in colon cancer (Bazan, 2002). In earlier studies, cancer invasion was shown to be enhanced in fibroblasts expressing oncogenic KRas, accompanied with increased adhesiveness and altered polarization (Liao, 2003). Moreover, upregulated carcinoembryonic antigen (CEA) expression and disturbance of epithelial cell polarization after oncogenic KRas expression was observed (Yan, 1997; Otori, 1997).

The development of CRC is categorized in three stages with different probabilities of oncogenic KRas mutation. Stage 1 characterizes the development of a small, benign tubular adenoma or polyp with sporadic KRas mutations. Stage 2 is defined as a more aggressive phenotype with patches and definite carcinoma cells. In case of stage 3, the cells start invading other tissues. KRas mutations occur in adenoma and carcinoma tissue, with carcinoma tissues being more frequently mutated (Forrester, 1987; Vogelstein, 1988).

KRas mutations occur in 10-30 % of lung cancers, accompanied with poor prognosis (Broermann, 2002) and a history of smoking. Despite the fact that NSCLC (non-small cell lung cancer) is known to frequently evolve activating EGFR (epidermal growth factor receptor) mutations, oncogenic KRas was detected in 21 % of NSCLC-tumor samples (Eberhard, 2005). Oncogenic KRas is inevitable for tumor cell survival at all stages of lung adenocarcinoma. Further, the presence of an additional mutation or loss of tumor suppressor function requires mutant KRas (Fisher, 2001).

Small molecule tyrosine kinase inhibitors (TKis) like Gefitinib (Iressa®) and Erlotinib (Tarceva®) are used as the second line therapy in patients with NSCLC after failure of standard chemotherapy. In the presence of mutant KRas, a poorer response and shortened survival is observed. Thereby oncogenic KRas functions as a prediction marker to elucidate resistance to targeted therapy after EGFR inhibition (Massarelli, 2007; Katzel, 2009). In colorectal car-

cinomas, the KRas status has to be evaluated carefully, because treatment with monoclonal antibodies targeting EGFR, Cetuximab (Erbitux®) and Panitumumab (Vectibix®), fails when mutant KRas is expressed (Lièvre, 2006; Amado, 2008) . Even the “gold standard” for CML (chronic myeloid leukemia) Imatinib (Glivec®) was found to be ineffective in patients with frequently expressed oncogenic KRas (Agarwal, 2008). In order to derive benefit from EGFR-TKis, the status of KRas as a biomarker should be considered for targeted inhibition. According to Singh et al., (Singh, 2009), cancers can be divided into oncogenic KRas dependent and independent which would give information about therapeutic prognosis. Additionally, KRas was found to dominantly activate Raf kinase, a downstream effector, while the other Ras proteins activate another branch of downstream signaling, the PI3K pathway (Phosphoinosite-3 kinase), and causing survival.

There have been attempts to inhibit oncogenic KRas by farnesyltransferase inhibitors (FTIs), which were demonstrated to work *in vitro* and in xenografts (Omer, 1997; A, 1997), shown to inhibit anchorage-independent growth of both KRas-transformed mouse fibroblasts and human tumor cells with KRas and NRas mutations, but failed in clinical studies (Blum, 2005). FTIs inhibit the C-terminal farnesylation on Ras proteins without affecting geranyltransferase activity, which might preserve Ras activity (Lerner, 1997) by taking over the catalysis of lipid modifications.

3.3 Lipidated Ras proteins localize to different cellular compartments

Apart from their GTPase activity and plasma membrane localization, all three Ras isoforms harbor lipid modifications, which are essential for their function and specific localization. This is achieved by posttranslational lipidation in the hypervariable region, an additional feature of the majority of Ras superfamily proteins (Hancock, 1989; Hancock, 1990).

After ribosomal protein translation, Ras proteins are irreversibly farnesylated by farnesyltransferase at the cysteine residue of the CAAX-box motif (Gelb 1997). Farnesyltransferases and geranylgeranyltransferase I recognize the CAAX-sequence and catalyze the binding of isoprenoids (farnesyl or geranylgeranyl) to the cysteine residue by forming a covalent thioether bond. At the cytosolic

surface of the ER, (endoplasmic reticulum) the AAX motif is cleaved by the local protease Rce1 (Ras-converting enzyme 1) and the C-terminal carboxyl residue is subsequently methylated by Icmt (Rajalingam, 2007). KRas4B is directly transported to the plasma membrane whereas HRas, NRas, and KRas4A are further modified (Swarthout, 2005), before reaching the plasma membrane.

In general, lipid modifications are either irreversible, or reversible. Irreversible lipidations remain on a functional protein and are only removed by proteasomal degradation. There are three kinds of irreversible lipid modifications in eukaryotes: N-linked acyl groups in case of myristoylation (Martin, 2011), S-linked isoprenoids (Hougland, 2009), like farnesylation of Ras proteins, and O-linked cholesterols (Milenkovic, 2010).

HRas, NRas and KRas4B undergo two types of lipidation: an irreversible farnesylation at the C-terminal cysteine of the CAAX-Box motif and a reversible (figure 2). Briefly, HRas is doubly palmitoylated (position C181 and C184), which correlates with a more prominent plasma membrane localization as compared to NRas. N-Ras contains only a single S-palmitoylated cysteine residue (position C181). The KRas4A splice variant is mono-palmitoylated and the splice variant KRas4B is only farnesylated (Hancock, 1989).

Due to their lipid modifications, all Ras isoforms localize to the plasma membrane and endomembranes. The degree of association with endomembranes differs among the Ras isoforms N>H>KRas (Choy, 1999). HRas and NRas additionally populate the Golgi apparatus mediated by localized palmitoyltransferases activity, thereby locally enhancing their membrane affinity (Rocks, 2006).

3.4 The GDI-like solubilization factor PDEδ

It has been proposed that intracellular Ras trafficking involves prenyl-binding proteins (Nancy, 2002; Hanzal-Bayer, 2002). PDEδ, which functions as a GDI-like solubilization factor for farnesylated proteins (Chandra, 2012; Zhang, 2004), by solubilizing these membrane-anchored proteins, thereby enhancing their effective diffusion in the cytosol (Schmick, 2014a; Schmick, 2015).

PDEδ (PDE6D) is a soluble 17 kDa protein, which was first identified as the fourth subunit of rod cell-specific photoreceptor cGMP phosphodiesterase (PDE6) (EC 3.1.4.35) located in retinal tissue. It was discovered as a co-

precipitate of rod PDE (Gillespie, 1989) and found to play a major role in the phototransduction cascade. The holoenzyme is a heterodimer, consisting of two α- and β-subunits, regulated by two γ-subunits (Baehr, 1979; Fung, 1990). The α- and β-subunits are post-translationally modified with a farnesyl (C15) or geranylgeranyl (C20) moiety, localizing PDE6 to the membrane. PDEδ solubilizes PDE from the rod outer segment disc membrane, without affecting its catalytic activity (Florio, 1996). PDEδ is expressed in various tissues and in eyeless invertebrates such as *C. elegans*, suggesting additional functions besides the solubilization of PDE in the eye (Li, 1998).

The core domain structure of PDEδ shows an immunoglobulin-like β-sandwich fold with two β-sheets that pack against each other, followed by an N-terminal α-helix. The structural comparison with RhoGDI (guanine-nucleotide dissociation inhibitors) gave the best hit (Z-score 9.8). RhoGDI solubilizes C-terminally prenylated proteins (Rac, Rho, and Cdc24) from cellular membranes. Although the sequence homology is very low, the fold and also the composition and position of specific residues, which form the inner surface of the lipid-binding pocket are identical, indicating the common features of both PDEδ and RhoGDI (Hanzal-Bayer, 2002). Nonetheless, PDEδ lacks an N-terminal helix-loop-helix motif, which allows interactions with the switch region of GTPases, meaning it has no binding preference for the nucleotide state of its interaction partner (Nancy, 2002; Hanzal-Bayer, 2002). Instead, PDEδ is a non-selective prenyl-binding protein, which targets hydrophobic prenylated C-termini of a variety of polypeptides with a stoichiometry of 1:1. Notably, it strongly interacts with farnesyl but to a lesser extent with geranylgeranyl side chains as a soluble transport factor (Zhang, 2004).

PDEδ was shown to act as a solubilization factor for KRas molecules as well as for depalmitoylated isoforms (Chandra, 2012). In fact, PDEδ does not extract proteins from membranes rather it passively sequesters farnesylated cargo from endomembranes. The presence of PDEδ is essential to counter the entropic tendency of farnesylated Ras proteins to randomly distribute to all endomembranes (Schmick, 2014a; Schmick, 2015). By facilitating diffusion of Ras proteins in the cytoplasm, the kinetics of being enriched at a different perinuclear compartments are elevated. If HRas or NRas are solubilized by PDEδ, the probability of these farnesylated but depalmitoylated proteins being

trapped at the Golgi apparatus is high, due to their higher mobility in complex with PDEδ and local PAT activity (Rocks, 2005). In case of KRas, an enrichment at the recycling endosome and the plasma membrane is maintained (Schmick, 2015).

Another interaction partner of PDEδ is the farnesylated protein RheB (Ras homolog enriched in brain) (Hanzal-Bayer, 2002; Chandra, 2012; Schmick, 2014), a regulator of the mammalian target of rapamycin (mTOR). RheB is active on lysosomes to recruit mTOR via Rag GTPases, facilitating formation of the mTOR complex 1 (mTORC1), which couples information about the availability amino acid to cell growth and autophagy. The mTORC1 activity is regulated by various input signals, such as growth factors, stress, energy status and amino acids (Sancak, 2008; Sancak, 2010; Jewell, 2013). In contrast to the Ras isoforms, RheB lacks an additional reversible palmitoylation and has no polybasic sequence. In this way, it is not trapped at a specific membrane compartment.

Beside the binding to Ras family members, PDEδ binds to truncated, non-modified Arl2 and Arl3 (Arf-like GTPase 2/3) proteins in a GTP-specific manner (Linari, 1999; Hanzal-Bayer , 2002; Ismail, 2011). In this way, PDEδ is an Arl effector, which has a higher affinity for the GTP-bound form of Arl2 and Arl3 (Hanzal-Bayer, 2002). The complex of Arl2:PDEδ shows typical GNBP:effector interactions (guanine nucleotide binding proteins), characteristic for the GTP conformation (Hanzal-Bayer, 2005; Hanzal-Bayer, 2002). The PDEδ-Arl2 interaction exclusively occurs in the perinuclear area and is strictly GTP-dependent, as only Arl2-GTP facilitates release of farnesylated cargo bound to PDEδ. It is still unresolved how the locally regulated nucleotide exchange on Arl2 is performed and if unknown GEFs are involved (Schmick, 2015). In summary, PDEδ is able to bind Ras, RheB, and other farnesylated proteins functioning as a solubilization factor in the cytoplasm and it interacts with Arl2-GTP in the perinuclear area to release its cargo, which is subsequently enriched at target membranes. In order to understand these functions and properties in more detail, the concept of protein cycles and localized release will be discussed in the following chapter.

3.5 The PDEδ-Arl2 delivery system serves many clients

It is already known, that the tight interplay between PDEδ-mediated solubilization of farnesylated Ras isoforms and Arl2-GTP-dependent localized release in the perinuclear area is inevitable to counter equilibration of Ras to all endomembranes (Schmick, 2015).

As described above, the hypervariable region (HVR) determines the localization of Ras proteins due to the respective posttranslational modification. Instead of the other isoforms, KRas is only irreversibly farnesylated but utilizes a polybasic stretch consisting of eight positively charged lysine residue in the hypervariable region. Electrostatic interactions between the negatively charged phospholipids at the inner leaflet of the plasma membrane and the lysine residues enhance the association of KRas to the plasma membrane (Hancock, 1990; Crouthamel, 2008; Quatela, 2008). Besides the plasma membrane, the positive charge allows additional intracellular electrostatic interactions with the negatively charged membranes of the recycling endosome compartment (Schmick, 2015).

Although, the combination of farnesylation and electrostatic interactions maintains KRas at the plasma membrane, vesicular internalization of the plasma membrane by endocytosis, phagocytosis, and pinocytosis constantly occurs. As the rate of plasma membrane vesiculation is five times higher than spontaneous dissociation of KRas from membranes, the fraction of KRas at the plasma membrane is constantly depleted (Schmick, 2014a). Internalized membrane loses its asymmetric charge due to the curvature of the formed vesicles. Endocytosis causes a positive curvature on the intracellular and a negative curvature on the extracellular leaflet of the plasma membrane, resulting in an equalized overall charge (Bohdanowicz, 2013). In this way, the electrostatic interactions between KRas and the lipid bilayer no longer exist and KRas can freely diffuse in the cytosol until it reaches membranes to associate with. The binding to endomembranes is highly dynamic and does not require additional targeting signals. Hence, KRas undergoes spontaneous intermembrane transfer via its soluble fraction (“hopping”) and equilibrates to all endomembranes with time due to a longer dwell time and the extensive surface area of the endomembranes system compared to the plasma membrane (Schmick, 2015).

As mentioned before, the solubilization factor PDEδ is important to sequester loosely bound KRas from endomembranes. The binding of KRas to PDEδ en-

hances its diffusion speed in the cytosol and leads to a faster depletion from endomembranes (Schmick, 2014a). Ectopic PDEδ expression was shown to reinstate the plasma membrane localization of Ras proteins in HepG2 cells, which lack endogenous PDEδ (Chandra, 2012), supporting results from PDEδ knockout and inhibitor studies, which demonstrated that the presence of PDEδ is essential to maintain KRas enrichment at the plasma membrane (Chandra, 2012; Zimmerman, 2013). Nonetheless, reaction diffusion simulations clearly demonstrate that PDEδ is indeed necessary but not sufficient to localize KRas at the plasma membrane (Schmick, 2014a).

In this way, neither the presence of the polybasic stretch nor PDEδ-mediated solubilization and not even a combination of both is sufficient to maintain KRas at the plasma membrane. As a consequence, KRas enrichment at the plasma membrane is not possible at thermodynamic equilibrium. Therefore, the enrichment at the plasma membrane has to be actively maintained by an energy-driven mechanism, which involves PDEδ and Arl2-mediated release in the perinuclear area (Schmick, 2014a; Schmick, 2015).

Farnesylated KRas in complex with PDEδ is released in the perinuclear area by local Arl2 activity. The interaction between PDEδ and the G-protein Arl2/3 (Ismail, 2011) leads to a GTP-dependent release of farnesylated cargo, which can then either be rebound by free PDEδ or associate with endomembranes. The presence of Arl2-GTP increases the dissociation rate of KRas 10-fold (Ismail, 2011). As verified by reaction diffusion simulations, the absence of perinuclear release causes KRas distribution to all endomembranes. Moreover, KRas has an increased probability of getting trapped at Rab11-positive endosomes (pericentriolar recycling endosome) (Schmick, 2015). Rab11 is a protein, which resides at the recycling endosome, a cellular compartment with negatively charged membranes, creating an environment similar to the plasma membrane but in close proximity to the nucleus. The presence of the polybasic stretch causes an elevated residence time of KRas on the recycling endosome, as charged membranes are electrostatically favored compared to endomembranes (Schmick, 2014a). Therefore, the dissociation rate of KRas from the recycling endosome is low. Hence, it traps and concentrates KRas, which is released from the PDEδ-Arl2 complex into the perinuclear space and ensures its directed vesicular transport to the plasma membrane (figure 8).

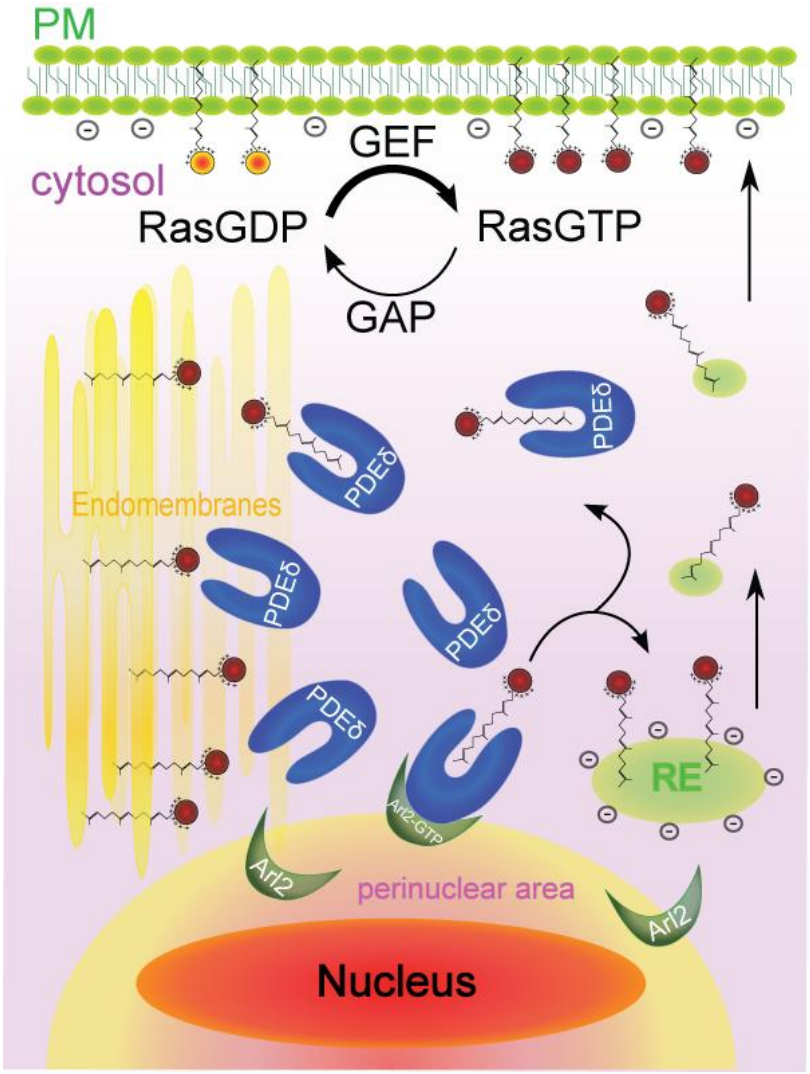

Figure 8: Spatial organization of KRas; Due to its polybasic motif in the HVR, KRas localizes to the negatively charged inner leaflet at the plasma membrane where it transmits signals from extracellular input inside the cell. Farnesylated KRas has the general tendency to bind to all endomembranes. In order to maintain an out of equilibrium distribution, PDEδ sequesters KRas from endomembranes and increases solubility in the cytoplasm. Farnesylated cargo bound to PDEδ is released in the perinuclear area by Arl2-GTP. Released KRas is either trapped on endomembranes or at the recycling endosome (RE) by electrostatic interactions. It is then transported back to the plasma membrane by directed vesicular transport.

This spatial asymmetry in the distribution of palmitoylated and depalmitoylated HRas and NRas is maintained by an acylation cycle (figure 9), which counteracts protein leakage from the plasma membrane into endomembranes by endocytosis, or fission, or by slow dissociation (Rocks, 2005; Goodwin, 2005). HRas and NRas are irreversibly farnesylated and reversibly palmitoylated. They localize to the plasma membrane and the Golgi apparatus, respectively. The compartmentalization of Ras signaling causes distinct cellular responses with

high specificity and the ability to act on multiple signal propagation pathways (Lorentzen, 2010).

Three cooperating factors counter the entropy-driven dilution of these Ras isoforms to all membranes to maintain an out-of-equilibrium distribution. First, iterative depalmitoylation and repalmitoylation cycles continuously occur, facilitated by local palmitoyltransferases (PATs) and cytosolic acyl protein thioesterases (APTs) (Vartak, 2014). Upon cleavage of palmitoyl groups by thioesterases, the plasma membrane affinity is reduced, concomitant with an increased effective diffusion in the cytoplasm. Although the molecules are irreversibly farnesylated and they tend to populate endomembranes, their effective diffusion speed is high. This is achieved by PDEδ, which binds to farnesylated proteins and shields the hydrophobic tail from the cytoplasm, facilitating faster diffusion and the PDEδ-Arl2 systems enhances enrichment on target membranes close to the perimuclear area as described for KRas (Schmick, 2014a, Schmick, 2015).

Second, local PAT (palmitoyltransferase) activity traps farnesylated Ras at the Golgi surface, thereby generating a higher membrane affinity and a localized slower diffusion, concomitant with an elevated residence time (Rocks, 2005). As mentioned above, an additional regulation of the amount of solubilized Ras is facilitated by the interaction between PDEδ and the G-protein Arl2 (Ismail, 2011). In its GTP-bound state, Arl2 releases cargo from PDEδ in the perinuclear area, which can then either be rebound by free PDEδ or associate with endomembranes or directly attach to the Golgi membranes for repalmitoylation (Schmick, 2015).

Third, such kinetically trapped and palmitoylated proteins are unidirectionally transported via the secretory pathway from the Golgi apparatus to the plasma membrane where they can be activated, completing the acylation cycle (Rocks, 2005; Rocks, 2010).

In contrast to doubly palmitoylated HRas, the overall palmitoylation of NRas is less stable as it has only one reversible modification. NRas dissociates faster from the plasma membrane due to ubiquitous APT activity and gets lost on endomembranes (Rocks, 2010; Schmick, 2015). Additionally, thioesterases catalyze depalmitoylation of NRas on secretory vesicles. Hence, that fraction of NRas originally targeted to the plasma membrane does not reach its destination

and is again solubilized by PDEδ, likely to get retrapped at the Golgi apparatus. NRas has a lower membrane affinity and palmitate stability, resulting in a more pronounced steady-state Golgi localization when compared to HRas (Rocks, 2010). The palmitoylation pattern together with the ubiquitous APT activity and the localized PAT activity cause the different kinetics of HRas and NRas in the acylation cycle.

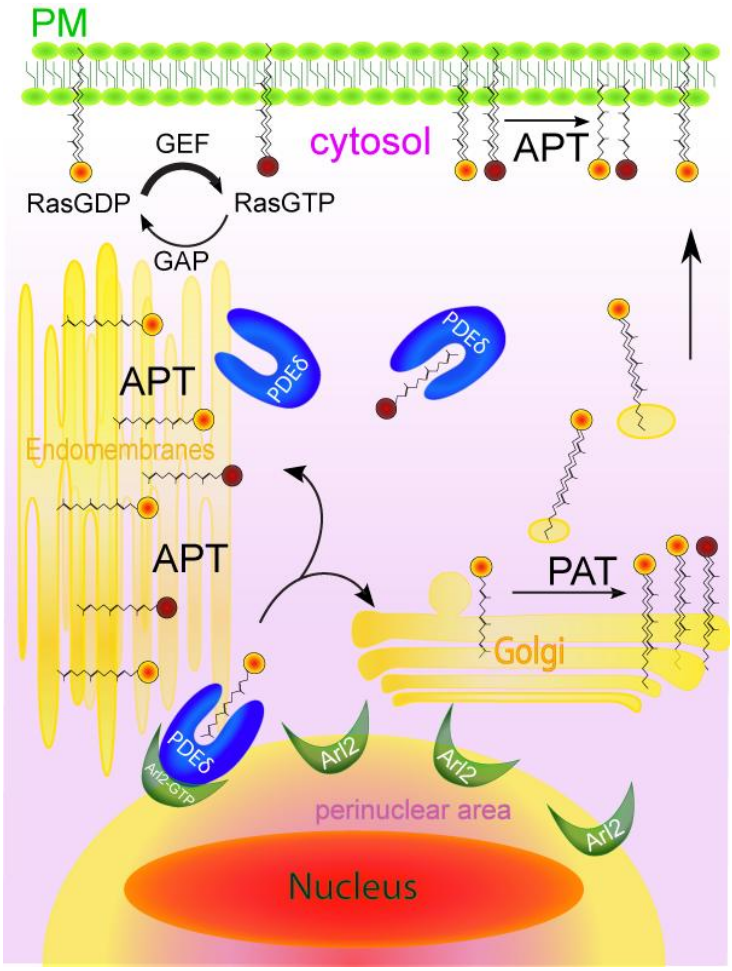

Figure 9: Spatial organization of NRas; NRas is farnesylated and palmitoylated at the plasma membrane, palmitoyl moieties are removed by cytosolic thioesterases (APT). Farnesylated NRas is solubilized by PDEδ and trapped at the Golgi apparatus for repalmitoylation, catalyzed by local palmitoyltransferases (PAT). Palmitoylated NRas is directed to the plasma membrane by vesicular transport. Arl2-GTP activity in the perinuclear area facilitates release of farnesylated NRas bound to PDEδ.

Besides HRas, NRas, and KRas, the PDEδ-Arl2 complex also interacts with the farnesylated Ras-family member RheB (Ras homolog enriched in brain) in the perinuclear area (figure 10). In contrast to the Ras isoforms, RheB is only farnesylated and has no other modifications or features, which would target it to a certain membrane compartment and lower its membrane dissociation. It re-

mains concentrated on perinuclear membranes and the weak association with membranes causes a stronger partitioning into the cytosol (Schmick, 2015). Due to the lack of any trapping membrane compartment, RheB equilibrates faster from these perinuclear membranes to the huge endomembrane surface (Schmick, 2015).

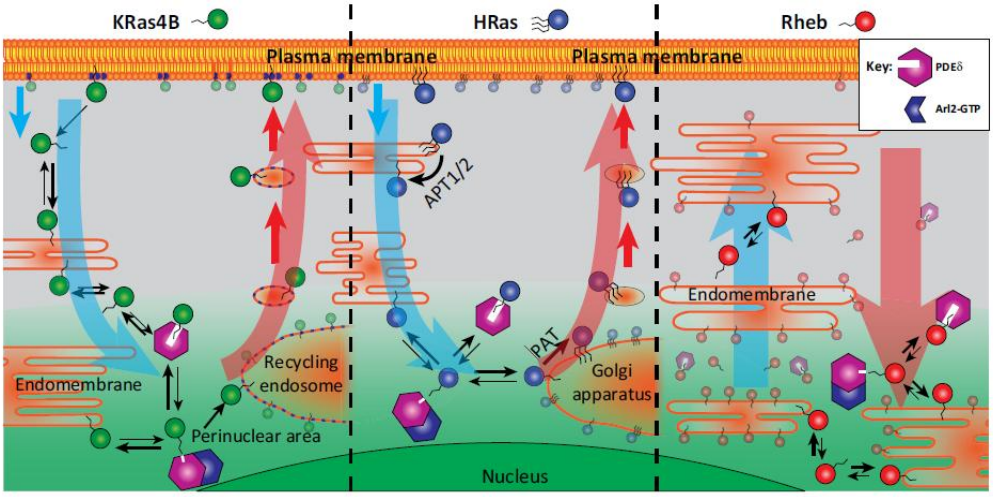

Figure 10: The displacement of farnesylated cargo from the PDEδ-Arl2 system in the perinuclear area is responsible for KRas (left) and HRas (middle) enrichment at the plasma membrane. RheB (right) is another client of the delivery system and enriches in the perinuclear area. With time, it rapidly equilibrates to endomembranes as it lacks an additional feature for trapping it at a vesicular transport compartment. Figure adapted from Schmick et al., 2015.

In this way, the PDEδ-Arl2 delivery system is the main driver for the different spatial localizations of HRas, NRas, KRas and RheB, facilitating trapping at the right membrane compartment. The release of farnesylated cargo on perinuclear membranes instead of delivery at the plasma membrane is a common mechanism in all cycles (figure 10). For Ras, its subsequent enrichment on a specific trapping compartments and the directed transport to the plasma membrane counter the equilibration to endomembranes. For RheB, the leakiness of perinuclear membranes causes an equal distribution to endomembranes.

3.6 PDEδ inhibition causes KRas delocalization

The importance of PDEδ in maintaining the spatial organization of Ras family proteins and convincing results from knockout studies (Chandra, 2012), demanded for the development of small molecule PDEδ inhibitors.

In 2013, a highly potent PDEδ inhibitor ($K_D < 5$ nm), Deltarasin, was published to have an impact on KRas-dependent cells by interference with the spatial or-

ganization of KRas. Deltarasin has a benzimidazole-based lead structure and was the first inhibitor found to specifically bind to PDEδ thereby indirectly targeting oncogenic KRas-dependent growth and signaling by depleting KRas from the plasma membrane. This inhibitor mimics a farnesyl moiety and binds to the farnesyl-binding pocket of PDEδ with high affinity thereby affecting the localization and Ras-induced proliferative information, transmitted via the MAPK pathway (Zimmermann, 2013).

Upon PDEδ inhibition, KRas cannot compete with the drug bound to the hydrophobic pocket and is therefore not solubilized in the cytoplasm. With time, the fraction of KRas at the plasma membrane decreases and the spatial organization is disrupted as PDEδ is essential to maintain the out-of-equilibrium distribution and KRas gets enriched on endomembranes (figure 11).

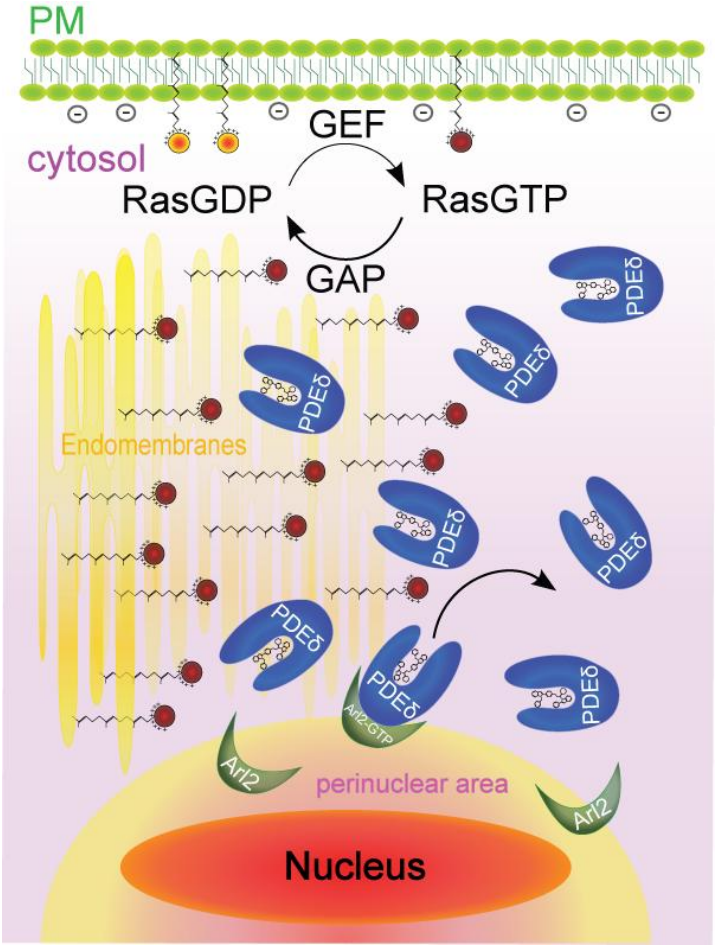

Figure 11: Schematic representation of the KRas cycle in the presence of Deltarasin. The farnesyl-binding pocket is blocked by Deltarasin and PDEδ is incapable to solubilize KRas. KRas populates all endomembranes and the fraction at the plasma membrane decreases with time. Deltarasin can be released in the perinuclear area by Arl-2, hence a higher effective inhibitor concentration is inevitable to rebind to the hydrophobic pocket to stop the KRas cycle.

For Deltarasin, an 'in cell' K_D of 41 ± 12 nM was calculated from dose-response data acquired with FLIM, demonstrating its high affinity. Moreover, experiments in human pancreatic cancer cells, as KRas is regularly mutated in such tumors, demonstrate that PDEδ inhibition causes death in KRas-dependent cell lines but not in KRas-independent cell lines (Zimmermann, 2013).

One year later, a second compound, named Deltazinone 1 was found to bind to PDEδ with very low nanomolar affinity (K_D < 5 nm). Deltazinone 1 is based on a pyrazolopyridazinone scaffold and exhibits an 'in cell' K_D of 58 ± 17 nM (Papke, 2015). Both inhibitors mimic farnesylated proteins and bind to the hydrophobic binding pocket of PDEδ in the same manner and with high affinities at nanomolar concentrations. Figure 12 shows the formation of hydrogen bonds between Deltarasin and three residues (Y149, R61, and C56) of the PDEδ binding pocket (Zimmermann, 2013).

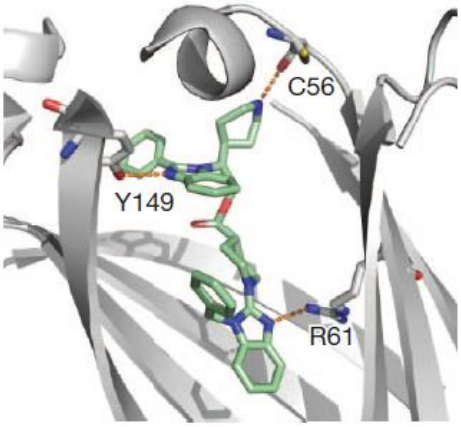

Figure 12: Binding mode of Deltarasin to PDEδ. The molecular docking proves the existence of three hydrogen bonds between Deltarasin and the hydrophobic binding pocket of PDEδ. The piperidine moiety interacts with the backbone carbonyl of cysteine 56 and the benzimodazole units with arginine 61 and tyrosine 149. Figure adapted from Zimmermann et al., 2013.

In order to validate PDEδ as a suitable target, genetic downmodulation with doxycycline-inducible shRNA against PDEδ was already performed in pancreatic cancer cell lines. The data corroborates the growth inhibitory effects after inhibitor treatment in KRas-dependent cells.

In this way, it is promising to further study and compare the effects of genetic downmodulation and small molecule PDEδ inhibition on a larger panel of different cancer cells with known dependencies on oncogenic KRas. In this work, I was particularly interested to further explore the relationship between PDEδ and the KRas status in different settings and to emphasize possible strategies for targeted cancer therapy.

3.7 Genetic validation of PDEδ in human cancer cells

It was already proven in 2013, that RNAi-mediated downmodulation of PDEδ leads to death in KRas-dependent but not in KRas-independent human PDACs (Zimmermann, 2013).

For the experimental design of this work, a panel of human cancer cell lines lines from pancreatic, colorectal, lung, and cervix carcinomas were chosen for genetic manipulation of PDEδ by doxycycline-inducible shRNA. These cell lines were selected due to their known KRas status (Singh, 2009; Babij, 2011; Singh, 2012) and are listed in table 1. They are a representative panel in terms of response and tumor origin, as these cancers are all known to gain oncogenic KRas mutations with time.

The PDAC cells Panc-TuI, Panc-1, Capan-1 and BxPC-3 were already shown to have a KRas-dependent growth behavior after PDEδ depletion (Zimmermann, 2013). The cell lines HCT-116 and Hke-3 are isogenic in the way that oncogenic KRas was depleted by homologous recombination in HCT-116 to become Hke-3. In this way, they represent an ideal system to study oncogenic KRas dependency. The cell line HT-29 harbors an oncogenic BRaf mutation and has a KRast wildtype background. As BRaf functions downstream of KRas, such mutant cell lines are not likely to gain an additional KRas-dependency.

Table 1: Human cell lines subjected to RNAi-mediated PDEδ downregulation with known KRas dependencies. Pancreatic cancer cell lines are depicted in red. Colorectal carcinoma cells are shown in blue and lung cancer cell lines are shown in green. A431 is a cervix carcinoma cell line with overexpressed EGFR and colored in black. (1 = Singh, 2009, 2 = Singh, 2012) (3 = Babij, 2011)

KRas dependent	KRas dependency (border)	KRas independent	KRas wild-type	unknown KRas dependency
Panc-TUI [1]	HCT-116 [2]	Panc-1 [1,3]	BxPC-3 [3]	SW480 (KRas mut)
Capan-1 [1,3]		A549 [1]	HT-29 [3] (BRaf V600E)	
MIAPaCa-2 [3]			Hke3 [2]	
H358 [1]			A431 (EGFR overexpr.)	
H441 [1]				

The idea is, that genetically inducible downmodulation of PDEδ mirrors the effect of specific inhibitors without unwanted side effects. It was already shown, that siRNA against PDEδ causes a delocalization of Ras from the plasma membrane to endomembranes (Chandra, 2012). In this way, the depletion of endogenous PDEδ leads to an interference with the spatial organization of Ras, by causing a random distribution to all endomembranes and diminishing the plasma membrane fraction. In order to correlate the effects of PDEδ knockdown with the respective KRas status, all cell lines were subjected to proliferation studies after stable shRNA insertion in the presence and absence of doxycycline. Further, the growth behavior of genetically modified cells was compared to small molecule inhibition by either Deltarasin or Deltazinone 1.

3.8 The mPDAC model system

Apart from the subset of human cancer cell lines with different tumor origins and heterogenious protein expression patterns, murine pancreatic ductal adenocarcinoma cells were also subjected to small molecule inhibition of PDEδ. They were designed to express oncogenes under control of endogenous promoters, using Cre-Lox technology (Hingorani, 2003; Tuveson, 2005; Hingorani, 2005) These mouse models clearly demonstrated that conditional activation of oncogenic KRas via Pdx1 (pancreatic progenitor cell gene promoter) leads to neoplasm formation, similar to the human disease (PanINs) (Tuveson, 2005). As such, they are a defined, homogenous, and characterized system to study PDAC (pancreatic ductal adenocarcinoma), allowing for studies on basic regulatory mechanisms of the MAPK pathway in an oncogenic KRas environment.

In this project, mPDAC (murine pancreatic ductal adenocarcinoma) cells, with either a single oncogenic KRas G12D knock-in ($KRas^{G12D(-/+)}$, KC, single knock-in, single mutant) or with $KRas^{G12D(-/+)}$ and $p53^{R270H(-/+)}$ (KPC, double knock-in, double mutant), a contact mutant, which tends to accumulate, were used. Only mice with mutant gain-of-function p53 develop pancreatic cancer metastasis, in contrast to p53 knockout animals (Morton, 2010). The single mutant (mPDAC 79990, $KRas^{G12D(-/+)}$, KC) represents early stage PDAC, whereas the double mutant (mPDAC 79751, $KRas^{G12D(-/+)}$ and $p53^{R270H(-/+)}$, KPC) mimics late stage PDAC progression in humans (Olive, 2004; Hezel, 2006).

4 Objectives

How are human cancer cells from different tumor origins affected by the induced downmodulation of PDEδ? Is there a correlation between the availability of PDEδ and the KRas mutation status? Are there differences in KRas-dependent and -independent cell lines after PDEδ knockdown or inhibition? Is PDEδ a valid target to inhibit oncogenic KRas-dependent signaling and does it affect downstream signaling (MAPK-pathway)?

Is there a correlation between the p53 status and the resistance towards PDEδ inhibition? Is the knock-in of oncogenes and/or corrupt tumor suppressor genes sufficient to change the network behavior and to drive oncogene addiction/synthetic lethality?

5 Results

5.1 Generation and characterization of stably transformed human cancer cell lines

The panel of human cell lines (table 1) was lentivirally transduced to stably express doxycycline-inducible shRNA against PDEδ and selected with puromycin (see M&M). In order to determine the time-point of efficient PDEδ downmodulation, all cell lines were treated with doxycycline for up to 3 days. Efficient PDEδ downmodulation was observed after 72 h doxycycline induction in all cell lines, shown in figure 13 for Panc-TUI cells as a representative example. PDEδ was already described to be a stable protein (Chandra, 2012), which requires several days of RNAi-treatment to see changes in the protein level. In general, the knockdown level was proven to be time-dependent and further experiments were carried out after 72 h doxycycline treatment.

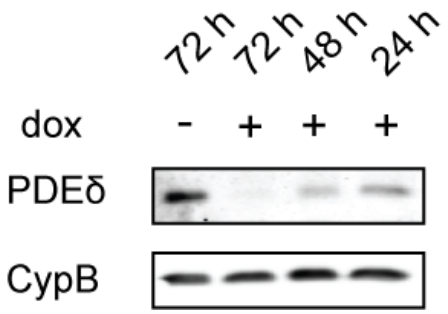

Figure 13: Western Blot analysis of PDEδ downmodulation by doxycycline induction for Panc-TUI cells. Blots were stained for PDEδ and Cyclophilin B (loading control). With different doxycycline incubation times as indicated, a time-dependent downmodulation of PDEδ was visible. An efficient downmodulation could be observed after 72 h doxycycline incubation. The induction was carried out with 0.2 µg/ml doxycycline.

To evaluate the level of PDEδ downmodulation in all previously mentioned human cancer cell lines, Western Blots were carried out with a constant amount of total protein, determined by Bradford assay, in lysates from cells before and after doxycycline induction (figure 14).

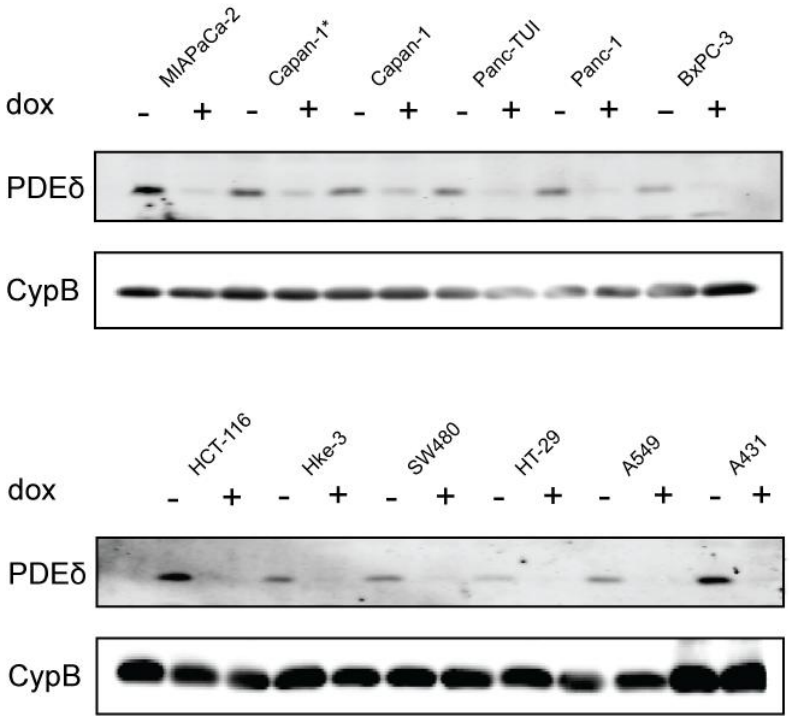

Figure 14: PDEδ and CyclophilinB (loading control) levels shown by Western Blot for each stably transduced cell line. The human PDAC cells are shown on top .Capan-1* cells were selected with higher puromycine concentrations (4 µg/ml). The CRC, lung, and cervix carcinoma cells are shown below. Doxycycline was incubated for 72 h prior to cell lysis and subsequent SDS PAGE. A total protein concentration of 50 µg was loaded for each protein sample.

All stably transfected cell lines responded to doxycycline as the endogenous PDEδ levels were mostly depleted when compared to the corresponding un-treated sample (figure 14). This proves that the shRNA was sucessfuly inserted and functioning after doxycycline incubation. This is corroborated by the fact, that control cell lines with stably expressed scrambled shRNA showed no effect on PDEδ after doxycycline addition, as demonstrated by Panc-TuI and HT-29 cells in figure 15.

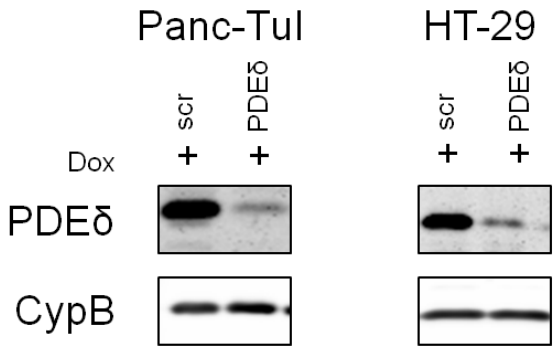

Figure 15: PDEδ and CyclophilinB (loading control) levels shown for scrambled shRNA and shRNA against PDEδ by Western Blot for Panc-TuI and HT-29 cells. Doxycycline was incubated for 72 h in both conditions. A clear decrease in the PDEδ level was only observed with the targeting shRNA but not with scrambled shRNA.

When comparing the basal amount of PDEδ in all cell lines, MIA PaCa-2, HCT-116, and A431 cells exhibited increased levels, whereas BxPC-3 and HT-29 cells showed lower band intensities (figure 14). MIA PaCa-2 and HCT-116 cells were reported to be oncogenic KRas-dependent and BxPC-3 and HT-29 are KRas wild-type cells. Solely, the Capan-1 cell line showed the highest level of remaining PDEδ protein after 72 h doxycycline treatment even with higher selection pressure (Capan-1*). Another interesting observation is, that HCT-116 and Hke-3 cells, which are isogenic exhibit different levels of endogenous PDEδ. HCT-116 cells are KRas dependent and have elevated PDEδ levels as compared to Hke-3 cells, pointing towards a connection between the KRas mutation status and the amount of PDEδ inside the cell.

To further quantify the endogenous amount of PDEδ in all cell lines, information can be inferred by using a calibration curve with known concentration of purified PDEδ. Again, the lowest endogenous amount of 2-25 ng was measured in BxPC-3 and HT-29 cells, which are KRas-independent. HCT-116 cells exhibited overall the highest level of endogenous protein (200 ng) and in the remaining cell lines the amount was between 50-100 ng. The isogenic cell line Hke-3 was also confirmed to have high levels of PDEδ but still less than HCT-116 cells (figure 16).

In general, the amount of endogenous PDEδ was lower in KRas-independent (wild-type) cells and this might correlate with the susceptibility towards downmodulation of PDEδ. As the wild-type cell lines BxPC-3 and HT-29 are not KRas-dependent, they might require lower basal PDEδ levels and tolerate the knockdown, as seen with HCT-116 and Hke-3. Further, yet unknown solubilization factors might compensate the role of PDEδ in these cell lines.

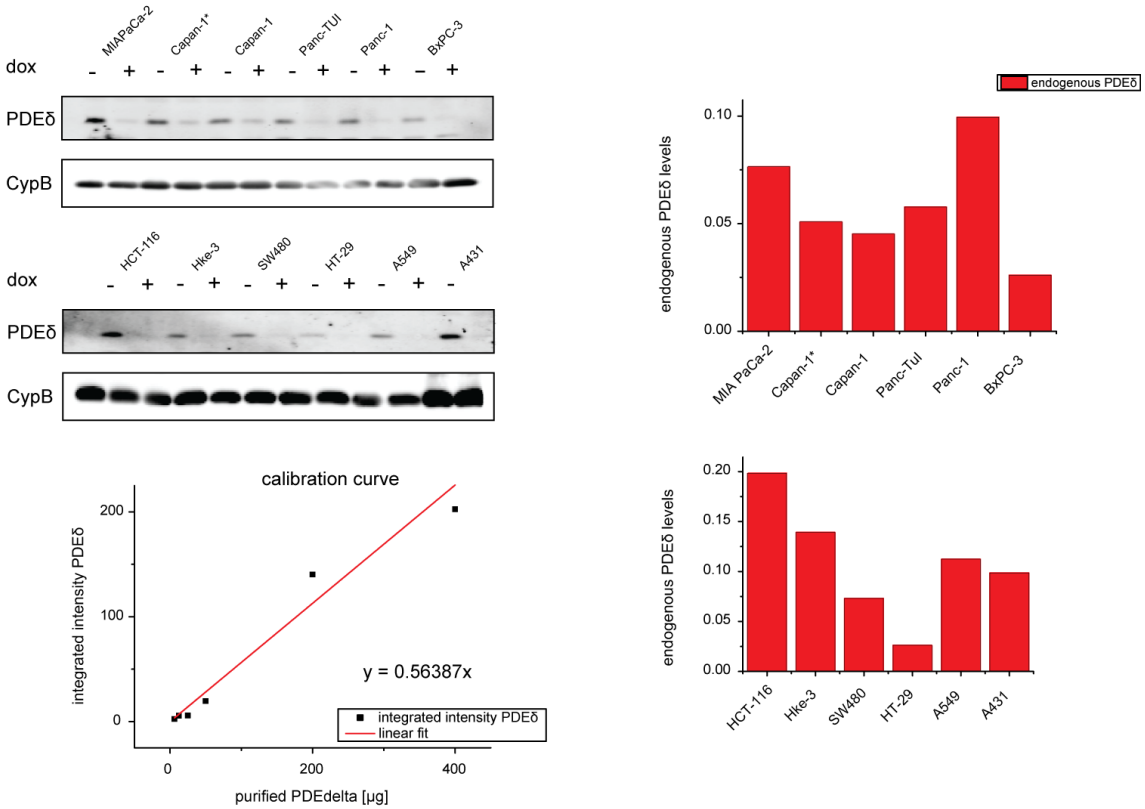

Figure 16: Calibrated PDEδ-levels of the human cancer cell lines shown in figure 14. A calibration curve was derived from a dilution series of purified PDEδ protein and used to determine the endogenous PDEδ concentration in all cell lines.

5.2 Inducible RNAi has an effect on cell proliferation in human cancer cell lines

As Deltarasin was published to have a dose-dependent growth inhibitory effect on oncogenic KRas dependent human PDACs (Zimmermann, 2013), all cell lines were subjected to real-time cell proliferation measurements, monitored by RTCA (real-time cell analyzer). For this, 10,000 cells were plated in each well of a 16-well E-plate and half of the samples were grown under doxycycline conditions to start PDEδ downmodulation. The red curves represent the change in the Cell Index (A.U.) with time in presence of doxycycline and the black curves represent the control measurements of the same cell line without doxycycline addition (figure 17).

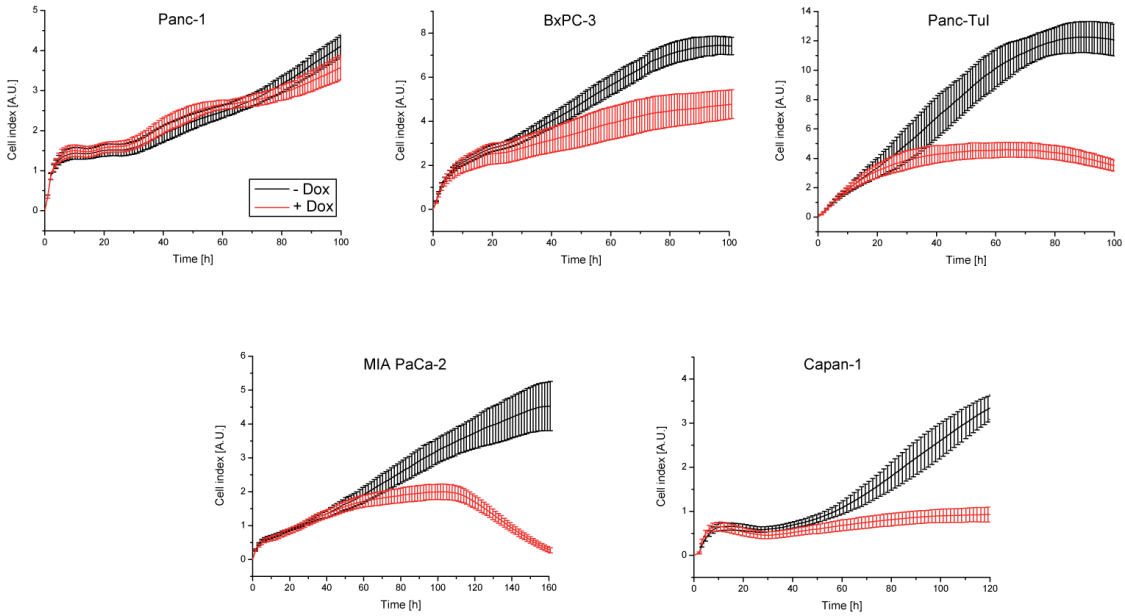

Figure 17: RTCA measurements of human pancreatic cancer cell lines. The oncogenic KRas-independent cell lines Panc-1, the KRas wild-type cell line BxPC-3 and the oncogenic KRas-dependent Panc-Tul cells are shown on top. The cell lines from Bochum (MIA PaCa-2 and Capan-1) are shown below. Dr. B. Papke performed the RTCA measurements for the Capan-1 cells. The effect of doxycycline-induced PDEδ knockdown is shown for each cell line, where the black curve represents cells under serum conditions and the red curve cells in the presence of 0.2 µg/ml doxycycline. Doxycycline was initially added.

The oncogenic KRas-dependent cell lines Panc-Tul and MIA PaCa-2 exhibited strong growth inhibitory effects after doxycycline-induced downmodulation of PDEδ, as shown by the red graph (figure 17). Interestingly, the KRas wild-type bearing BxPC-3 cells also changed the growth behavior after PDEδ knockdown. The oncogenic KRas-independent Panc-1 cells exhibited minor growth effects.

Second, the human colorectal cancer cell lines HCT-116, Hke-3, HT-29, and SW 480 were used to validate possible growth inhibitory responses by RTCA (figure 18). As aforementioned, the red curves represent the presence and the black curves the absence of doxycycline.

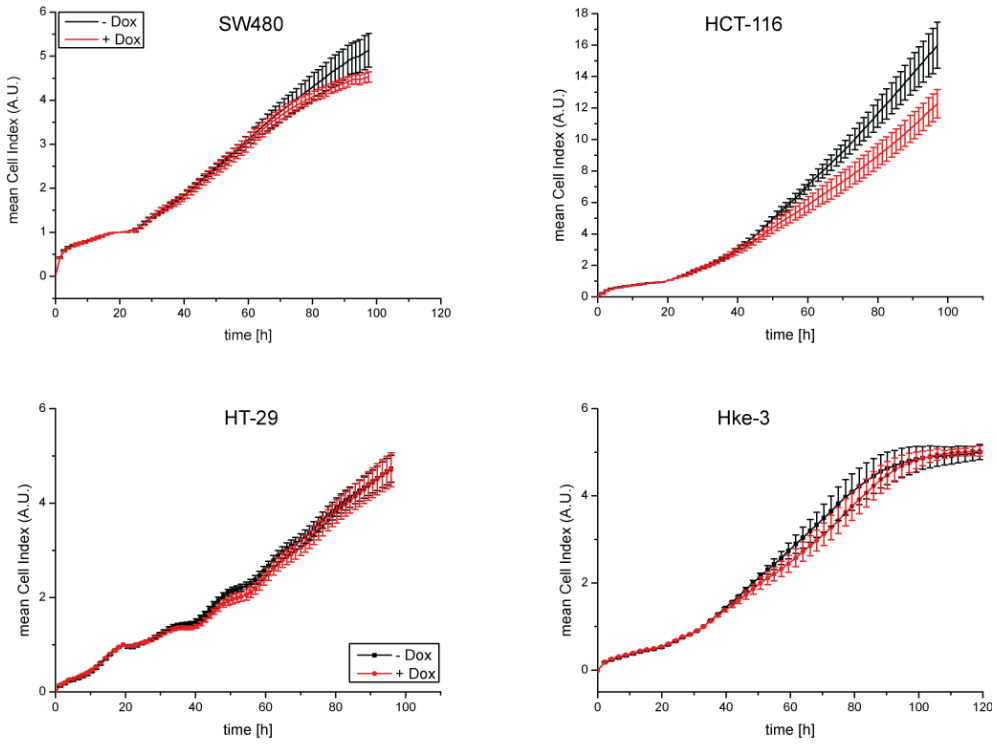

Figure 18: RTCA measurements in human colorectal carcinoma cells in the presence of doxycycline-inducible shRNA against PDEδ. The effect of doxycycline-induced PDEδ knockdown is shown for each cell line, where the black curve represents cells under serum conditions and the red curve cells in the presence of 0.2 µg/ml doxycycline. Doxycycline was added after 24 h.

In case of all human CRC cells, no major effect of PDEδ downregulation on proliferation could be observed. The black and red graphs overlapped, indicating no effect on the Cell Index. Solely, the HCT-116 cell line displayed a slight tendency towards PDEδ-mediated growth effects at later time points (figure 18). HCT-116 harbors oncogenic KRas. As discussed before, HCT-116 and Hke-3 cells are isogenic, where mutant KRas was deleted by homologous recombination in the latter. Accordingly, Hke-3 cells were defined as KRas wild-type cells (Singh, 2012) and unlikely to respond to PDEδ inhibition. The small difference in their proliferation could therefore point towards an effect of oncogenic KRas. The Western Blot data support the fact that any effect on growth obtained by RTCA is exclusively caused by varying amounts of PDEδ.

HT-29 cells were reported to have wild-type KRas in combination with an additional BRaf (V600E) mutation, which functions downstream of KRas and causes resistance to certain chemotherapeutics (Di Nicolantonio, 2008). Moreover, this cell line clearly showed low endogenous PDEδ levels, determined by Western Blot and its proliferation seems to be unaffected by PDEδ downmodulation.

Finally, the human lung cancer cell lines A549, H441, and H358 and the cervix carcinoma cell line A431 were selected for transduction with inducible shRNA against PDEδ. Unfortunately, H441 and H358 cells did not tolerate viral infection and underwent apoptosis during further maintenance within 2 weeks. In summary, 2 out of these 4 cell lines could be generated to stably express PDEδ shRNA. Only the oncogenic KRas-dependent H358 cell line could be used for a single RTCA measurement (figure 19) but not further due to a complete loss of cultured cells within days. Nonetheless, the effect on the cell growth after doxycycline application was clearly visible, as these cells are known to be dependent on the KRas oncogene.

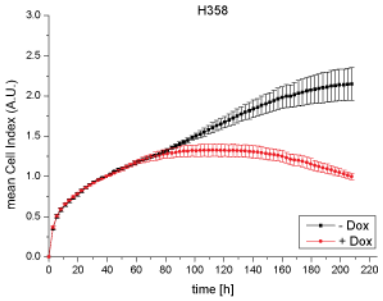

Figure 19: RTCA measurements of the human lung cancer cell line H358 in the presence of doxycycline-inducible shRNA against PDEδ. The black curve represents cells under serum conditions and the red curve cells in the presence of doxycycline. Doxycycline was added after 24 h.

To validate possible growth inhibitory responses in the cervical cancer cell line A431 and in A459 lung cancer cells after doxycycline addition, they were monitored by RTCA (figure 20).

From the data it could be concluded that these cell lines responded to PDEδ downmodulation, as visualized by growth effects at later time points (figure 20). Although A459 cells are classified to be KRas-independent, a clear difference after PDEδ depletion was observed. A431 cells are characterized by overexpressed EGFR. As Ras is a downstream integrator for EGFR signaling, proliferative signaling via Ras might be affected by PDEδ downmodulation in these cells.

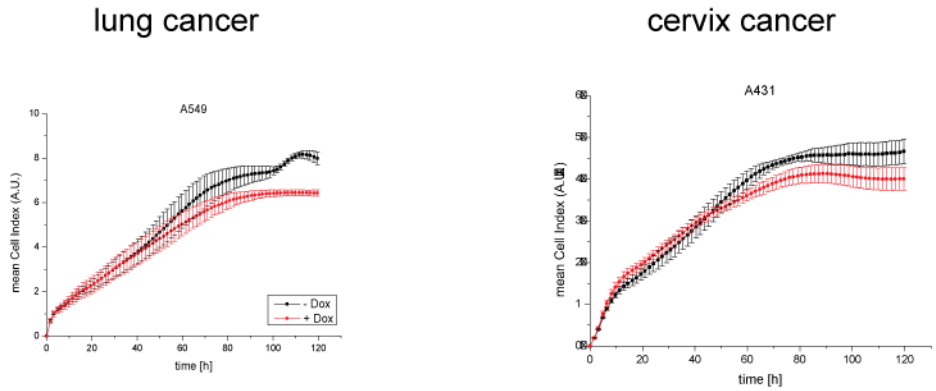

Figure 20: RTCA measurements in human lung (left) and cervix carcinoma cells (right) in the presence of doxycycline-inducible shRNA against PDEδ. The effect of doxycycline-induced PDEδ knockdown is shown for each cell line, where the black curve represents cells under serum conditions and the red curve cells in the presence of doxycycline. Doxycycline was added at the beginning of the experiment.

5.3 Comparison between small molecule inhibition and RNAi in human cancer cell lines

As mentioned before, the idea was to compare data from the genetic validation of PDEδ with small molecule PDEδ inhibition. The genetic approach ideally represents chemical PDEδ inhibition without side effects. To allow for a clear correlation between PDEδ depletion and genetic interference, the acquisition of cell growth in hPDACs (figure 21) was performed with doxycycline-inducible shRNA and compared to varying inhibitor concentrations of Deltarasin and Deltazinone 1 (inhibitor data generated by Holger Vogel).

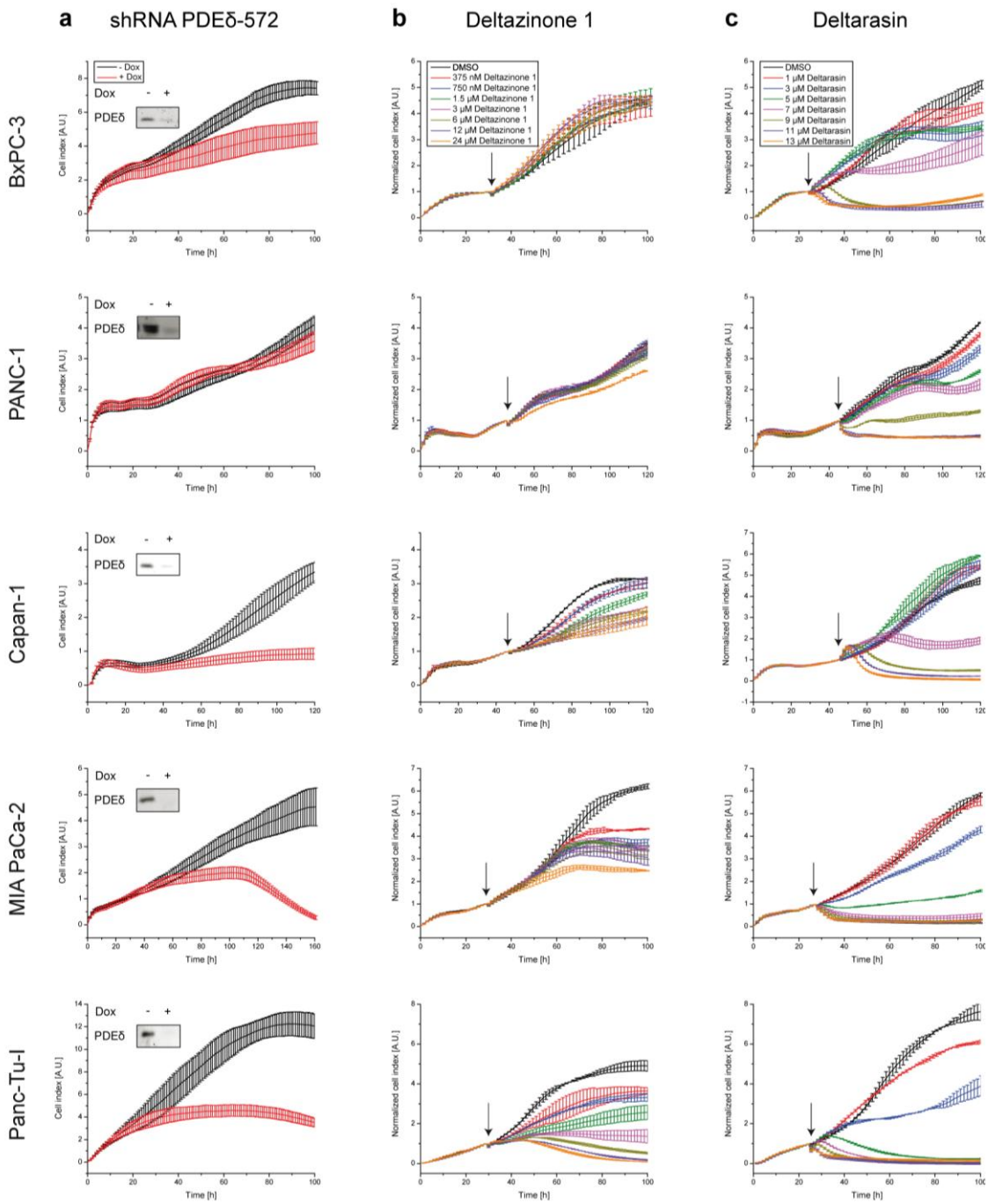

Figure 21: RTCA measurements of human pancreatic cancer cell lines. The effect of doxycycline-induced PDEδ knockdown is depicted on the left. The black curve represents cells under serum conditions and the red curve the addition of doxycycline. Doxycycline was initially added. The respective PDEδ protein levels in the presence or absence of doxycycline (72 h) are determined by Western blots. The dose-dependent effects on growth caused by Deltazinone 1 (middle panel) and Deltarasin (left panel) are shown (data acquired by Holger Vogel). Both PDEδ inhibitors were added at the indicated time points (arrow) in the respective concentrations. For b and c, the cell indices were normalized to the time of drug addition. Data for Capan-1 cells, including Weatern Blot and RTCA were generated by Dr. B. Papke. Figure adapted from Papke et al., 2015.

Again, the strongest effects on cell growth could be measured in KRas-dependent cell lines (Panc-TuI, MiaPaCa-2, Capan-1). The KRas-independent Panc-1 cells showed no significant reduction in growth, neither with shRNA nor

Deltazinone 1. Only the BxPC-3 cell line, which is classified to be KRas-independent, displayed a stronger reduction in growth with shRNA when compared to Deltazinone 1. With Deltarasin, a dose-dependent cell death was measured in all cell lines.

The comparison between shRNA-mediated PDEδ downmodulation and the two PDEδ inhibitors was also extended to CRC (figure 22) and lung cancer cells (figure 23)

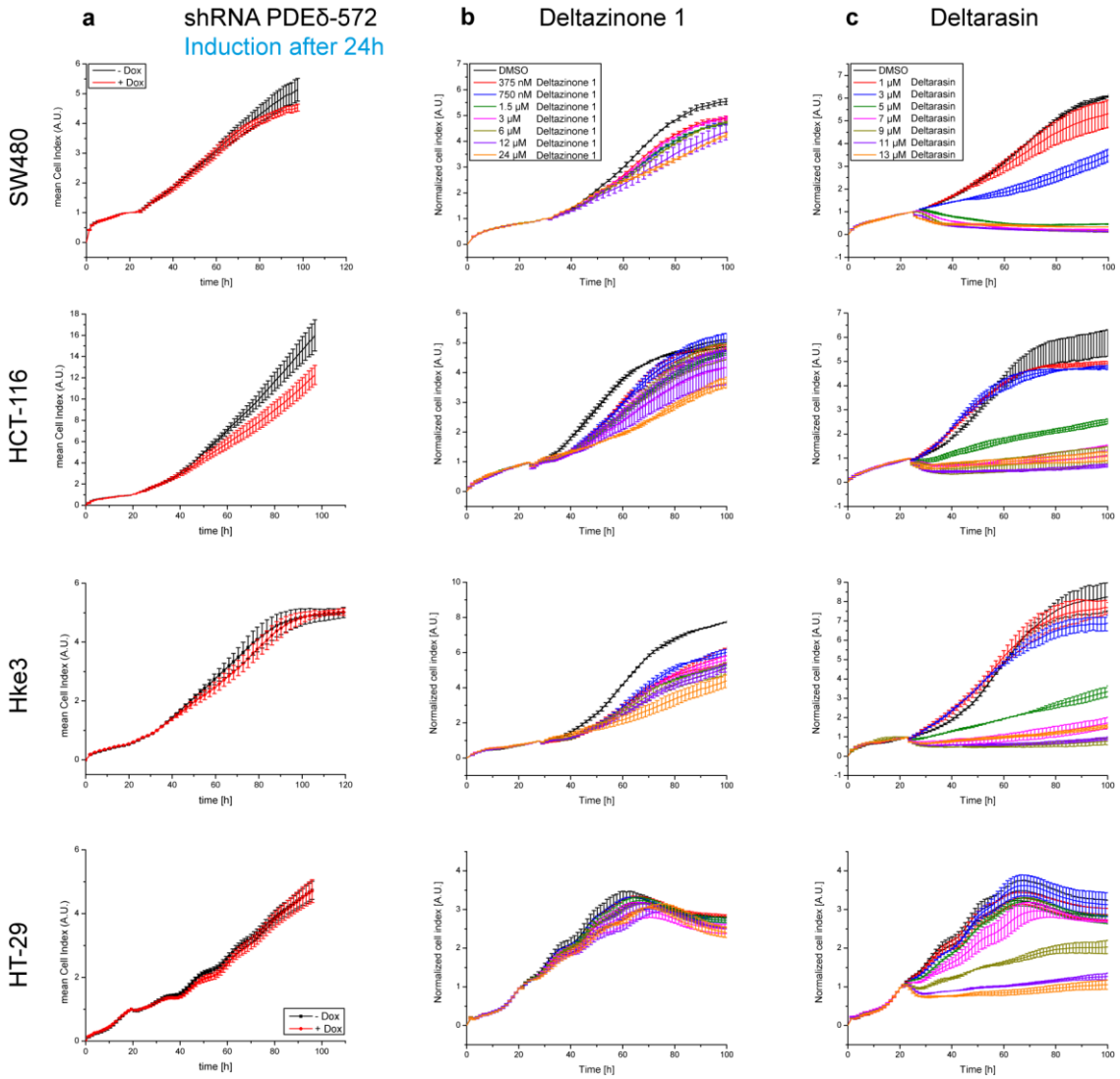

Figure 22: RTCA measurements of human colon rectal carcinoma cell lines. The effect of doxycycline-induced PDEδ knockdown is depicted on the left, where the black curve represents cells under serum conditions and the red curve cells in the presence of doxycycline. Doxycycline was added after 24 h. The dose-dependent effects on growth caused by Deltazinone 1 (middle panel) and Deltarasin (left panel) are shown (data acquired by Holger Vogel). Both PDEδ inhibitors were added at the indicated time points (arrow) in the respective concentrations. For b and c, the cell indices were normalized to the time of drug application.

As expected, the CRC cell lines showed little, in case of HCT-116 cells, or no response to PDEδ downmodulation (figure 22, left). HCT-116 cells are on the border to KRas-dependency, whereas all other CRC cell lines are published to be KRas-independent. The isogenic cell lines HCT-116 and Hke-3 showed a similar growth behavior when treated with Deltzinone 1 and Deltarasin, respectively. The oncogenic BRaf mutation in HT-29 cells seems to also cause resistance to chemical PDEδ inhibition. Here, no effect of Deltazinone 1 could be observed, even at higher concentrations. As observed for hPDACs, Deltarasin causes cell death at higher doses in all cell lines with time.

The lung cancer cell lines A549 and A358 were also compared to Deltazinone 1 and Deltarasin (figure 23).

Unfortunately, no further data than a single RTCA measurement could be performed with the oncogenic KRas-dependent lung cancer cell line H358. Nevertheless, a clear effect on growth could be measured, as it was expected and which is mirrored in the presence of Deltazinone 1. A549 cells only showed a slight reduction in proliferation with Deltazinone 1.

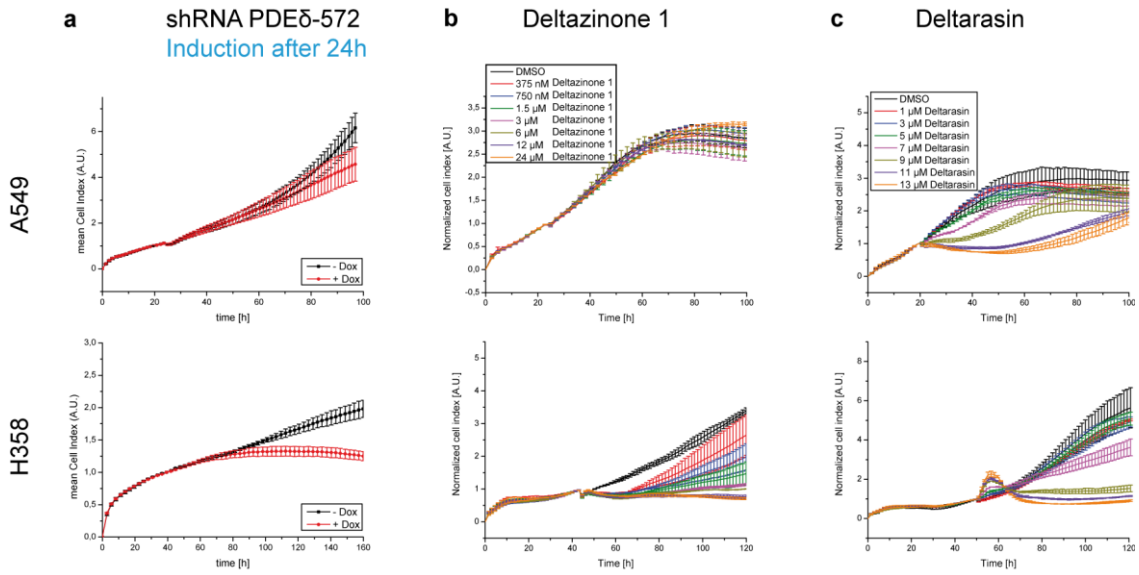

Figure 23: RTCA measurements of human lung cancer cell lines. The effect of doxycycline-induced PDEδ knockdown is depicted on the left, where the black curve represents cells under serum conditions and the red curve cells in the presence of doxycycline. Doxycycline was added after 24 h. The dose-dependent effects on growth caused by Deltazinone 1 (middle panel) and Deltarasin (left panel) are shown (data acquired by Holger Vogel). Both PDEδ inhibitors were added at the indicated time points (arrow) in the respective concentrations. For b and c, the cell indices were normalized to the time of drug application.

In summary, the impedance-based measurements in the presence of genetic PDEδ knockdown highly correlate with those generated in the presence of

Deltazinone 1 in all cell lines. Moreover, Deltazinone 1 exhibits higher specificity for PDEδ and a broader herapeutic window and less cytotoxicity when compared to Deltarasin. Nonetheless, the general tendency of growth inhibition in the presence of Deltarasin is also mirrored by the genetic knockdown.
From this it can be inferred that the genetic validation proves the importance of available PDEδ in oncogenic KRas-dependent cells.

5.4 Clonogenic assays to study long-term effects of PDEδ knockdown

Efficient PDEδ downmodulation by shRNA was achieved after 72 h doxycycline treatment in all cell lines, as demonstrated by Western Blots for Panc-TuI cells (figure 13). RTCA measurements showed clear growth inhibitory effects in oncogenic KRas-dependent hPDACs, slight effects in lung and cervix cancer, but not in CRCs. This is corroborated by data with the small molecule inhibitor Deltazinone 1. The slight effects on growth at longer time points gave reason for the following experimental approach.
Clonogenic assays with or without doxycycline were performed in triplicates to study long-term effects on growth in the stable transfected human cancer systems (figures 24, 25, 26). For this, sparsely seeded cells (2,000/ well for hPDACs and CRC and 1,000/well for A459 and A431) were maintained in a 6-well plate in the presence or absence of doxycycline for 7-10 days and then fixed and stained with crystal violet to visualize individual colonies. The quantification was performed on IR-scanned (Licor, Odyssey) images with equal sizes. ImageJ was used to track (particle tracking tool) and measure the particles of each well to plot their average size, the colony number, and the plate coverage. In general, clonogenic assays give information about cytostatic effects, where the colony size is reduced when compared to the control condition and about cytotoxic effects, which means that colonies vanish with time. In addition to clonogenic assays, long-term RTCA measurements were carried out for the respective cell lines for 7-10 days. Previous RTCA measurements were carried out for only 100-120 h (figures 24, 25, 26). First, all hPDACs were subjected for studying long-term effects after PDEδ downmodulation (figure 24). Second, long-term growth effects were studied in CRC cell lines (figure 25) and third in cervix and lung carcinoma cells (figure 26).

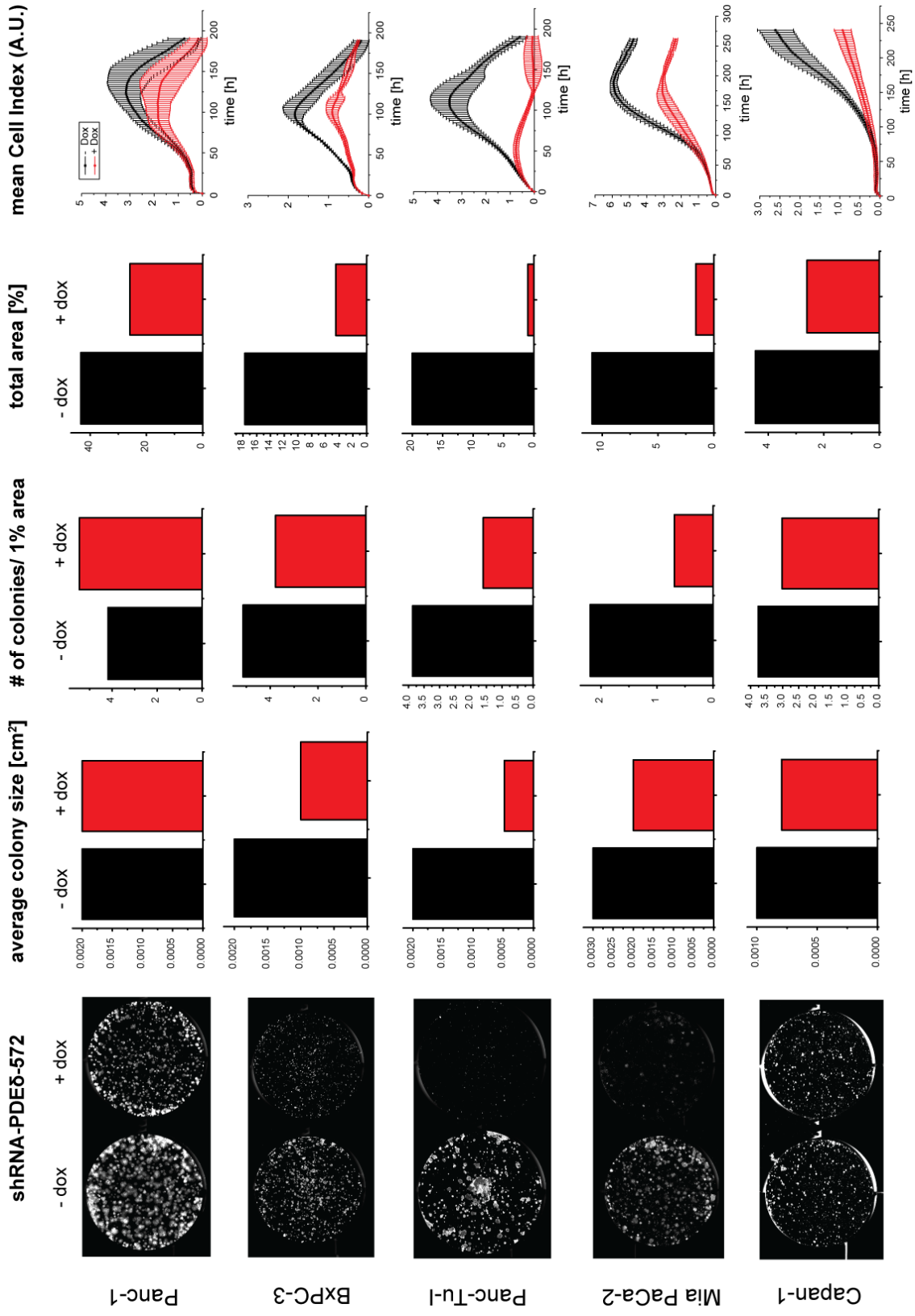

Figure 24: Clonogenic assays and the respective quantification of hPDACs after 7-10 days with and without doxycycline (left). All cell lines were seeded sparsely at 2,000 cells/well in a 6-well plate and incubated with or without doxycycline. The average colony size, the number of colonies and the total area in untreated samples is represented by the black bar and the doxycycline conditions are shown in red (middle). The respective long-term RTCA measurement (2,000 cells/well) is shown on the right, where the black curves represents the serum condition and the red curve the induced downmodulation after doxycycline addition. Doxycycline was initially added in all experiments.

The quantification of each clonogenic assay in all human PDACs clearly showed long-term effects of PDEδ knockdown by RNAi (figure 24). The oncogenic KRas-dependent Panc-TuI and MIA PaCa-2 cells displayed the strongest effects, because no or very few colonies remained when PDEδ was downmodulated, indicating that PDEδ is inevitable for their survival (cytotoxicity). The Capan-1 cells, published to be dependent on oncogenic KRas, showed only minor effects on the colony size and plate coverage. BxPC-3 cells, which also responded to PDEδ downmodulation in RTCA measurements, displayed a clear reduction in colony size but not in the total number of colonies. The Kras-independent Panc-1 cells showed a slight reduction in the colony size (figure 25, left). Sadly, the quantification regarding the increase in the number of colonies, but a decrease in the total area, is not meaningful. This means, that for certain cell lines, the particle tracking has to be improved to allow for a more representative quantification of the respective image.

In all long-term RTCA measurements, an RNAi-mediated growth inhibition could be demonstrated at later time points. Again, Panc-TUI cells displayed the strongest inhibition on cell growth by PDEδ downmodulation and Panc-1 cells the lowest. This RTCA data mimicked the growth effects observed by clonogenic assays in the presence of PDEδ shRNA. The long-term studies corroborated the results generated by short-term RTCA, which show that KRas-dependent cells are more susceptible to PDEδ knockdown. Nonetheless, long-term studies prove an effect of PDEδ RNAi on cell growth in all hPDACs at longer time points.

As aforementioned, clonogenic assays with or without doxycycline were performed to also study long-term effects on growth in the stable transfected human CRCs (figure 25).

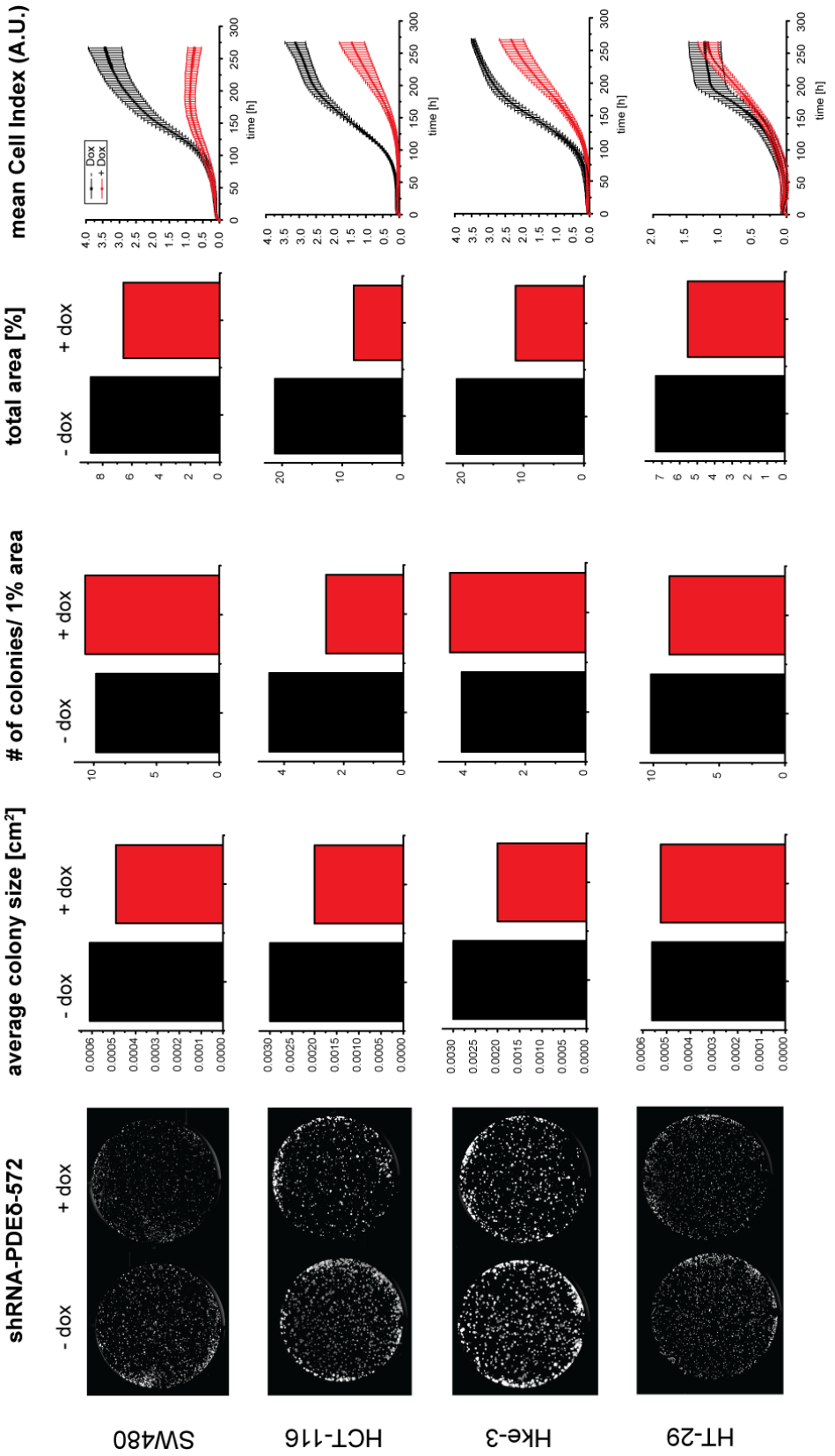

Figure 25: Clonogenic assays and the respective quantification of human CRC cell lines after 7-10 days with and without doxycycline (left). All cell lines were seeded sparsely at 2,000 cells/well in a 6-well plate and incubated with or without doxycycline. The average colony size, the number of colonies and the total area in untreated samples is represented by the black bar and the doxycycline conditions are shown in red (middle). The respective long-term RTCA measurement (2,000 cells/well) is shown on the right, where the black curves represents the serum condition and the red curve the induced downmodulation after doxycycline addition. Doxycycline was initially added in all experiments.

In 3 of 4 human colon rectal cancer cells, the clonogenic assays showed long-term effects on growth after PDEδ knockdown by doxycycline-inducible shRNA. The mutant KRas-harboring cell line HCT-116 exhibited the strongest reduction in colony size, colony number and plate coverage. As discussed for short-term RTCA data, Hke-3 and HCT-116 are isogenic cell lines that differ in their KRas mutation status, the effect of PDEδ downmodulation was expected to vary. HCT-116 cells indeed showed a stronger reduction in growth, as indicated by the respective percentage of plate coverage for both cell lines (figure 25). Their isogenic counterpart, Hke-3, showed a clear reduction of the colony size, but the amount of colonies seemed to be unaffected, which explains a reduction the overall plate coverage. SW 480 cells were similarly affected as Hke-3 cells in clonogenic assays, but showed a clear time-dependent cell death in long-term RTCA measurements. It could be argued that SW480 cells are more susceptible to nutrient supply, as no medium exchange was performed during RTCA measurements. For clonogenic assays, the medium was replaced every three days. Hence, in RTCA measurements the additional depletion of nutrients could have also influenced cell growth. The mutant BRaf cells HT-29 did not show any change in growth, neither when subjected to RTCA measurements nor in clonogenic assays, thereby lacking any long-term response. Again, the results from long-term studies corroborated the RTCA data and PDEδ downmodulation seemed to affect nearly all cell lines on a longer time scale.

The stable transfected human lung cancer cell line A549 and the cervix carcinoma cells A431 were also used for clonogenic assays. Cells (1,000 cells /well) were incubated for 7-10 days with or without doxycycline to study long-term effects on growth (figure 26).

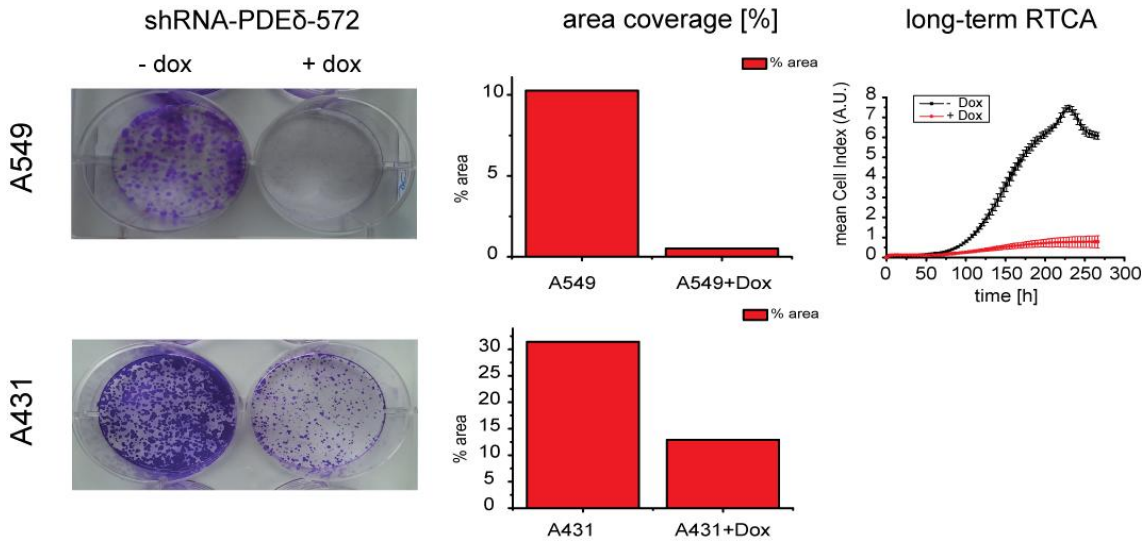

Figure 26: Clonogenic assays and the respective quantification of lung and cervix cells after 7-10 days with and without doxycycline (left). All cell lines were seeded sparsely (1,000 cells/well) in a 6-well plate and 24 h later doxycycline was applied. The average colony size (middle panel) in untreated samples is represented by the left bar and the doxycycline conditions are shown on the right. The area coverage for each sample is shown in the right panel. Again, the left bar indicates growth conditions in the absence and the right bar in the presence of doxycycline.

After doxycycline addition, A459 colonies vanished nearly completely, comparable to the data from oncogenic KRas-dependent hPDACs. The remaining colony spots were hard to resolve with the particle tracking algorithm. Again, further improvements are needed to allow for a meaningful representation and quantification of long-term data. Nonetheless, the RTCA long-term studies indicated strong effects on colony growth. For the cervix carcinoma cells A431, with overexpressed EGFR, a reduced colony size and probably a reduction of the total colony size could be visualized in clonogenic assay. This cell line could not be monitored by long-term RTCA as these cells are highly proliferative and quickly populate RTCA wells, which might also cause nutrition problems as discussed for SW 480 cells.

The long-term studies in all human cancer cell lines strongly support the observation that PDEδ RNAi has long-term effects on cells, predominantly and more severe in oncogenic KRas-dependent cancer cells.

5.5 Visualization of endogenous Ras by immunofluorescence

So far, it could be inferred from all previous experiments that RNAi-mediated knockdown of PDEδ resulted in cell death in KRas-dependent cells and caused varying degrees of long-term growth inhibitory effects in all tested cells, except for HT-29 cells. To further study the underlying mechanism, which causes cell death and if there is spatial interference with KRas by PDEδ inhibition or genetic depletion, endogenous Ras staining was performed. For this, Ras was visualized using a primary pan Ras antibody and an Alexa488-labeled secondary antibody in the absence or presence of doxycycline, in combination with Deltarasin or Deltazinone 1. The induction of PDEδ shRNA decreases the endogenous amounts of PDEδ. By additional application of PDEδ inhibitors, the remaining endogenous PDEδ should be inhibited thereby causing a complete relocalization of Ras to endomembranes. As discussed before, PDEδ inhibitors disrupt KRas and PDEδ binding and thereby the out-of-equilibrium distribution of KRas, which should allow to visualize this process.

Prior to immunostaining, cells were treated for 30 h with doxycycline, as longer incubation time might have already killed the cells as observed by RTCA. The respective inhibitor was added 2 h before fixation.

Here, MIA PaCa-2 cells exhibited a strong accumulation of fluorescence in the perinuclear area in the presence of doxycycline and Deltarasin but only with higher amounts of Deltazinone 1 (20 µM). The combination of doxycycline-induced downmodulation and Deltarasin seemed to enhance perinuclear Ras enrichment (figure 27). MIA PaCa-2 cells are dependent on oncogenic KRas and their growth was shown to be affected by genetic downmodulation and small molecule inhibition, respectively. Hence, it is likely that the observed elevated fluorescence on endomembranes in this experiment represents the perturbed spatial organization of Ras.

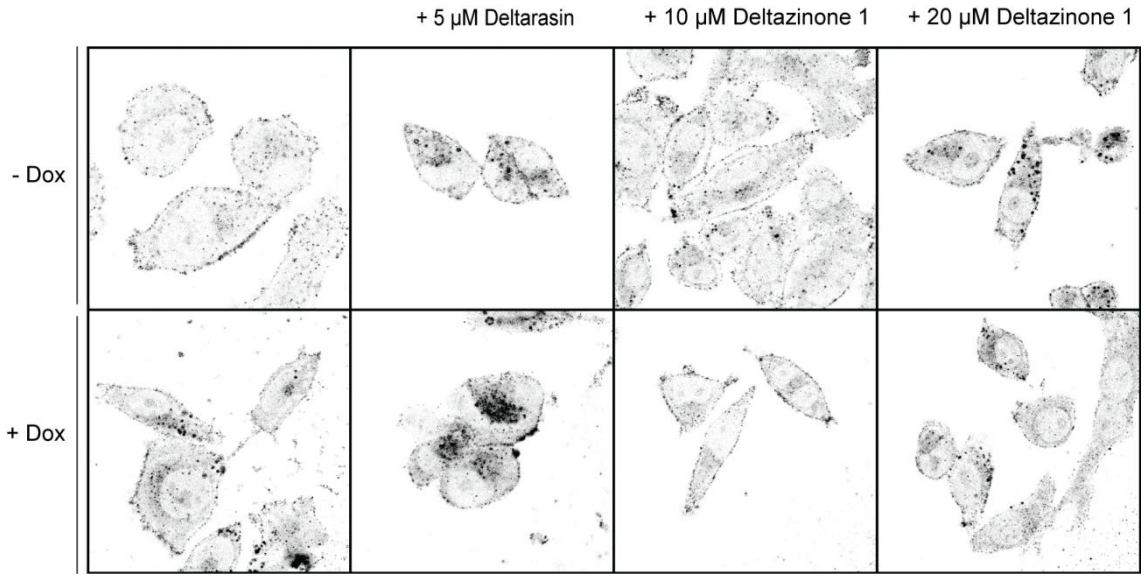

Figure 27: Immunofluorescence images with a primary anti pan Ras and an Alexa488-labeled secondary antibody in MIAPaCa-2 cells. Doxycycline was added 30 h before fixation (lower panels). Both inhibitors were applied to the respective sample 2 h prior to fixation.

In contrast to MIA PaCa-2 cells, the KRas-independent Panc-1 cells were positively stained for pan Ras mainly at the cell periphery. This could be observed in all conditions, indicating plasma membrane bound Ras. The presence of doxycycline showed slightly enhanced perinuclear staining compared to control samples (figure 28). The addition of Deltazinone 1 seemed to enhance the fluorescence intensity at the plasma membrane (figure 28).

The comparison between the two cell lines supported the idea that oncogenic KRas-dependent cells seem to be susceptible to interference with the spatial organization of Ras. This is corroborated by immunofluorescence images from CRC cells, which showed no perinuclear enrichment of fluorescence after PDEδ inhibition (data not shown).

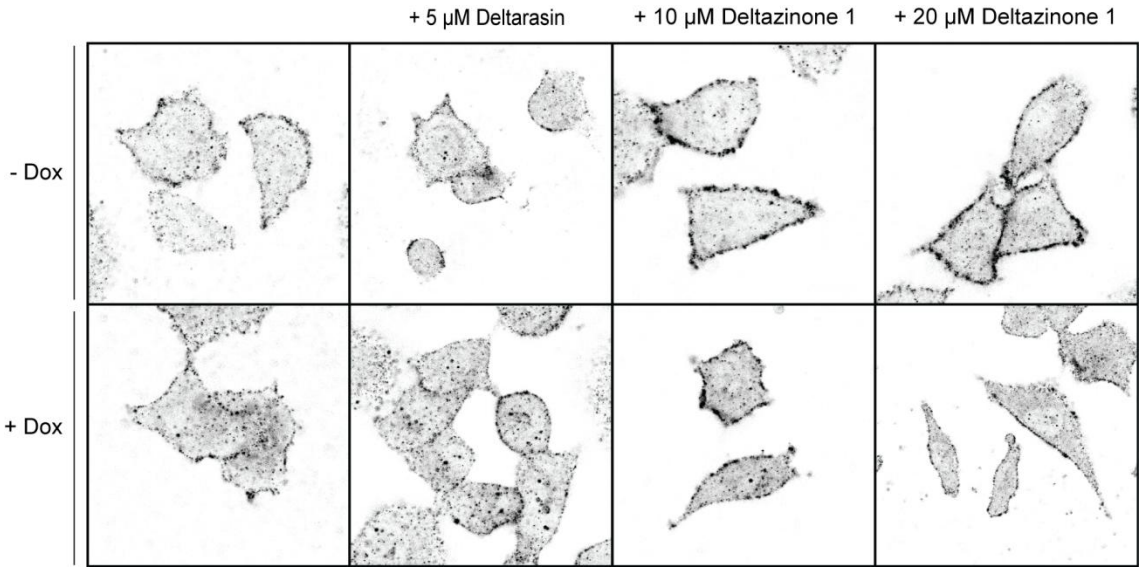

Figure 28: Immunofluorescence images with a primary anti pan Ras and an Alexa488-labeled secondary antibody in Panc-1 cells. Doxycycline was added 30 h before fixation (lower panels). Both inhibitors were applied to the respective sample 2 h prior to fixation.

5.6 PhosTag-FLIM to determine Erk2 activity in Panc-TuI

In summary, PDEδ inhibition and RNAi-mediated downmodulation exhibited clear effects on growth in mutant KRas-dependent cells and endogenous Ras delocalization to endomembranes was determined by immunofluorescence. As already mentioned in the beginning, the presence of oncogenic KRas likely enhances MAPK signaling. To study possible effects on signaling by PDEδ inhibition, the following experiment, based on PhosTag-FLIM, was designed to quantify Erk2 phosphorylation under different environmental conditions (DMSO control, PDEδ inhibitors, and shRNA). For this, mCitrine-Erk2 was transfected in Panc-TUI cells, either with 36-48 h doxycycline or 2 h inhibitor incubation prior to fixation and subsequent PhosTag-Cy3.5 staining.

Minimum 4 cells for each set were measured with FLIM and analyzed by global data analysis (Grecco, 2010). The average change in the donor lifetime per cell and the corresponding mean α value were represented in box plots (figure 31).

In the presence of FRET, Erk2 is phosphorylated and thereby activated and interacts with PhosTag, a phosphor-sensitive probe. The donor fluorophore mCitrine was linked to Erk2 and the acceptor fluorophore Cy3.5 was bound to PhosTag.

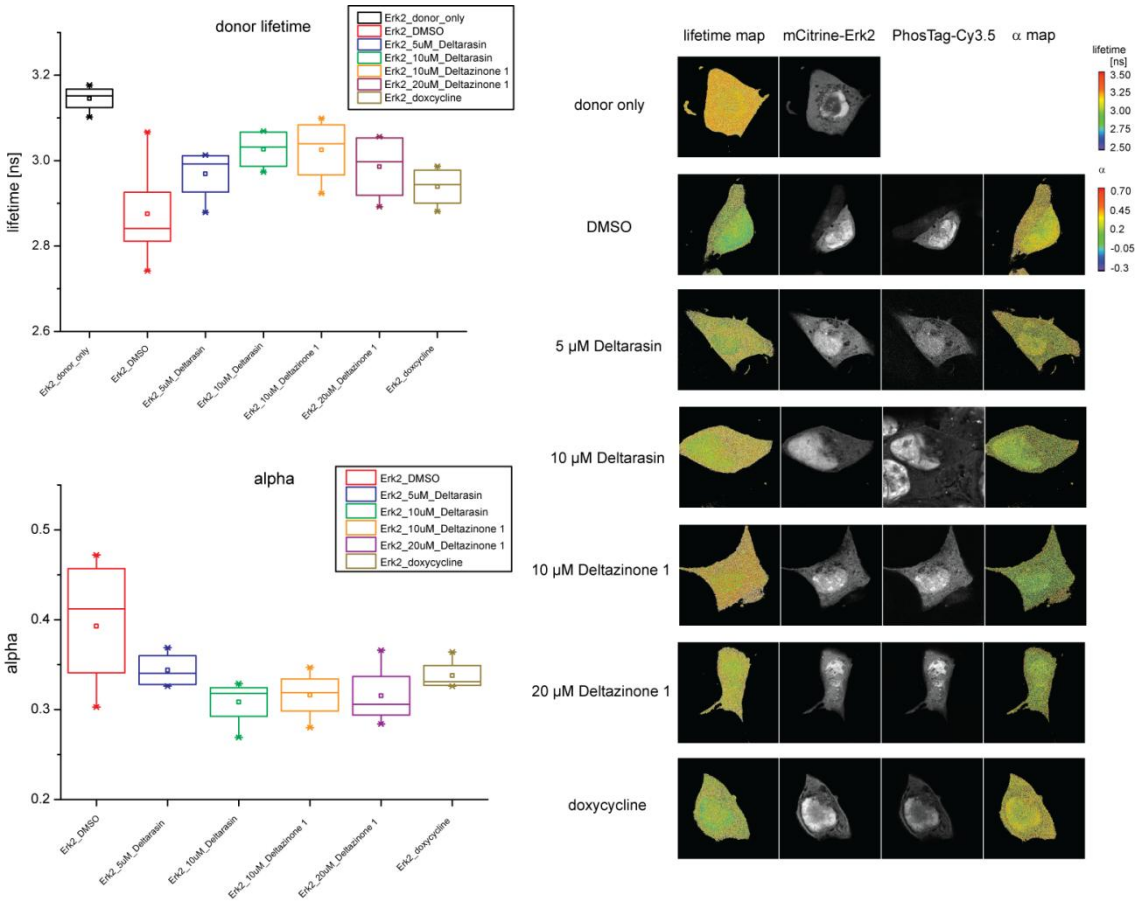

Figure 29: PhosTag-FLIM in Panc-TUI cells in the presence and absence of Deltarasin, Deltazinone 1, doxycycline, or DMSO. The fluorescence image shows mCitrine-Erk2, the lifetime is shown in the middle row and the α map in the bottom row (right). The corresponding average lifetime and the bound fraction α per cell are represented in box Plots (left).

The resulting quantification of the donor fluorescence intensity showed that the lowest lifetime and inversely correlated highest α values were measured under control conditions in the presence of DMSO. Beside this, the highest variance for both parameters was found in the control condition. Upon Deltarasin treatment, the lifetime increases with increasing Deltarasin doses. For Deltazinone 1, a similar loss of pErk2 was confirmed by elevated lifetime values. RNAi-mediated downmodulation of PDEδ resulted in a moderate change in the donor lifetime and α, when compared to both inhibitors.

In accordance with previous observations by Zimmermann et al. already demonstrating decreased phosphoErk levels in Western Blots (Zimmermann, 2012) this data showed the same effect on a molecular basis. It can be concluded that PDEδ inhibition, either by genetic or chemical approaches, has an effect on KRas and thereby on downstream molecules as demonstrated by the decreased activation of Erk2.

5.7 Characterization of the mPDAC system

The panel of genetically modified human cancer cell lines clearly showed a strong correlation between the KRas status and the availability of free PDEδ inside cells. All human cell lines were were chosen due to their known KRas status but derived from various tumor origins. Hence, they represent heterogeneous populations and might have acquired additional mutations with time.

To further allow a direct correlation between the KRas status and the response to PDEδ inhibition, two cell lines, derived from genetically engineered mouse models, demonstrated to mimic different stages of human PDAC (Hingorani, 2003; Olive, 2009; Hezel, 2006) were examined in the following experiments. The model system has the advantage of a known mutation status as both cell lines express oncogenic KRas. The additional p53 mutation is characteristic for late stage pancreatic cancer.

First, these cell lines were screened for the intracellular amount of active Ras. Both cell lines, $KRas^{G12D(-/+)}$(KC, mPDAC 79990) and $KRas^{G12D(-/+)}p53^{R270H(-/+)}$ (KPC, mPDAC 79751) are expected to have high levels of GTP-bound KRas because of the oncogenic KRas mutation on one allele. Regarding the initiation of the MAPK pathway, active Ras recruits cytosolic Raf to the plasma membrane, which binds via its RBD (Ras-binding domain of Raf) exclusively to Ras-GTP. The binding of RBD to active Ras and its recruitment from the cytosol to the plasma membrane are indicators for active GTP-bound Ras.

In order to demonstrate the presence of active Ras, pulldown experiments with purified 3x Raf-RBD were performed. For this, cell lysates of the respective cell line, grown under serum conditions, were incubated with GST-tagged 3x Raf-RBD, pulled down with GSH-beads and loaded on acrylamide gels. The mock control was prepared from cell lysates, incubated with GSH-beads but no 3x Raf-RBD-GST was present. After Western Blotting, the membranes were stained for anti-pan Ras, due to the lack of specific KRas antibodies. A positive pan Ras staining indicated the presence of comparable levels of GTP-bound Ras in both cell lines (figure 32). The mock control showed only faint and unspecific bands indicating that the pan Ras staining in the presence of 3x Raf-RBD was specific. From this it can be concluded that both cell lines express active Ras in equal amounts.

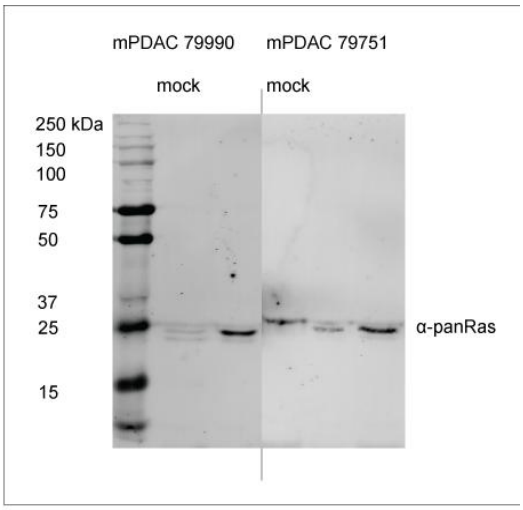

Figure 30: GST-pulldown experiment with 3x Raf-RBD-GST in both cell lines as depicted above, (mPDAC 7999 left and mPDAC 79751 right). Anti-pan Ras staining indicates the presence of activate Ras in both cell lines, the mock control is derived from lysates without 3x Raf-RBD-GST incubation and subsequent GSH-pulldown. In the double mutant cell line, two pulldown samples with different concentrations are shown next to the mock control.

5.8 Raf-RBD-GST immunostaining

In the presence of GTP-bound Ras, the PDEδ/Arl2 delivery system was shown to be crucial for the out-of-equilibrium maintenance of KRas at the plasma membrane.

As shown for the panel of human cancer cells and reported in previous studies, a delocalization of KRas from the plasma membrane to endomembranes can be observed after PDEδ-specific RNAi treatment (figure 33). In figure 33, the delocalization of active Ras was visualized by fluorochrome-labeled 3x Raf-RBD in one of the murine PDAC cell lines (Chandra, 2012).

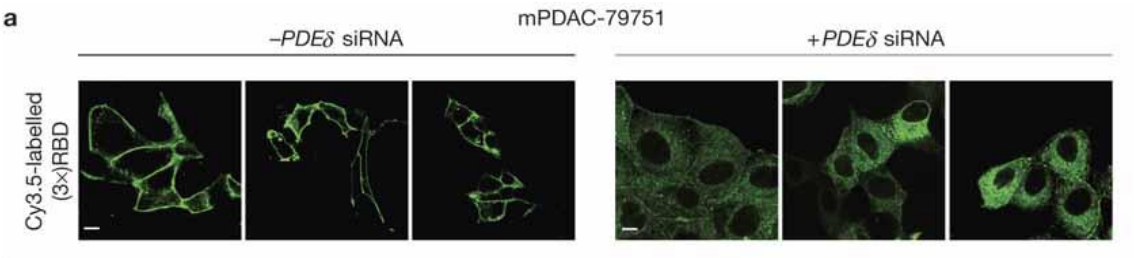

Figure 31: Ras staining with 3x Raf-RBD in the double mutant cell line. Active Ras randomly distributes to endomembranes after PDEδ downmodulation by siRNA. (Figure adapted from Chandra, 2012)

This experiment could not be reproduced with the aforementioned labeled 3x Raf-RBD. That is why an indirect immunostaining approach was designed, which will be discussed further.

To visualize active Ras, cells were treated with either DMSO or Deltarasin (5 µM) for 6 h, fixed, permeabilized and incubated with unstained 3xRaf-RBD-GST. An Alexa 488 conjugated anti-GST antibody was used in the second step to detect GST and thereby indirectly active Ras using fluorescence microscopy (figure 34).

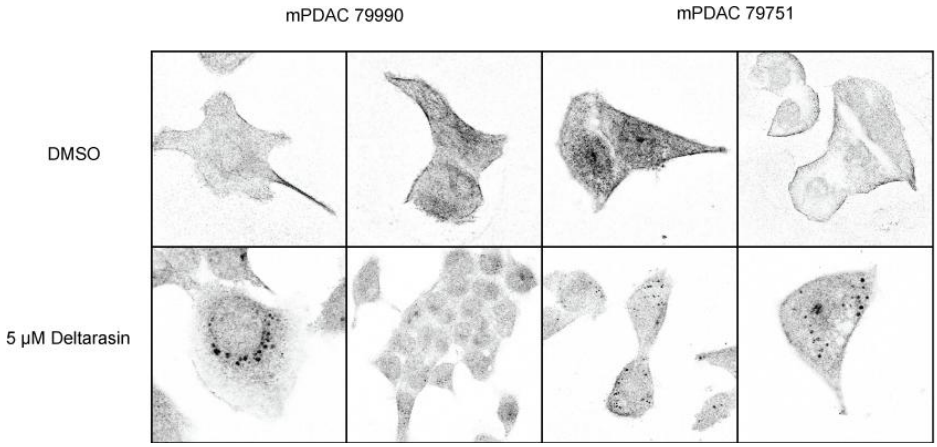

Figure 32: Immunofluorescence with 3xRaf-RBD-GST, followed by anti-GST Alexa488 staining in both cell lines with each two samples (single mutant left and double mutant right). The staining indicates the presence of activated Ras at the plasma membrane (upper panel). Ras delocalizes from the plasma membrane to endomembranes (lower panel) after 6h Deltarasin treatment (5 µM).

The GST-staining in DMSO-treated cells was predominantly visible at the plasma membrane in both models. DMSO treatment was used as the control condition to exclude possible phenotypic effects caused by DMSO itself, as PDEδ inhibitors were all dissolved in DMSO prior to use. As shown in figure 34, DMSO seemed to have no effect on the Ras localization at the plasma membrane. After Deltarasin addition, active Ras diluted to endomembranes and the peripheral staining dissolved. Dot-like structures appeared in the perinuclear area and in close proximity to the plasma membrane. The double knock-in cell line was found to have vesicles distributed throughout the cell, whereas the majority of single mutant cells showed perinuclear accumulation. The mismatch in localized fluorescence between DMSO and Deltarasin treated cells evinces that Deltarasin binds to PDEδ, interrupts the Ras cycles and causes a randomized Ras distribution to all membranes with time.

5.9 Effects on KRas localization after PDEδ inhibition

To further characterize the system and visualize specifically the inhibitor-induced delocalization of ectopically expressed KRas from the plasma membrane to endomembranes, live-cell imaging was carried out. Fluorescently labeled KRas (mCitrine-KRas) was transfected into both cell lines and changes in the localization of KRas before and after the addition of Deltarasin or Deltazinone 1 were followed over time (figure 35 and 36):

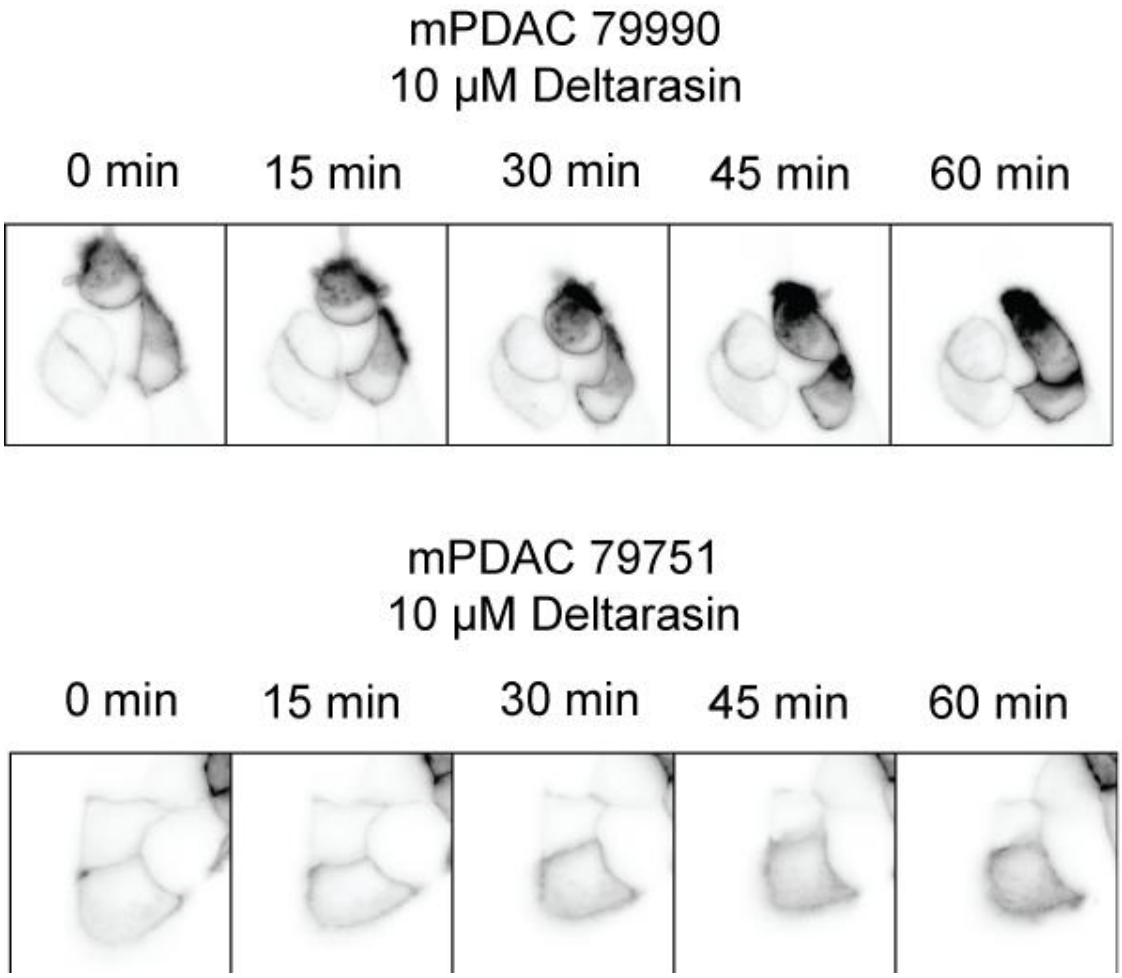

Figure 33: Murine PDAC cells were transfected with mCitrine-KRas and acquired before (0 min), and 15, 30, 45, and 60 min after 10 µM Deltarasin addition. The single mutant cell line is depicted on top and the double mutant cell line on the bottom.

Deltarasin caused cell shrinkage and within 60 min a clear depletion of KRas fluorescence from the plasma membrane could be observed in both cell lines. With proceeding time, Deltarasin-treated cells became more round-shaped and the fluorescence signal seemed to dominantly arise from endomembranes (figure 35). With low doses of Deltazinone 1, no such clear effects could be moni-

tored (data not shown) and even with higher concentrations (50 µM) only cell shrinkage could be observed in both cell lines (figure 36).

This indicates that Deltazinone 1 is less effective in targeting the PDEδ/Arl2 system as there was no visible dilution of KRas to the endomembranes. Although both inhibitors possess the same PDEδ binding mode, they are based on different chemical scaffolds. Hence, it is likely that theiy obey differences in their efficiency or induce unwanted side effects, which could be shown for Deltarasin in human cancer cell lines.

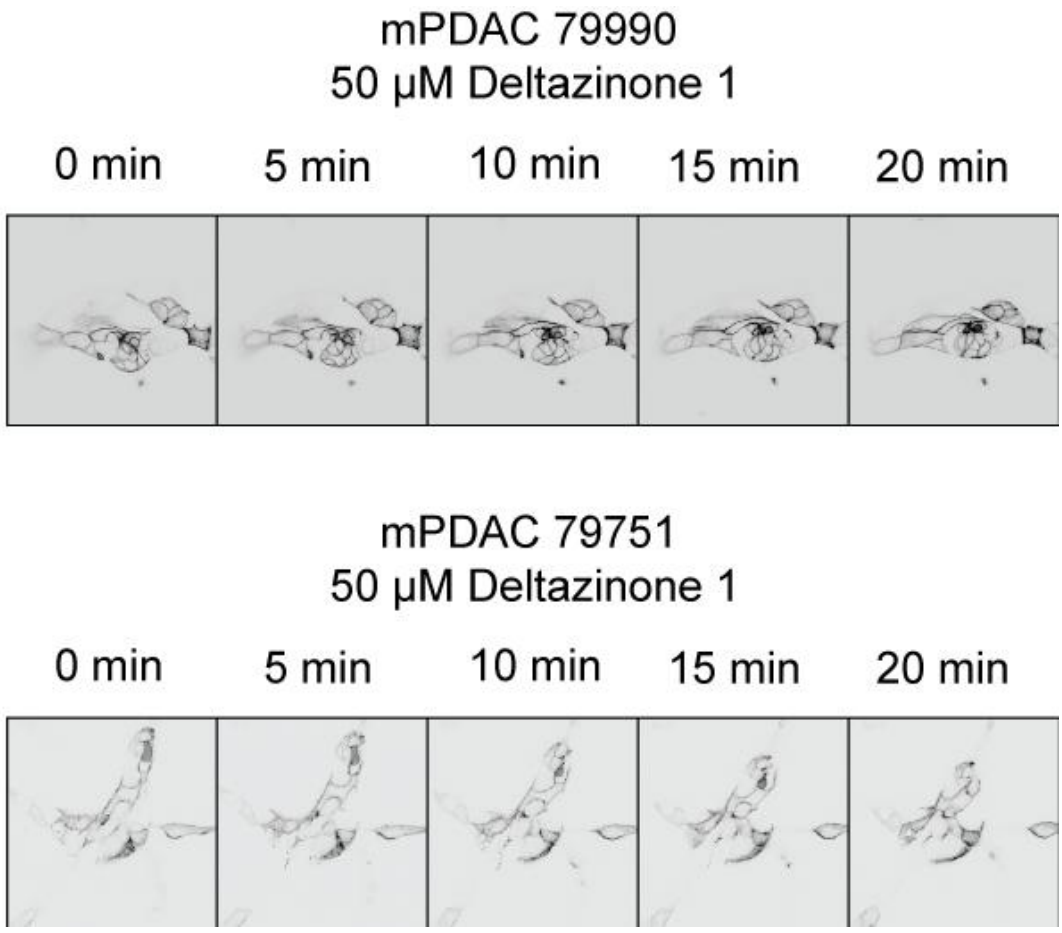

Figure 34: Murine PDAC cells were transfected with mCitrine-KRas and the fluorescence intensity was acquired before (0 min), 5, 10, 15, and 20 min after 50 µM Deltazinone 1 incubation. The single mutant cell line is depicted on top and the double mutant cell line below.

5.10 PDEδ inhibition affects cell growth in mPDACs

As Deltarasin was published to have a dose-dependent growth inhibitory effect on oncogenic KRas dependent human PDACs (Zimmermann, 2013), the murine system was also subjected to impedance-based real-time cell proliferation measurements, monitored by RTCA (real-time cell analyzer). The measurements were carried out for 4-5 days with 5,000 cells/well in 16-well E-Plates where each condition was duplicated. The mean value and the standard deviation were calculated. The real-time acquisition of cell growth was performed with varying inhibitor concentrations of Deltarasin and Deltazinone 1, respectively (figure 37).

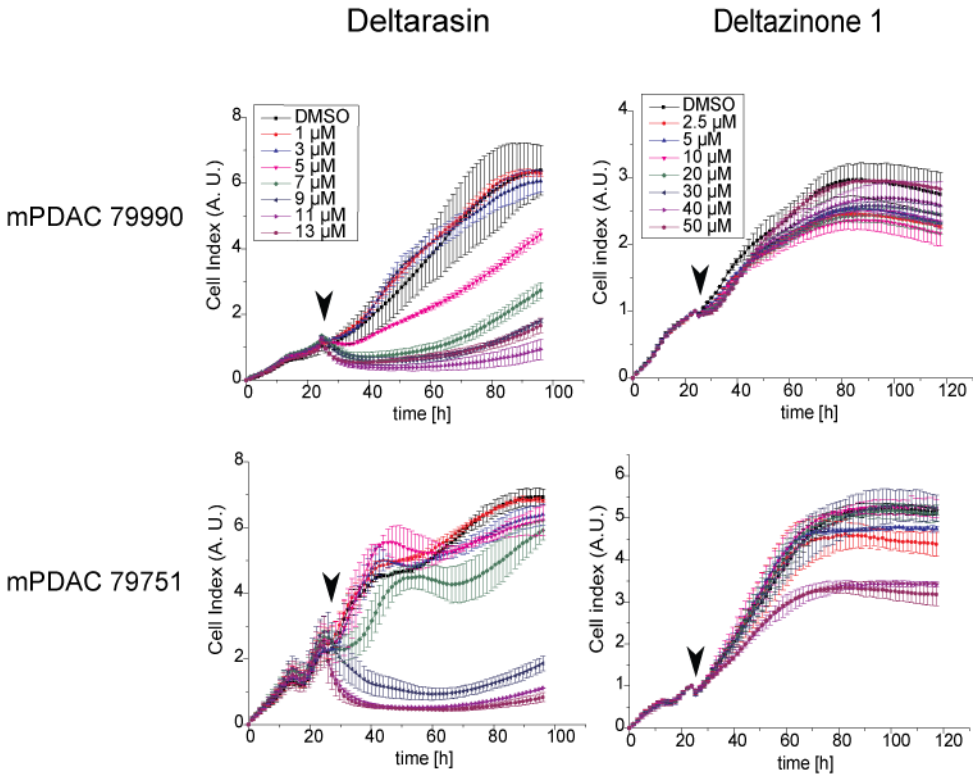

Figure 35: Growth response after Deltarasin and Deltazinone 1 administration. The left column shows the cell growth after different doses of Deltarasin and the right column after Deltazinone 1 application. The single mutant cell line (79990) is shown in the upper row and the double mutant cell line (79751) in the lower row. The mean value of two parallel measurements under each condition is plotted. The error bars represent the standard deviation. Deltarasin causes a dose-dependent response in both cell lines. At 5-7 µM growth is inhibited in the single mutant cell line, whereas the double mutant cell line tolerates up to 9 µM. Deltazinone 1 seems to have only minor effects on the double mutant cell line at high doses and no effects are visible in the single mutant cells. The black arrow indicates the time point of inhibitor addition.

In case of Deltarasin, growth inhibitory effects were visible between 5-7 µM in the single knock-in cell line, whereas the double mutant reacts at 9 µM and seemed to be more resistant to Deltarasin. The new inhibitor was previously

tested in human PDACs and shown to require higher inhibitor concentrations as Deltarasin (Papke, 2015). Hence, Deltazinone 1 doses up to 50 µM were applied to mPDACs. Within 4 days, no reduced proliferation could be observed by RTCA in the KRas(G12D) cell line, but the double mutant cell line exhibited effects on growth, starting at 40 µM. The growth behavior after Deltarasin administration was more affected than with Deltazinone 1 and in case of mPDAC 79751, a switch-like response for Deltarasin between 7 and 9 µM was visible. Concentrations above 9 µM resulted in immediate cytotoxicity. Although Deltazinone 1 was shown to have the same binding mode as Deltarasin and less cytotoxic effects (Papke, 2015), only minor growth effects for one cell line could be monitored in this timeframe (figure 37, right column).

The measurable effects on growth by Deltarasin vanish if the cells were initially seeded at higher densities (figure 38). Here, the KC cells tolerated Deltarasin concentrations >7 µM. The KPC cells showed a change in their growth behavior, starting at 7 µM but less prominent than with lower cell densities.

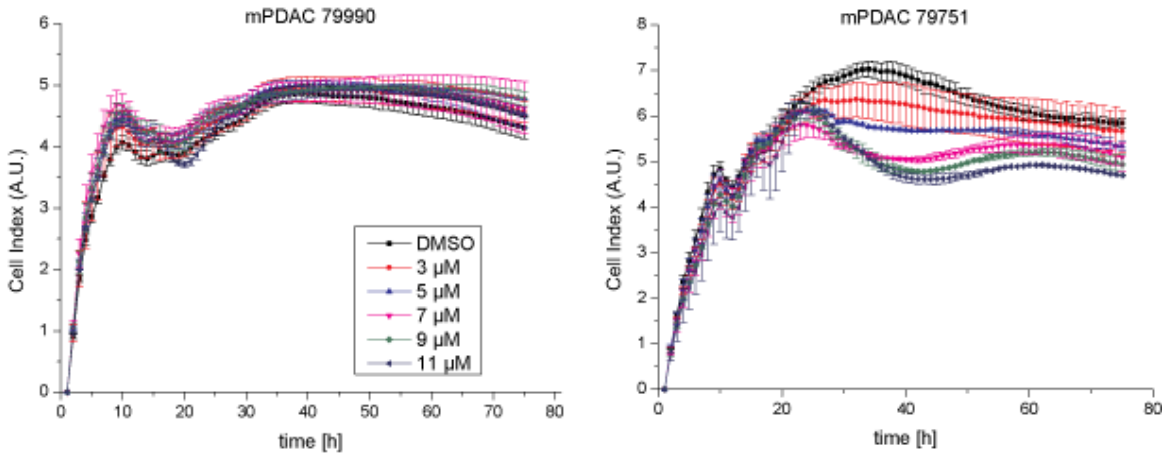

Figure 36: RTCA measurements for both mPDAC cell lines, seeded at higher densities, in the presence of varying Deltarasin concentrations, as indicated. These doses showed an effect on growth in less confluent samples, which was not noticeable here.

5.11 Clonogenic assays to study long-term effects in mPDACs

To further study long-term effects of both inhibitors on growth in the murine cell systems, clonogenic assays with varying inhibitor concentrations were performed (figure 39). As shown for the human cancer cell lines, clonogenic assays allow discriminating between cytostatic - the colony number remains but the size decreases - and cytotoxic effects - reduction of the colony number.

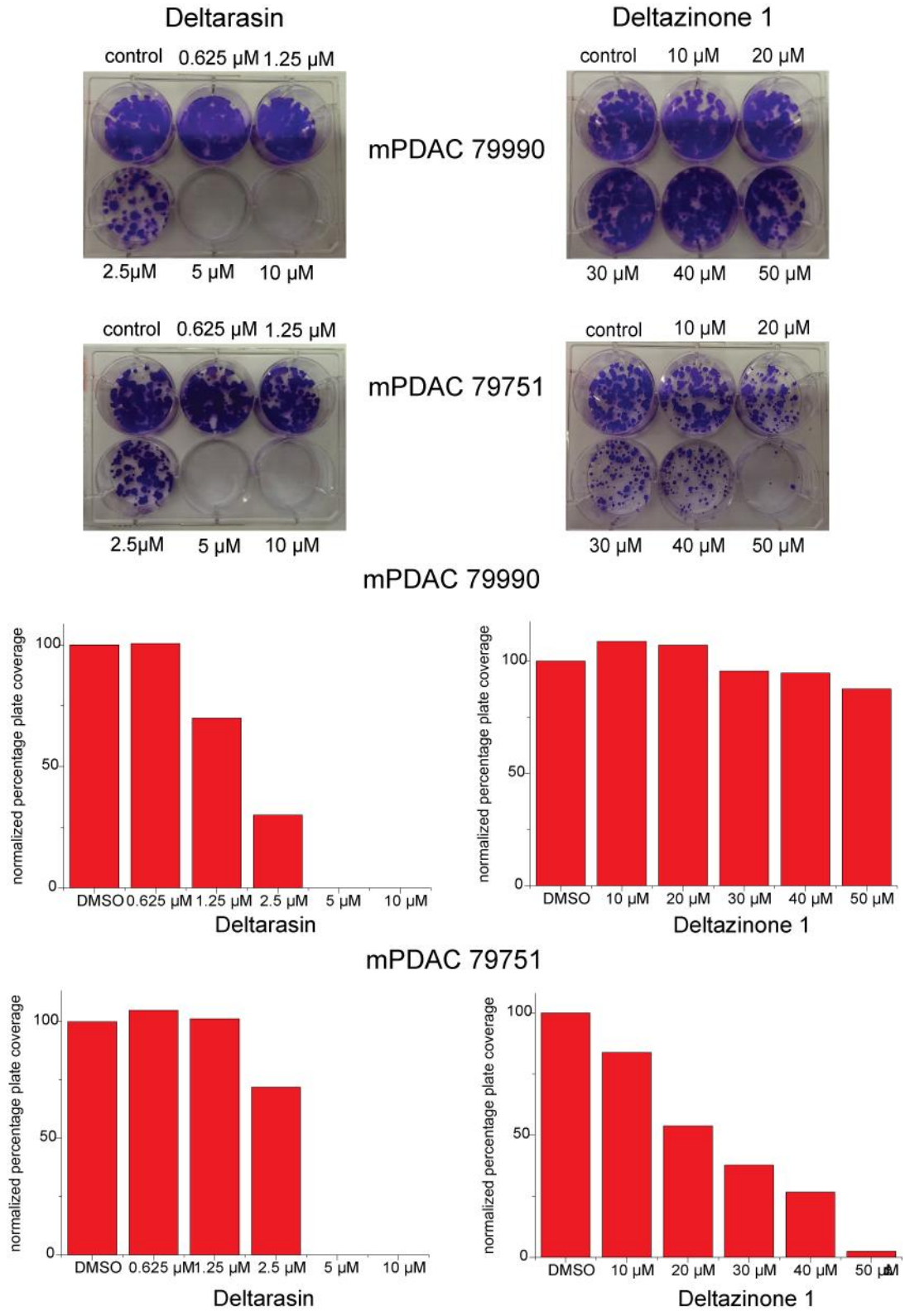

Figure 37: Clonogenic assays with varying concentrations of Deltarasin and Deltazinone 1 for both cell lines (top). The KC cell line is depicted in the upper row and the KPC cell line in lower row. The quantification for the corresponding inhibitor and cell line is shown below. Deltarasin causes cell death at 2.5 µM in long-term studies in both cell lines, whereas Deltazinone 1 seems to have a dose-dependent effect only in the double mutant cell line. The DMSO concentration is equal to the highest dose of inhibitor used in the experiment. All clonogenic assays were performed in triplicates.

Deltarasin treatment for 7 days caused cell death in both cell lines between 2.5-5 µM, as visualized by the lack of crystal violet staining. Deltarasin concentrations >5 µM were likely to cause unspecific cytotoxic effects due to the abrupt change in cell growth (figure 39, top, left).

The quantification was performed on IR-scanned (Licor, Odyssey) images with equal sizes and ImageJ was used to measure the particles of each well. As mPDAC cells are highly proliferative, even when sparsely seeded, the well bottom is overgrown by undistinguishable colonies within 7 days. Hence, the quantification information was reduced to measure the plate occupancy because single colonies could not be correctly defined. As discussed for the human cancer cell lines, an improved particle tracking algorithm would probably give more information about the colony number and the colony size.

Nonetheless, the resulting diagram clearly showed a dose-dependent behavior for the KC cell line and the KPC cell line seemed to tolerate increasing Deltarasin concentrations up to 2.5 µM (figure 39). In case of Deltazinone 1 the growth inhibitory effects are only visible in mPDACs 79751 at high concentrations and for long incubation times, corroborating the RTCA data. Moreover, a dose-dependent colony decrease could be observed for the double knock-in cell line, whereas the mPDAC 79990 cell line was unaffected even at concentrations >40 µM. The single knock-in cell line was slightly affected by DMSO, as indicated in the quantification, because the DMSO concentration was equal to the highest inhibitor dose applied in this assay, which could explain the elevated percentage of plate coverage at 10 and 20 µM (figure 39, top). The KPC cells, harboring the additional p53 mutation seemed to become resistant to Deltarasin treatment (figure 39), but clearly showed a long-term effect in presence of Deltazinone 1. Interestingly, concentrations of 10 µM Deltazinone 1 and below seemed to have no effect on the plate occupancy (figure 40).

That implies that the new scaffold Deltazinone 1 exhibited less cytotoxicity on both cell lines but long-term effects on the KPC cells at higher concentrations.

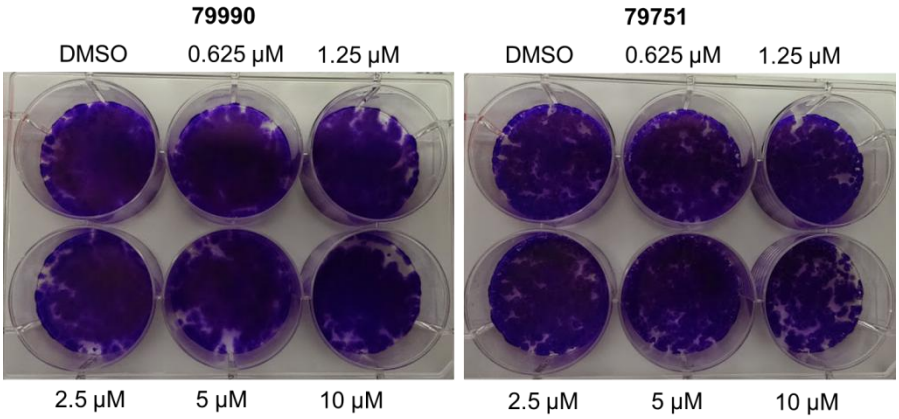

Figure 38: Clonogenic assays with varying concentrations Deltazinone 1 for both cell lines as depicted above. The DMSO concentration is equal to the highest dose of inhibitor used in the experiment. Cells are grown for 7 days in the presence of the inhibitor.

In order to allow for a more quantitative statement about the impact of higher cell densities on the growth-inhibitory effect of Deltarasin, both cell lines were seeded at higher densities and grown for 7 days in the presence of the respective inhibitor or DMSO (control). From the colony staining it can be inferred, that both cell lines die at concentrations >2.5 µM (figure 41). The single mutant cell line exhibits a similar staining in all four wells. For the KPC cells, a slight reduction in the plate coverage at 1.25 µM can be seen by eye. None of the populated wells could be used for further quantification as there were no distinguishable colonies.

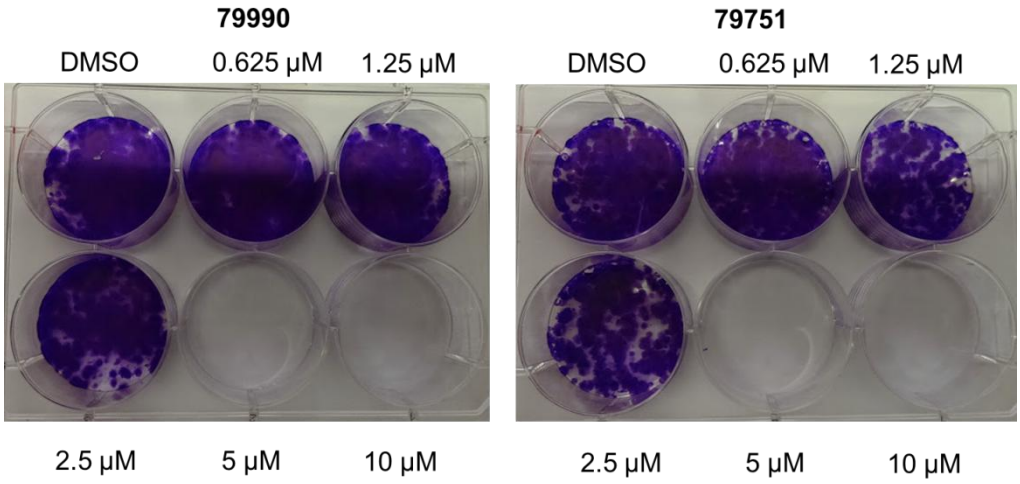

Figure 39: Clonogenic assays with varying concentrations of Deltarasin for both cell lines, seeded at higher densities. Deltarasin causes cell death at 2.5 µM. No dose-dependent growth inhibition could be observed. The DMSO concentration is equal to the highest dose of inhibitor used in the experiment. Cells are grown for 7 days in the presence of the inhibitor.

5.12 PDEδ inhibitors break the interaction between RheB and PDEδ

It was already shown that Deltarasin and Deltazinone 1 are able to break the interaction between the Ras-family member RheB and PDEδ (Zimmermann, 2013; Papke, 2015). RheB is a farnesylated but non-palmitoylated protein, which also binds to PDEδ. In contrast to KRas it lacks any polybasic motif or other feature to localize to a specific trapping membrane compartment hence it is enriched on perinuclear membranes.

To address the question whether the PDEδ inhibitors are also able to break the molecular interaction in the murine model system, mCitrine-labeled RheB and mCherry-fused PDEδ were transfected in both cell lines and FRET (Förster Resonance Energy Transfer) was determined by FLIM (Fluorescence Lifetime Imaging Microscopy) in the absence and presence of the respective inhibitor in live cells. The genetically encoded fluorophores, mCitrine and mCherry are a suitable FRET pair, in which mCitrine functions as the donor fluorophore and mCherry as the acceptor. In the absence of any drug, both fusion proteins are soluble in the cytoplasm, accompanied with a high RheB fluorescence signal in the nucleus. Data analysis reveals initially the binding of RheB to PDEδ indicated by a higher interacting fraction (α) and a lower lifetime as compared to donor-only or inhibitor-treated samples.

Upon drug treatment, RheB delocalized to endomembrane structures and its fluorescence intensity in the nucleus dropped, indicating less soluble material. The lifetime increased and α decreased, confirming the loss of interaction between the two fluorescently labeled proteins (figure 42). PDEδ is a soluble molecule and remained soluble throughout the experiment, whereas the RheB fluorescence appeared to be predominantly delocalized to perinuclear membrane structures after inhibitor addition. This experiment confirmed that both inhibitors are functional in murine cells and they efficiently break the interaction between RheB and PDEδ.

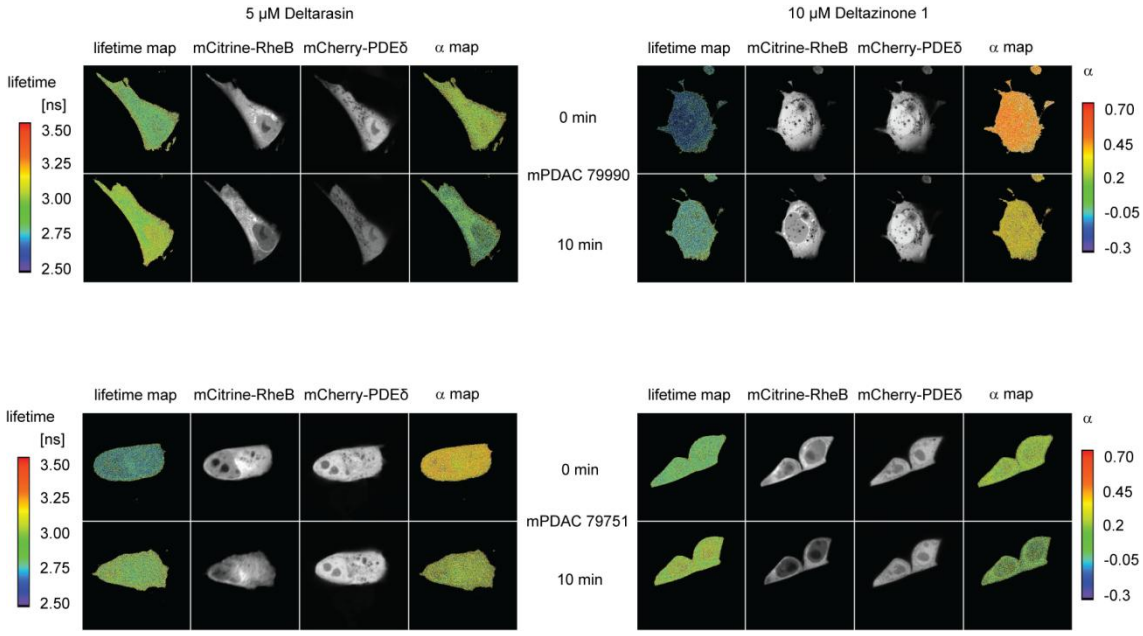

Figure 40: Deltarasin and Deltazinone 1 break the interaction between RheB and PDEδ in mPDAC cells. FLIM images show that RheB and PDEδ interact in the cytosol, as indicated by a lower donor lifetime and the increase in the bound fraction (α). After inhibitor treatment, the donor lifetime increased and the inversely correlated bound fraction decreased. The single knock-in cell line is shown on the top and the double knock-in cell line on the bottom. Each, 5 µM Deltarasin (left) and 10 µM Deltazinone 1 (right) were used.

5.13 Effects on MAP kinase signaling after PDEδ inhibition

The previous experiments demonstrated that both inhibitors exhibit different effects on cell growth in both murine cell lines. Deltarasin gains cytotoxic properties at concentrations above 5 µM or even lower for longer incubation times, whereas Deltazinone 1 did not. Nonetheless, both compounds break the interaction between PDEδ and RheB. That is why it is likely that a perturbation of the KRas cycle would have additional effects on downstream signaling.

As afore mentioned, Ras-induced signaling is transmitted via the MAPK pathway, resulting in proliferation. Oncogenic KRas is constitutively active, and should therefore enhance the MAPK signaling output. As an activity read-out for oncogenic KRas signaling, phosphorylation of Erk - the terminal node of the MAPK pathway - was studied by Western Blot. Different concentrations of each inhibitor were applied to both cell lines and incubated for 6 h and stained for pErk (figure 43 and 44). For data quantification, pErk levels were normalized to Cyclophilin B levels.

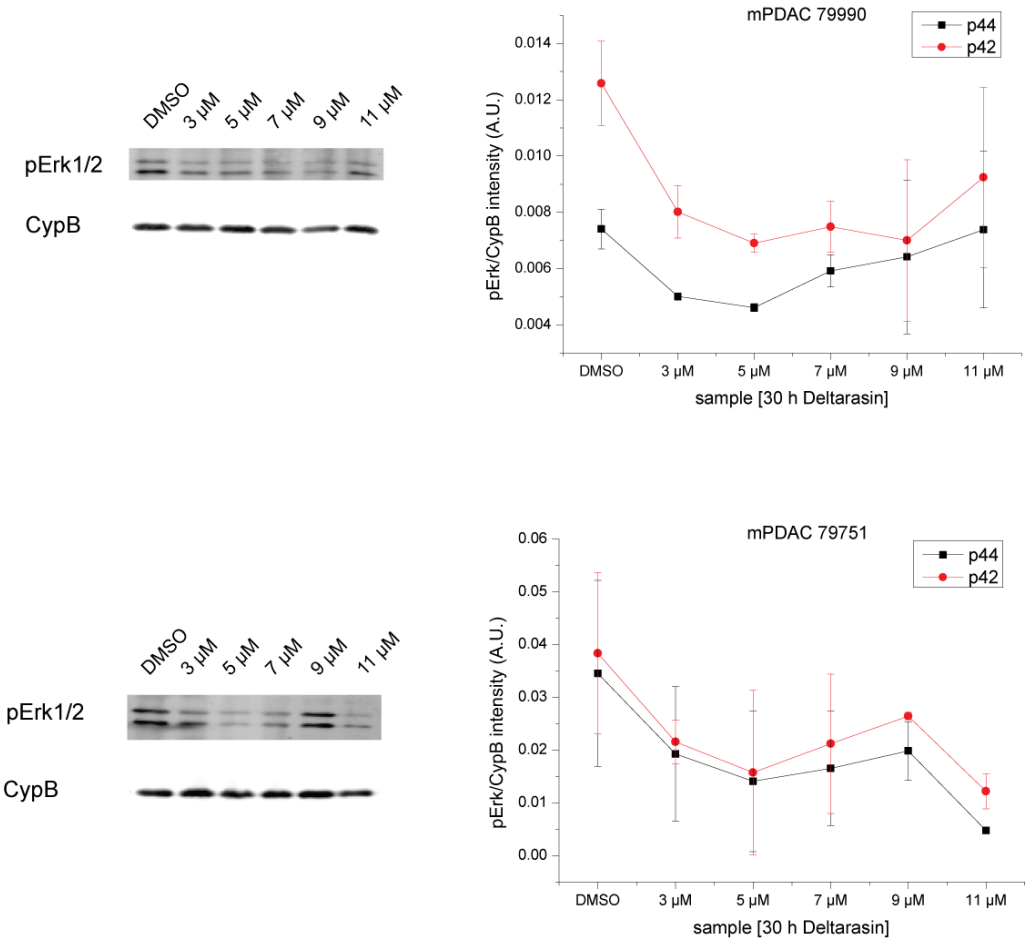

Figure 41: PhosphoErk levels for both mPDAC cell lines in the presence or absence of Deltarasin were determined by Western Blots (left). The quantification of three independent experiments is shown on the right with the respective standard deviation. In case of the KC cell line, p44 values for low Deltarasin concentrations are shown as single values due to the lack of detectable bands. Cells were incubated with Deltarasin for 30 h. The phosphoErk and Cyclophilin B bands are shown for different Deltarasin concentrations and from their quantification (N=3), it can be inferred that the single knock-in cell line (top) and the double knock-in cell line (bottom) have decreased pErk level with increasing amounts of Deltarasin.

After Deltarasin incubation for 30 h, a dose-dependent decrease of phosphoErk levels (p42, p44) was visible in both cell lines. Regarding the overall trend, Deltarasin caused a dose- and time-dependent decrease of pErk levels in both cell lines.

In case of Deltazinone 1, no such effect on downstream signaling after PDEδ inhibition neither in the single (data not shown), nor in the double knock-in cell line could be detected in this timeframe. The pErk levels were nearly constant in each condition (figure 44).

.

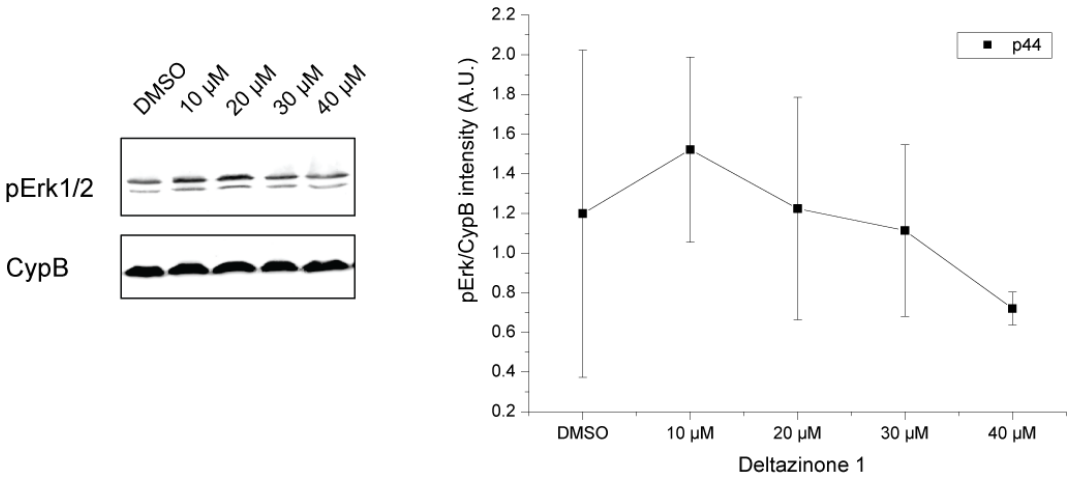

Figure 42: PhosphoErk levels after Deltazinone 1 and DMSO treatment (control) in mPDAC cells (79751) were determined by Western Blots (left). The quantification of three independent experiments is shown on the right with the respective standard deviation. Cells were incubated with Deltazinone 1 for 24 h. The phosphoErk and Cyclophilin B bands are shown for different Deltarasin concentrations and from their quantification (N=3) it can be inferred that pErk levels were not affected by increasing amounts of Deltazinone 1.

5.14 Monitoring pErk2 by PhosTag-FLIM in mPDACs

To further quantify any change in Erk activity in single cells, PhosTag-FLIM was utilized (Karajannis, 2015). PhosTag is a phosphate-binding probe, which allows the detection of phosphorylated (serine, threonine, tyrosine) proteins. As Erk has to be phosphorylated for its full activity, mCitrine-labeled Erk2 was transfected in both cell lines and treated with different amounts of both inhibitors, fixed, permeabilized and stained with PhosTag-Cy3.5. The amount of FRET correlates with Erk2 activity (figure 45).

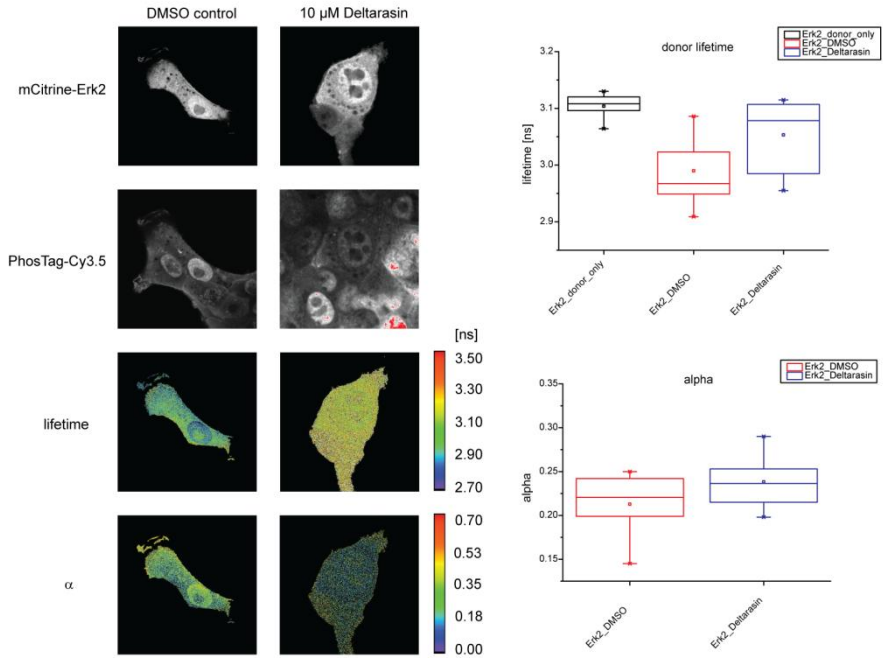

Figure 43: Deltarasin treatment reduces the level of phosphorylated Erk2 in mPDAC cells. PhosTag-FLIM on (79990) cells with mCitrine-Erk2 (donor) fluorophore and PhosTag-Cy3.5 (acceptor). The fluorescence images, the lifetime map and α map of a representative example cell are depicted on the left. The respective quantification of the donor lifetime (upper graph) and the bound fraction (lower graph) of 2 datasets is shown on the right.

As depicted in figure 45, Deltarasin treatment resulted in a loss of phosphorylated Erk2 when compared to the DMSO control condition. In DMSO-treated cells a clear phosphorylation gradient of Erk2 in the nucleus and throughout the cell could be detected, whereas Deltarasin-treated cells did not exhibit such a gradient. For quantification, the average lifetime and α values of the whole cell were used. The resulting box plots showed for the average lifetime in >4 cells the tendency to increase after Deltarasin addition. DMSO-treated cells usually exhibited a higher FRET signal. This indicates that Deltarasin caused a decrease in Erk2 phosphorylation.

Next, Deltazinone 1 was applied to cells with ectopically expressed mCitrine-Erk2, incubated, fixed, permeabilized and stained with PhosTag-Cy3.5 and FLIM was performed (figure 46).

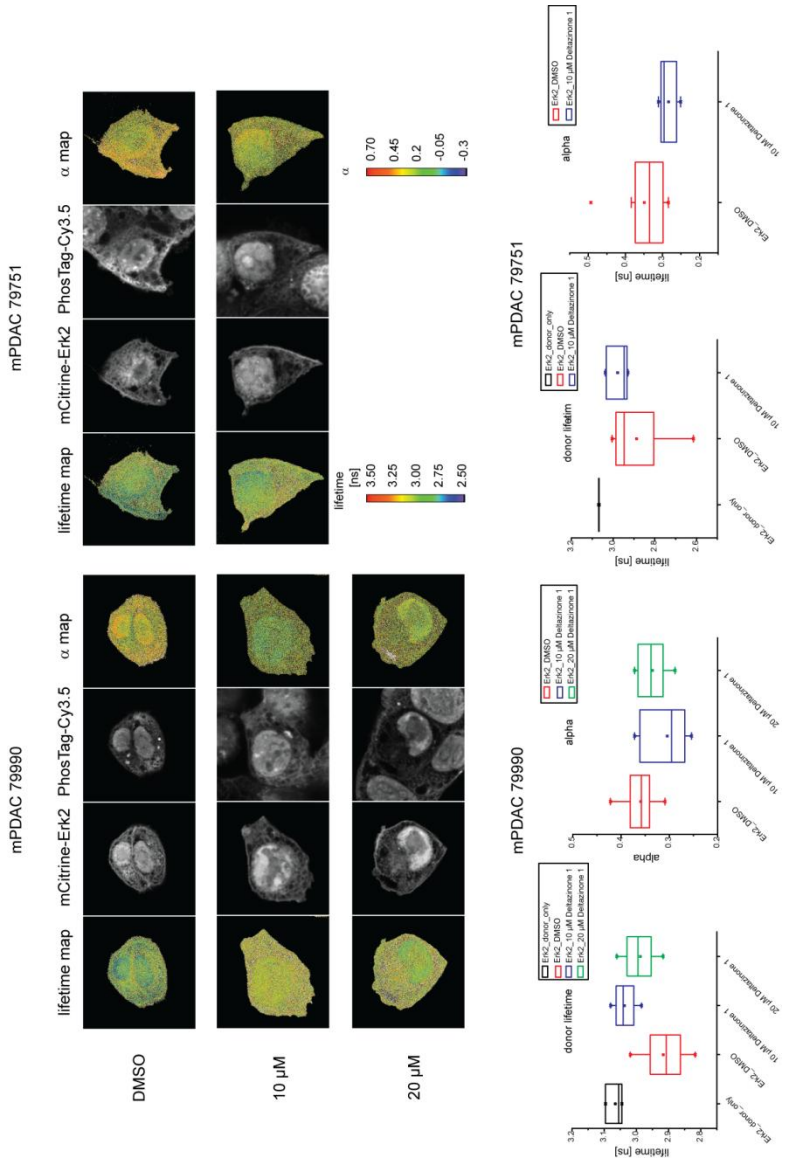

Figure 44: Deltazinone 1 treatment reduces the level of phosphorylated Erk2. PhosTag-FLIM on mPDAC 79990 (left) and MPDAC 79751 (right) with mCitrine-Erk2 (donor) and PhosTag-Cy3.5 (acceptor). The fluorescence images, the lifetime map and α map of a representative example cell are depicted on the left for the KC and on the right for the KPC cell line with DMSO and 10 µM (Deltazinone 1) for both cell lines and 20 µM (Deltazinone 1) for the single mutant cell line. The respective quantification of the donor lifetime and the bound fraction (α) of 2 datasets is shown below.

Regarding the effects of Deltazinone 1 on downstream signaling, the quantification of the FLIM data in both cell lines showed an increased lifetime and decreased bound fraction, when compared to the DMSO control and in case of the lifetime additionally to the donor-only sample as well. This clearly showed a decrease of Erk2 phosphorylation in the presence of both inhibitors after 2 h.

5.15 Doxycyclin-inducible downmodulation of PDEδ in mPDACS

The most elegant way to target PDEδ would be genetic downmodulation of PDEδ by lentiviral transduction of doxycycline-inducible shRNA in the murine models, demonstrated to work in human cells. Previous data with commercially available siRNA and transient shRNA indeed showed an effect on pErk in correlation with the amount of downregulated PDEδ (Chandra, 2012). The idea was to use the sequence from the commercial shRNA, used by Chandra et al. and introduce it into the pLKO backbone. The induction of shRNA (shRNA cloning performed by Dr. A. Konitsiotis) showed no significant change in the growth behavior in both cell lines (figure 47). In order to prove the downregulation efficiencyi, Western Blots were carried out and stained for PDEδ. Unfortunately, no significant reduction in the band intensities after doxycycline-treatment was detectable (figure 49). Hence, the designed construct is not targeting endogenous PDEδ in the murine system and the slight change in the growth behavior of the 79990 cells, measured by RTCA, is not caused by a specific downmodulation of PDEδ.

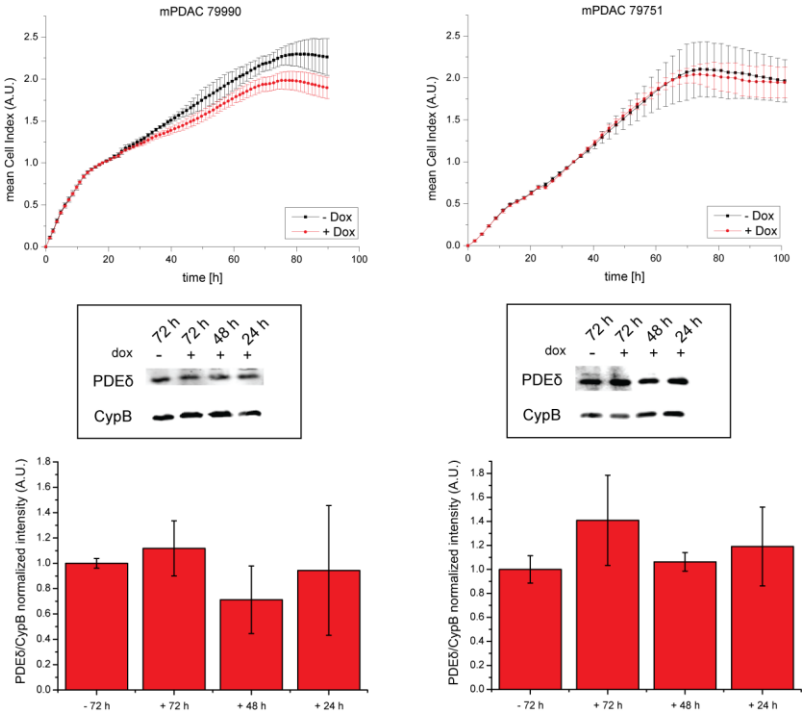

Figure 45: RTCA data for the respective murine cell line (top). The single mutant cell line is shown on the left and the KPC cell line on the right. Doxycycline was added after 24 h. The corresponding Western Blot data to show time-dependent downregulation of PDEδ, including CyclophilinB as the loading control, is shown below.

6 Discussion and conclusions

6.1 Genetic downmodulation of PDEδ in stably transduced human cancer cell lines

The initial idea was to generate a panel of human cancer cell lines with stable shRNA expression (table 1). For this hPDAC cells (Panc-1, Panc-TUI, Capan-1, and BxPC-1), CRC cells (HT-29, HCT-116, Hke-3, and SW480), the lung cancer cell lines (A549, H358, and H441) and the cervix carcinoma cells A431 were subjected to lentiviral transduction with shRNA against PDEδ. Out of this panel, only the lung cancer cell lines H358 and H441 could not be generated because they did not tolerate viral infection and subsequent puromycine selection. Even with multiple rounds of viral supernatant transfer, shown in parallel to work in other cell lines, this did not yield stably transduced cells. Nonetheless, the single RTCA measurement for H358 cells pointed in the direction that also here oncogenic KRas-dependent cell lines are more affected than KRas wildtype cells (A549).

The subset of hPDACs represent a reproduction from experiments performed in 2013 (Zimmermann, 2013). As demonstrated in the results section, the response in RTCA measurements could be reproduced in this work (figure 17). The MIA PaCa-2 cells and the Capan-1 cells were kind gifts from Prof. S. Hahn from the Ruhr-University Bochum. The Capan-1 cells I generated in my work showed a different behavior after doxycycline induction. Even selection with high amounts of puromycine (5 µg/ml) for 2 weeks did not show a stronger growth inhibition after doxycycline addition (figure 46).

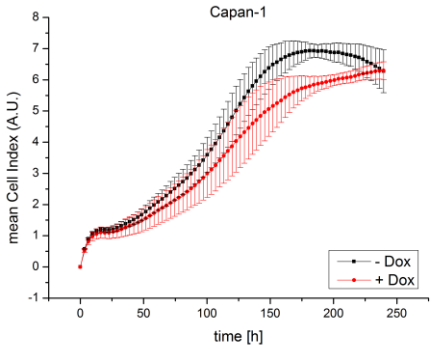

Figure 46: RTCA data for Capan-1 cells under high puromycine selection (top graph). The doxcycycline induction is represented by the red curve and shows no significant reduction in cell proliferation.

Although lentiviral systems provide high and efficient transduction, the insertion and positioning of artificial DNA in the genome cannot be controlled. That means, whenever a stable cell line is generated, it still remains questionable if a good knock-down, in case of shRNA, is achieved. Very likely, the cell lines used for the publication in 2013 (Zimmermann, 2013) and for figure 17 (data generated by Dr. B. Papke for Capan-1), were more efficiently targeted, probably due to a more efficient insertion or positioning of shRNA. The reproduction of a new stably transduced Capan-1 cell line would not necessarily yield better results, as the place of insertion of the viral DNA is not controllable.

Moreover, the Capan-1 cells, which were generated in this work, exhibited the highest amounts of PDEδ levels after doxycycline-induced depletion, as shown by Western Blot (figure 16). According to reaction-diffusion simulation data (Schmick, 2015), even a small fraction of free PDEδ in the perinuclear area is sufficient to maintain KRas at the plasma membrane by the PDEδ/Arl2 delivery system. As Capan-1 cells are oncogenic KRas-dependent and were shown to react to PDEδ downregulation, the remaining fraction of PDEδ after knockdown might be sufficient to prevent cell death hence, the out-of-equilibrium distribution is still maintained. In this way, the Western Blot data corroborates the slight growth changes observed by RTCA and might provide information why this system does not behave as it was supposed to be.

Nonetheless, the downmodulation of PDEδ was successful in all the remaining cell lines, as shown by Western Blots. The data from RTCA measurements and demonstrated that KRas-dependent cells are more susceptible to PDEδ downmodulation or small molecule inhibition. All human PDACs showed the expected sensitivity to PDEδ inhibition, which correlated with the KRas status. Interestingly, the CRC cells seemed to be unaffected by modulated PDEδ levels. Only the KRas-dependent cell line HCT-116 showed decreased proliferation in the absence of PDEδ, whereas the isogenic counterpart Hke-3 did not. The most striking behavior could be detected in HT-29 cells. The PDEδ knockdown worked in these cells, as demonstrated by Western Blots, but they did not respond to any PDEδ modulation, neither by RNAi nor small molecule inhibition. HT-29 cells have an oncogenic Braf mutation, which is downstream of KRas. This means that such cancers are not likely to gain additional Ras mutations and that the BRaf mutation alone is sufficient to drive cancer progression.

Moreover, BRaf mutations seemed to be unaffected by varying PDEδ levels, as BRaf is a soluble protein and does not require a solubilization factor for its distribution. In addition, the new small molecule inhibitor Deltazinone 1 showed the same growth profiles in RTCA measurements as the inducible shRNA did. This confirms that PDEδ is a valid target for oncogenic KRas-dependent cancer cells and this might offer new therapeutic strategies in cancer treatment. It would have been nice to include an additional CRC cell line with a known KRas-dependency, to really prove the correlation between oncogenic KRas and the level of PDEδ and if this is an omnipresent feature of all oncogenic KRas-dependent cells.

The clonogenic assays, which were performed in triplicates, showed a smiliar growth inhibition in all samples as with RTCA. Again, this proves that the knockdown of PDEδ works and is accompanied by long-term growth effects in all cell lines. The HT-29 cells displayed again the lowest effect on colony growth, concomitant with RTCA data.

Clonogenic assays with both small molecule inhibitors were also performed by Dr.B. Papke and first results showed similar growth effects in the presence of Deltazinone 1 and unspecific cytotoxicity with Deltarasin at higher doses.

To further optimize the information output from clonogenic assays, one has to establish better particle tracking methods for the different cells lines to allow for better quantification of the colony number and size. All cell lines are from different tumor origins and are heterogenous. In this way, it is difficult to identify single colonies with a general algorithm and for further quantification an individual solution for each cell line is demanding.

6.2 PDEδ inhibition causes a modulated response in murine PDACs

Recapitulating all experimental results, the two mPDAC systems exhibited different behaviors after PDEδ inhibitor treatment. Both cell lines were shown to have detectable amounts of GTP-bound Ras, proven by GST-pulldown. GTP-bound Ras was visualized at the plasma membrane and relocalized to endomembranes after Deltarasin treatment, indicating that PDEδ was efficiently inhibited and the out-of-equilibrium distribution could not be maintained. Hence, the entropic tendency of KRas to occupy all membranes dominated. One draw-

back is that the RBD-staining detects all Ras isoforms and does not give direct information about active KRas. To gain further knowledge, these experiments, using 3xRaf-RBD fused to GST could be repeated for both murine cell lines in the presence of Deltazinone 1 to achieve better comparability between both chemical compounds. It could well be that Deltazinone 1 is not as effectively relocalizing KRas, which can already be seen when comparing figure 33 to figure 34.

As measured by RTCA, there was a clear difference in the cell indices between both cell lines when subjected to increasing Deltarasin concentrations. The double knock-in cells seemed to be more resistant than the KC cells. They tolerated doses up to 9 µM instead of 5-7 µM and exhibited a switch-like response, rather than a gradual dose-response, as measured in the single mutant cells. With Deltazinone 1, not even short-term growth effects could be detected for the single knock-in cells (figure 35), whereas the KPC cells were slightly affected at higher concentrations and longer incubation times, as demonstrated by clonogenic assays (figure 37). Therefore the question arises whether both inhibitors exhibit long-term effects on both cell lines. From clonogenic assays it could be inferred, that Deltarasin caused cell death at a concentration >2.5 µM and Deltazinone 1 seemed to have long-term effects at higher concentrations in KPC but not in KC cells (figure 37).

Beside the higher resistance of KPC cells to Deltarasin, higher cell densities or even monolayers prevented inhibitory effects. The dose-dependent growth behavior completely vanished when cells were seeded at higher concentrations (figure 36). Hence, the elevated level of cell-cell contacts and the increased amount of extracellular messengers due to a higher cell number probably prevented cytotoxic effects at the indicated concentrations, which were previously demonstrated to cause death in this system (figure 35).

In a tumor, the phenomenon of cell aggregation and self-organization in time and space decreases the susceptibility of single cell in contrast to the organized structure. In human pancreatic cancer, chemotherapy was shown to be ineffective because of collagen-rich shielding layers around the tumor, which provide an additional incapability to penetrate central cancer cells (Bardeesy, 2002). As a result, certain cells (Hermann, 2007) may have survived any drug or radiation treatment and probably additionally gained mutations that guarantee cellular

fitness under these conditions and they continue to grow and probably metastasize into other organs and tissues (Weinstein, 2006; Marusyk, 2008; Torti, 2011).

As demonstrated by FLIM measurements with ectopically expressed RheB and PDEδ, an interaction break was indeed observed after addition of Deltarasin or Deltazinone 1 within minutes in both murine cell lines. This proves that both inhibitors are able to block the PDEδ binding-pocket to release farnesylated cargo, which dilutes to perinuclear membranes (figure 40). Since both compounds demonstrated an interaction break between PDEδ and farnesylated cargo, it is likely that a perturbation of the KRas cycle would have additional effects on downstream MAPK signaling. Decreased pErk levels were already described in the presence of Deltarasin (Zimmermann, 2013). Biochemical data in mPDACs by Western Blot confirmed decreased pErk1/2 levels after Deltarasin treatment (figure 41) but no decreased pErk levels with the new scaffold Deltazinone 1 (figure 42). In contrast, PhosTag-FLIM experiments supported the loss of pErk1/2 after PDEδ inhibition for both inhibitors (figure 43 and 44). All in all this is consistent with previous observations with siRNA/shRNA against PDEδ (Chandra, 2012).

Western Blots represent a cell population, whereas FLIM measurements exhibit molecular resolution. This might give an explanation why the Deltazinone 1 Western Blot data showed no measurable decrease in the Erk2 phosphorylation levels. Further data is necessary for better statistical confidence and to really prove if there are differences in the murine model systems.

6.3 Higher inhibitor concentrations are necessary to target KRas signaling

The FLIM data in mPDACs and recent studies in MDCK cells (Papke, 2015) showed that nanomolar concentrations of both Deltarasin and Deltazinone 1 are sufficient to break the interaction between RheB and PDEδ in *in vitro* assays. Nonetheless, it could be demonstrated that even small amounts of unbound PDEδ were capable to enrich KRas at the plasma membrane (Schmick, 2015; Schmick, 2014a), demanding higher doses of the inhibitor concomitant with cytotoxicity. As a consequence, to clearly see effects on Ras relocalization and growth, higher amounts of each inhibitor are required to completely block PDEδ

and interfere with the Arl2-mediated release in the perinuclear area (Schmick, 2015), as already demonstrated by *in vitro* assays (Zimmermann, 2013; Papke, 2015).

The conflicting difference in working concentrations could be explained by reaction-diffusion simulations (Schmick, 2015). Although both inhibitors were shown to work at nanomolar concentration and RheB-PDEδ FLIM assays, interference with the KRas localization requires higher concentration of the respective drug (Papke, 2015). Simulations prove that the PDEδ-Arl2-mediated release is inevitable for the KRas enrichment at the plasma membrane (Schmick, 2015). Low inhibitor concentrations are not sufficient to completely block PDEδ, meaning the Arl2-facilitated release is unaffected, which then guarantees a continuous fraction of free PDEδ in the perinuclear area. This small fraction of unbound PDEδ still exhibits functionality and can solubilize Ras family proteins or rebind to the inhibitor, counteracting complete depletion.

The differences between Ras and RheB localization are consequences of membrane leakage and the distinct PDEδ-Arl2 activity, depicted as a waterwork in figure 47. The different compartments (plasma membrane and perinuclear area) are shown as dams, which function as reservoirs to keep the pool of Ras (figure 47, left) and RheB (figure 47, right) in place. Leakage into the endomembrane system is represented by holes in the respective dam. The PDEδ-Arl2 system is compared to a pump and vesicular transport to a pipe, which connects both reservoirs. The trapping compartment is shown as an extension of the perinuclear area (Schmick, 2015).

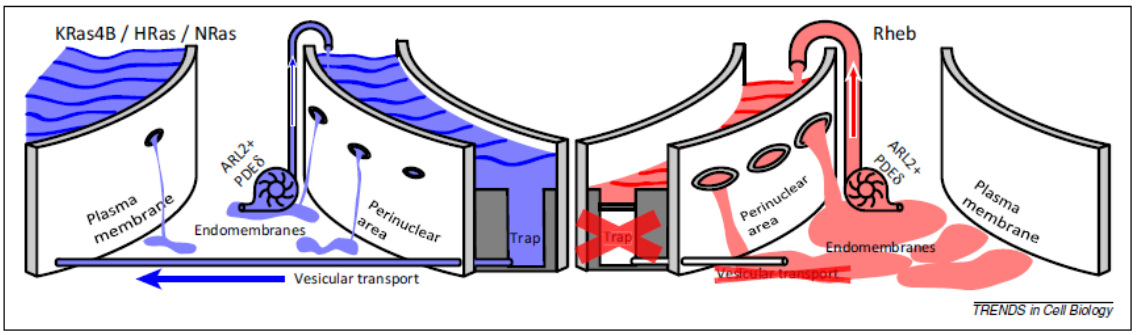

Figure 47: Schematic waterworks representation of the Ras (left) and RheB (right) localization. The plasma membrane and the perinuclear area are shown as dams. The PDEδ-Arl2 complex is represented by a small turbine which enriches farnesylated cargo in the perinuclear area. All Ras isoforms are trapped by their respective trapping compartment and directed to the plasma membrane by vesicular transport (pipe). The RheB enrichment in the perinuclear area requires higher PDEδ-Arl2 activity as the leakage from the perinuclear area is fast. Figure adapted from Schmick et al., 2015.

As already discussed, RheB is farnesylated but lacks any feature, which targets it to a trapping compartment. KRas owns an additional polybasic stretch, which is able to interact with the negatively charged inner leaflet of the plasma membrane by electrostatic interaction. Therefore, leakage of KRas from the plasma membrane is far lower than leakage of RheB from the perinuclear membranes. The weaker membrane binding of RheB when compared to all Ras isoforms, is demonstrated by a highly leaky perinuclear area. As there is neither a trapping compartment, nor directed vesicular transport, a high PDEδ-Arl2 activity is required to compensate for the loss of RheB in the perinuclear area. This leakiness of RheB in combination with the high PDEδ-Arl2 pumping activity implies that perinuclear enrichment is sensitive to perturbations. Therefore, pharmacological interference with the PDEδ-Arl2 system is likely to affect RheB localization more than it does with any of the Ras isoforms.

In case of HRas, NRas, and KRas, the protein leakage into endomembranes is lower than for RheB, as all Ras isoforms harbor distinct features, which allow for trapping at a certain membrane compartment. Here, a normal PDEδ-Arl2 pumping activity is sufficient to deplete the cytosolic and endomembrane-bound fraction of Ras to enrich it at its trapping compartment, prior to directed plasma membrane transport.

Regarding the effects on KRas and RheB after PDEδ inhibition, it is questionable if Erk phosphorylation really reflects KRas-dependent downstream signaling or if it is solely caused by affecting RheB. As KRas is involved in a multitude of signaling networks, one should consider the connection between PI3K/Akt and mTor and additional downstream targets, which could be compared in the presence of small molecules targeting PDEδ. Combinatorial approaches with a PI3K inhibitor (LY295004) could be measured with RTCA and confirmed by Western Blot to further untangle the effects on downstream modules.

Further, it could be speculated that Deltazinone 1, shown to be less cytotoxic as higher concentrations are tolerated, affects the mTor pathway (survival signals) more than Deltarasin does in accordance with its potency to solubilize RheB. The ability to solubilize KRas might completely differ between the tested compounds. As stated above, no KRas delocalization could be monitored with Deltazinone 1. Therefore, any growth inhibitory effects might be caused by efficiently targeting RheB.

Finally, it has to be determined why Deltarasin and more prominently Deltazinone 1 seem to be less effective in the murine system and if it is a result of MDR (multi-drug resistance) or if another GSF is present in mice. Another GSF might be either exclusively responsible for the solubilization of KRas in mice or it can take over PDEδ-mediated solubilization when PDEδ is blocked.
For Deltazinone 1 a stability test in murine liver microsomes showed that this compound is less stable (LDC, Dortmund). Microsomal stability determines the intrinsic clearance of the drug *in vivo*. This might explain why Deltazinone 1 works in human cell lines but only exhibits effects on mPDAC cells at high concentrations and long incubation times. As mouse metabolism differs from the human metabolism, the drugs might have been modified in such a way that they become effectless by unspecific enrichment (e.g. endomembranes) of the drug in the cell. Fluorescently-labeled Deltazinone 1 would indicate whether the cells are still able to incorporate the drug and gain insights about the time it stays inside.

Although PDEδ is a valid target to inhibit oncogenic KRas-dependent signaling in human cell lines, which broadens the spectrum of possible inhibitors that would cause alone or in combination a reduction in tumor growth in KRas-dependent cells, the two murine cell lines behaved completely different after small molecule inhibition of PDEδ and among themselves. The results, including RTCA, FLIM and clonogenic assay data, point towards the activation of different pathways after inhibitor treatment, as the only genetic difference in the murine system is the presence of mutant p53. Hence, new or alternative pathways might be activated, as both cell lines exhibit a different oncogenic mutation pattern. In general, this demonstrates that information about the status of oncogenes such as KRas or p53 should be evaluated prior to therapeutic intervenability. An oncogenic KRas mutation usually has an impact on the MAPK signaling pathway. The additional p53 mutation represents a defective tumor suppressor, meaning the important cellular check-point p53 has lost its function to transmit antiproliferative signals upon stress or oncogene activation (Zilfou, 2009). It would be interesting to further study the contribution of each oncogenic mutation on the behavior of the system after PDEδ inhibition.

7 Outlook

In this work it was shown, that the genetic downmodulation of PDEδ in human cancer models worked out. It would be interesting to see if the effects on growth, observed here, could be transferred to other cancer models. It would be nice to include an oncogenic KRas-dependent CRC cell line into the panel of cells to really correlate the effects on growth with oncogenic KRas-dependency. Moreover, the results in lung carcinomas should be reproduced or a transient knockdown with siRNA could be performed, as these cells already reacted to PDEδ downmodulation but did not tolerate viral transduction. Further, new inhibitors with more hydrogen bondings between the PDEδ binding pocket and the backbone of the compound could be tested in the human and murine models.

The genetic validation of shRNA-mediated downmodulation should be repeated in the mPDACs model systems, probably with different cloning methods and designs. This would allow a clear statement if the absence of PDEδ is crucial for long-term survival in mPDAC cell lines. Additionally, one could state that if the cells behave differently, the p53 status is essential for survival.

It would be interesting to study the effects of PDEδ inhibitors in pancreatic cells from the wild-type mouse, which was used as the genetic background for the transgenic animals. As these cells are not cancerous, RTCA experiments would directly give information about the growth behavior after inhibitor treatment, dependent on the genetic background.

Moreover, it would be interesting to study the effects of PDEδ inhibition on stem cells from different tissues. As the lab is currently establishing organoids from the small intestine, the effects on organoid growth and stem cell survival could be investigated. Additionally, the organoid system could be expanded to other organs (pancreas, liver) and further tested for any effects of PDEδ inhibition.

In both cell panels, the PhosTag-FLIM approach in the presence of EGF, to achieve maximal MAPKK and MAPK activity, could be performed to see clearer effects on Ras-mediated signaling via the MAPK pathway. Initial data for Mek1 phosphorylation in the presence of Deltarasin or Deltazinone 1 pointed also towards deactivation of the MAPK pathway in the presence of small molecule inhibitors. Hence, Mek1 activation should also be considered. Further, Western Blot data in the presence of Deltazinone 1 could be performed with EGF-

stimulation to achieve a maximum of phosphorylated Erk2. In this way, a decrease of Erk2 phosphorylation should be easier detectable.
Finally, the MAPK module should be analyzed after shRNA-mediated PDEδ knockdown to allow a clear statement about PDEδ inhibition and MAPK signaling and to exclude possible side effects caused by small molecule inhibitors.

8 Materials and Methods

8.1 Molecular biology

8.1.1 Bacterial culture

Liquid cultures of *Escherichia coli* XL 10 Gold/Stbl3 are grown in LB or TB medium with the appropriate antibiotic at 37°C/30°C in an incubator at 180 rpm. Cells are plated on LB agar with the appropriate antibiotic (selection marker) and incubated at 37°C/30°C.

Single colonies are picked and inoculated in 5 ml growth medium for mini-prep and pre-culturing, respectively. Pre-cultures are transferred to 150 ml medium and incubated over night at 37°C/30°C and 180 rpm (midi prep).

8.1.2 Transformation of chemically competent *E. coli*

Transformation is an amplification method for recombinant DNA in bacteria.

For each transformation, 100 µl *E. coli* cells are thawed on ice, mixed with 3.5 µl DTT (2.25 mM) and ~1 µl DNA, and incubated on ice for 30 min, following heat-shock for 60 sec at 42°C and immediate incubation on ice for 2 min. 500 µl SOC medium is added and the transformation mixture is incubated at 37°C for 1 h while shaking. 10-50 µl are plated on LB agar plates containing the selection marker and incubated overnight.

In case of ligation product transformations, all bacteria are completely plated to enhance the number of positive colonies. For retransformation, the addition of SOC is neglected and 50 µl bacteria suspension is plated after heat-shock.

8.1.3 DNA preparation QIAprep® Spin Miniprep kit

Typically, 2 ml bacterial culture is used and the procedure is performed according to the manufacturer's protocol. DNA is eluted with H_2O for cloning and in EB-buffer for long-term storage.

8.1.4 DNA preparation M&N Midi kit (Endotoxin-free NucleoBond® Xtra)

In general, 150 ml cultures are handled according to the manufacturer's protocol for low-copy plasmids. DNA is eluted with H_2O (endotoxin-free). Endotoxins are amphiphilic lipopolysaccharides located at the outer layer of the inner mem-

brane of Gram-negative bacteria, such as *E. coli*. Endotoxins are usually released during cell growth and during plasmid preparation. Hence, their removal is essential to ensure contaminant-free circular DNA and thereby high transfection rates in mammalian cells.

8.1.5 Sequencing using BigDye® Terminator kit

Sequencing reactions are based on the Sanger's dideoxy chain terminating method, using fluorescently labeled 2',3'-dideoxy-nucleotides (ddNTPs) which cannot form phosphodiester bonds (missing an OH-bond). The synthesized DNA strand is terminated after the insertion of a ddNTP. Nucleotide-detection is performed with capillary gel electrophoresis (in-house facility).

Typical sequencing reaction:

- 500 ng of DNA
- 2 µl of ready reaction premix
- 3 µl BigDye® termination buffer
- 0.5 µl sequencing primer (10 pmol/µl)
- Adjusted with ddH_2O to 20 µl.

Table 2: PCR cycle for sequencing reaction

Step	Temperature [°C]	Time
Initial	96°C	1 min
Denaturation	96°C	10 sec
Annealing	50	5 sec
Extension	60	4 min

The denaturation, annealing and extension reaction are repeated 25x (table 2, highlighted in grey). Excess ddNTPs are removed using DyeEx® spin columns, soaked with 600 µl ddH_2O for 30 min prior to use, according to the manufacturer's manual. Cleaned PCR product is transferred to 0.5 ml tubes and dried in a speed vacuum centrifuge at 60°C for 30 min and subsequently send for in-house analysis.

8.1.6 Agarose gel electrophoresis

Electrophoresis is a separation method using electrical fields. Here, the negatively charged DNA migrates towards the anode in the electric field and smaller fragments migrate faster, resulting in a separation by fragment size. To be able to determine the correct size of a certain DNA fragment, a DNA standard (NEB, 2-log DNA ladder) is always used for comparison.

For dsDNA, agarose-containing gels are used. These have the advantage of a defined pore size according to the percentage of agarose content. Agarose is a polysaccharide and a natural polymer. The appropriate amount of agarose (table 3) is dissolved in 1x TAE buffer and heated in the microwave until completely solubilized and Red-safe is added to visualize DNA (5 µl in 100 ml 1x TAE with agarose) and then poured into a gel cast with comb. When cooled down to RT, agarose forms a stable hydrogel. Electrophoresis is carried out at 100-120 V, constant, depending on the size of the gel, for 20-30 min in 1x-TAE buffer.

Table 3: Agarose content and resolution of DNA fragment sizes

Agarose concentration in % [w/v]	Size of DNA fragments [kbp]
2	0.1-1
1.8	0.2-2
1.5	0.3-3
1	0.5-7
0.8	0.8-12
0.5	1-30

8.1.7 Purification of DNA

The QIAquick®/Zymo gel extraction kit for isolation of DNA fragments from agarose gels is used to isolate and purify DNA fragments and is performed according to the manufacturer's protocol. Columns with silica membranes facilitate DNA-binding at high salt concentrations and allow for washing steps. Purified DNA is eluted with H_2O.

8.1.8 Restriction digest of DNA

Restriction endonucleases type II bind to palindromic dsDNA sequences (restriction sites) and catalyze the hydrolysis of phosphodiester bonds (3'- to 5'-) in each strand, resulting in a double strand break with either sticky or smooth

ends. As such, restriction digest is used for cloning, DNA linearization, and ligation experiments. Usually, dsDNA is incubated with the appropriate restriction enzyme in 10x CutSmart® buffer (NEB) and H_2O for 1 h at 37°C for complete digestion. If possible, restriction enzymes are heat-inactivated at 67°C for 30 min after digestion.

8.1.9 Dephosphorylation of 5'-phosphorylated DNA

In order to prevent vector DNA from self-ligation, 5'-phosphorylated ends are dephosphorylated by alkaline phosphatases (CIAP) during restriction digest. Hence, 1 µl CIAP (NEB) is added to each restriction digest of the desired vector backbone and incubated for 1 h at 37°C.

8.1.10 Ligation of dsDNA

DNA-ligase (T4) catalyzes the ATP-driven phosphodiester bond formation between 3'-OH and the 5'-phosphate group of linear DNA fragments. Ligation of DNA fragments is performed with different ratios (1:3 -1:10) of purified and digested vector and insert. The required amount of insert was calculated as follows:

$$Insert[ng] = \frac{vector[ng] \cdot size(insert)[bp]}{size(vector)[bp]}$$

Usually, 1 µl of T4 ligase and 4 µl ligation buffer were used for each 20 µl reaction and incubated at 16°C overnight.

8.1.11 Polymerase Chain Reaction (PCR)

The Polymerase Chain Reaction (PCR) is based on thermal cycling (table 4) and was developed in the early 1980's (Mullis, 1986). In general, it is used for the amplification of a particular DNA sequence and offers a broad application spectrum for e.g. cloning, sequencing, gene analysis, phylogeny, genetic fingerprints, infectious diseases, forensic science, and paternity testing.

Table 4: Thermal cycles of the polymerase chain reaction

Step	Temperature [°C]
Initial	95°C
Denaturation	95°C
Annealing	45-65
Extension	60

First, dsDNA is denatured by heat (95°C), resulting in a single stranded template, followed by the annealing process of two oligonucleotide primers, flanking the region of interest. The hybridization temperature of the primers to the ssDNA depends on their length and G-C content and has to be adjusted for every primer pair, usually between 45-65 °C. A heat-stable DNA polymerase (e.g. Tac polymerase) binds to the specific primers and elongates the primers, by consumption of dNTPs, resulting in a perfect copy of the template strand. In every cycle the DNA sequence is doubled and cycle repetition leads to an exponential amplification of the template sequence (table 4, steps in grey are repeated). PCR can also be used to create genetic modifications in the template.

8.1.12 PCR product purification

The QIAquick® PCR purification kit is used for purification of DNA fragments according to the manufacturer's protocol.

8.1.13 Site-directed mutagenesis

The KRas-SAAX mutant is generated by site-directed mutagenesis because a single nucleotide has to be exchanged. As the template, mCitrine-KRas-CLL is used. The KRas-SAAX forward and reverse primers are designed to have x nucleotides in length and the nucleotide of interest in the middle.

- 300-500 ng of template
- 1 µl dNTPs (10 mM)
- 50 pM primer 1
- 50 pM primer 2
- 1 µl Pfu polymerase
- 10x Pfu polymerase buffer
- 1.5 µl DMSO
- Adjusted with H_2O to 50 µl

The reaction is performed as following with 16-18 cycles of the steps marked in grey:

Table 5: Site-directed mutagenesis PCR cycles, repetitions are shown in grey

temperature	**time**
95°C	2 min
95°C	30 sec
55°C	1 min
72°C	6 min (1 min/kbp)
72°C	8 min
8°C	till end

Finally, the methylated parental template strands are digested with Dpn1 at 37°C for 1 h and the product is transformed into chemical competent bacteria.

8.2 Cell culture

Human pancreatic cancer cell lines, colon rectal, and cervix cancer cell lines (Panc-1, Panc-TuI, BxPC-3, MIAPaCa-2, Capan-1, HCT-116, Hke-3, SW480, A431) (ATCC, American Type Culture Collection, Manassas, VA, USA) cells are maintained in DMEM (Dulbecco's modified Eagle medium, Sigma-Aldrich Biochemie GmbH, Taufkirchen, Germany) supplemented with 10 % FCS (fetal calf serum), 2 mM L-glutamine (Sigma-Aldrich Biochemie GmbH, Taufkirchen, Germany) and 1 % NEAA (non-essential amino acids) (Sigma-Aldrich Biochemie GmbH, Taufkirchen, Germany), at 37°C, 5 % CO_2 in a humidified incubator.

Lung cancer cell lines H35 and H441 (ATCC, American Type Culture Collection, Manassas, VA, USA) are maintained in RPMI (Roswell Park Memorial Institute medium) (Sigma-Aldrich Biochemie GmbH, Taufkirchen, Germany) supplemented with 10 % FCS (fetal calf serum), 2 mM L-glutamine (Sigma-Aldrich Biochemie GmbH, Taufkirchen, Germany) and 1 % NEAA (non-essential amino acids) (Sigma-Aldrich Biochemie GmbH, Taufkirchen, Germany), at 37°C, 5 % CO_2 in a humidified incubator.

The colon rectal cancer cell HT-29 and the lung cancer cell line A549 (ATCC, American Type Culture Collection, Manassas, VA, USA) are maintained in Ham's medium, supplemented with 10 % FCS (fetal calf serum) and 1 mM L-glutamine (Sigma-Aldrich Biochemie GmbH, Taufkirchen, Germany), at 37°C, 5 % CO_2 in a humidified incubator.

8.2.1 Cell culture (mPDAC)

Murine pancreatic ductal adenocarcinoma cells (mPDAC) (Shokat/Tuveson lab) were maintained in DMEM, supplemented with 10 % FCS (fetal calf serum), 2 mM L-glutamine (Sigma-Aldrich Biochemie GmbH, Taufkirchen, Germany) and 1 % NEAA (non-essential amino acids) (Sigma-Aldrich Biochemie GmbH, Taufkirchen, Germany), at 37°C, 5 % CO_2 in a humidified incubator.

Table 6: General seeding procedure for mPDAC cells

dish	cell density	medium
T75	10^6	10 ml
10 cm	10^6	10 ml
6-well	150,000	2-3 ml
8-well LabTek	5,000-10,000	300-500 µl
RTCA	2,000-5,000	200 µl
clonogenic assay	250-500	3 ml

8.2.2 Cell splitting

In order to keep adherent cells alive and under perfect growth conditions, they need to be detached, diluted and seeded into a new culture dish in a regular manner to prevent confluency. This process is called cell splitting. In general, adherent cells grow as a monolayer and growth inhibition by confluency might transform the cells and as such it is not a controllable and predictable system anymore. Old growth medium is removed from the cells and they are washed with sterile 1x PBS. Subsequently, Trypsin/EDTA (Pan Bio) is added. Trypsin is a digestion enzyme which unspecifically recognizes positive amino acid residues (Lys, Arg). EDTA (ethylenediamine tetraacetate) functions as a chelator and complexes bivalent cations (Ca2+). Adhesion is strongly Ca2+-dependent and Trypsin/EDTA facilitates a proper detachment of the cells. The detached cells are resuspended in fresh growth media to inactivate Trypsin and to count the cells in order to seed them into new culture dishes in the desired amount.

8.2.3 Cryo preservation, thawing, and long-term storage of cell lines

It is essential to keep backups from all cell lines which are used for cell culture work for long-term storage in order to generate reproducible results for this work and future work.

For long-term storage, cells are cryo-preserved, using cryo-protectants such as DMSO and freezing temperatures below -80°C. DMSO prevents intracellular ice crystal formation, hence enhances the cell viability during freezing and thawing. Sub-confluent T75 flasks are split as described above, counted and collected by spinning down. The resulting cell pellet is diluted in cryo-medium (usually 90 %

DMEM and 10 % DMSO) to a concentration of $2x10^6$ cells/ml. 500 µl (10^6 cells) of the cell suspension is applied into cryo vials, stored on ice, and subsequently transferred to a NALGENE® Cryo 1°C freezing box and stored at -80°C for at least 1 day. These freezing boxes are filled with isopropanol and allow for controlled freezing rates of 1°C/min. The frozen aliquots are moved to a -150°C freezer for long-term storage.

Whenever a certain cell line is needed from the backup, frozen vials are thawed as quickly as possible in a 37°C water bath to avoid toxic effects of DMSO on the cells. The thawed cell suspension is transferred to an appropriate culture dish or flask with the appropriate amount of growth medium. Media is exchanged the next day and replaced with fresh growth medium, to remove traces of DMSO.

8.2.4 S2 Cell culture and lentiviral transduction

Murine PDAC cell lines (79990 and 79751), as well as all human pancreatic cancer cell lines Panc-1, Panc-TuI, Capan-1, BxPC3, colon rectal cancer cell lines HCT116, Hke3, SW480, HT-29, human lung cancer cell lines H441, H358, A549 and human epithelial cervix carcinoma cell line A431 are maintained in the appropriate medium as previously described.

All target cell lines are tested for puromycine tolerance, prior to transduction. Different puromycine concentrations are applied to each cell line and the growth inhibitory effects are monitored for four days. The minimal inhibitory concentration of puromycine is used for selection (table 7):

For knockdown experiments, cells are transduced with lentiviral particles containing PDEδ shRNA, vehicle only or GFP-control and selected with puromycine (Sigma Aldrich) for minimum 6 days and three passages.

Table 7: Target cell lines with their appropriate puromycine concentration for selection after lentivirus transfer

cell line	puromycine concentration [µg/ml]
Panc-1	2
Panc-Tul	1
BxPC-3	1.5
Capan-1	1.5-5
MIAPaCa-2	1
HCT-116	1
Hke-3	1
SW480	1
HT-29	1
A431	1
A549	1
mPDAC 79990	2
mPDAC 79751	2
H358	1.5
H441	1.5

8.2.5 Lentivirus production and transduction

All vectors are a kind gift of the Hahn lab (Bochum). The design of human shRNA PDEδ is published in Zimmermann et al., 2013.

On the first day, packaging cells (HEK 293 T) are seeded in 10 cm dishes ($2x10^6$) or 6 cm dishes (10^5) and cultivated in complete growth medium (DMEM with supplements) in a humidified incubator at 37°C, supplemented with 5 % CO_2.

On the next day, cells are transfected with a three-plasmid system, using $CaCl_2$ transfection (1x 10 cm dish). The corresponding concentrations for 6 cm dishes are shown in ():

- 12 µg (4 µg) pCMVΔR8.2
- 6 µg (2 µg) pHIT G
- 12 µg (4 µg) DNA of interest
- Ad 438 µl with ddH_2O
- 62 µl (25 µl) $CaCl_2$ solution (2 M) are applied and mixed with the plasmids
- 500 µl (200 µl) 2x HBS buffer is slowly added (dropwise, no mixing)
- the reaction mixture is incubated for 10 min at RT

The transfection mixture is carefully pipetted up and down and applied to the packaging cells.

On the third day, the growth medium for HEK 293 T is changed and the target cells are seeded in 6 cm dishes and incubated overnight at 37°C in a humidified incubator with 5 % CO_2.

On day 4, the viral supernatant is collected in a Falcon and filtered through a 0.45 µm filter in a fresh falcon tube with polybrene (c=4 mg/ml). Growth medium from all target cell lines is aspirated and all dishes are washed twice with 1x sterile PBS. The filtered viral supernatant containing polybrene is added (2-3 ml/6 cm dish) to the target cells. The target cells are incubated overnight at 37°C in a humidified incubator with 5 % CO_2. Usually, puromycine selection starts the day after with fresh growth medium.

8.2.6 Real time cell analysis (RTCA)

RTCA is performed using 16-well E-plates with gold electrodes on the bottom measured on a Dual Plate xCELLigence instrument (Roche Applied Science, Indianapolis IN). The system measures the impedance-based cell index (CI), a dimensionless parameter which evaluates the ionic environment at the electrode/solution interface and integrates this information on the cell number. Continuous impedance measurements are monitored every 15 min for up to 300 hours. Blank measurements are performed with growth medium. Depending on the cell line and if not stated elsewhere, 5×10^3- 1×10^4 cells are plated in each well of the 16-well plates in 200 µl of cell culture medium for short-term measurements and 1-2x10^3 cells/well for long-term measurements and then placed into the RTCA machine in a humidified incubator at 37°C with 10 % CO_2. After seeding, cells are allowed to reach steady growth for 24 h before inhibitor addition, whereas in case of cells stably expressing the inducible shRNA transgene, doxycycline is directly applied to the wells of interest. In case of Deltarasin and Deltazinone 1 measurements, the amount of DMSO is kept constant between the individual conditions and did not exceed 0.24 %. All assays are performed as minimum triplicate. The cell index is normalized to 1 at the time point of drug administration. For shRNA experiments there no normalization is applied.

8.2.7 Clonogenic assays

To study long-term effects on cell growth, clonogenic assays are performed. Briefly, 1,000 cells/well are seeded in 6-well plates and grown for 7-10 days in the respective growth medium with or without doxycycline (200 µg/ml) or the appropriate amount of inhibitor. Doxycycline and the inhibitors are applied 24 h after seeding. Clonogenic assays provide information regarding the colony size and the colony number. If the number decreases after inhibitor or doxycycline induction, the treatment causes cell death (cytotoxicity), whereas shrinkage of the colony is due to cytostatic effects.

After long-term growth, the medium is aspirated and the wells are carefully washed with 1x PBS. 500 µl PFA (Paraformaldehyde) 4 % is applied and 1-0.5 ml crystal violet solution (5 % in EtOH, prediluted in 1x PBS) is added to achieve a final concentration of 0.1-0.05 % crystal violet. The plates are incubated for 20 min at RT and then washed twice with 1x PBS (short 5 min and 10 min long washing step). The plates are dried at RT and scanned on the Odyssey IR imaging System (Licor). Scanned plates are analyzed by counting and measuring the colonies with ImageJ.

8.2.8 Inhibitor treatment

In general, both inhibitors Deltarasin and LDC 09577 are dissolved in DMSO. For dilutions, growth medium is used and added before the inhibitor and then mixed.

8.2.9 Transient transfection

All transient transfections in mPDAC and Panc-TUI cells are performed with Lipofectamine 2000 (Invitrogen). For this 240 µl OptiMem (Sigma) are mixed with 4 µg DNA in one tube. In a separate tube, 240 µl OptiMem and 9.6 µl Lipofectamine are applied. Both tubes are first incubated for 5 min at RT and then pooled and further incubated for 20 min at RT. 60 µl are applied to each well for an 8-well LabTek chamber.

8.3 Biochemistry

8.3.1 Whole cell Lysates

For protein analysis (Western Blots) whole cell lysates are prepared from mammalian cells cultured in petri dishes, according to the needed amount of total protein (6-well plates, 3.5 cm, 6 cm, and 10 cm dishes). The growth medium is aspirated and the cells are washed once with PBS, subsequently incubated with an appropriate amount of 1x RIPA buffer, supplemented with 1 tablet Complete Mini EDTA-free protease inhibitor and 100 µl phosphatase inhibitor cocktail 1 and 2. After 15 min, the cells are scraped with a plastic cell-scraper and the lysed content of each well is transferred to a prechilled 1.5 ml Eppendorf tube. If necessary, sonification for 12 sec is performed (30 % cycle 3). Samples are spun down at 14,000 rpm for 20-30 min and the supernatant is collected in fresh prechilled tube.

At this stage the samples can either be snap-frozen for long-term storage at -80°C or the total protein concentration is measured by Bradford assay. A BSA (bovine serum albumin) standard curve is recorded for calibration. All steps are performed on ice and in prechilled machines and tubes to avoid protein degradation.

8.3.2 Bradford assay

The Bradford assay is a colorimetric protein determination assay, based on the absorbance shift of Coomassie Brilliant Blue G-250 dye in presence of protein. Coomassie Brilliant Blue G-250 is red in its unbound, cationic form. Upon binding of the dye to proteins, the blue, anionic form is stabilized and the amount of blue complex is equivalent to the protein concentration. The absorbance is measured at 595 nm in a spectrometer.

Protein standards are prepared by serial dilution of BSA (1 mg/ml) in ddH_2O.

16 µl BSA is mixed with 984 µl H_2O and a serial dilution out of this, ranging from 1-16 µg/µl is performed. Each standard (500 µl) is added in a separate cuvette and mixed with 500 µl Bradford reagent. For each sample, 1 µl is added to 500 µl ddH_2O and mixed with 500 µl Bradford reagent. The absorbance values are obtained at 595 nm in a spectrophotometer and plotted against the standard protein concentration.

8.3.3 SDS-PAGE

SDS-PAGE is a method to separate proteins according to their size by electrophoresis in acrylamide gels. Sodium dodecyl sulfate (SDS) is an anionic surfactant which stoichiometrically binds proteins (1 SDS molecule per 2 amino acids). It breaks hydrogen and disulfide bonds, shields the overall charge, and causes an unfolding of proteins, resulting in negatively charged complexes which are separated only by size. The uniformly charged SDS-protein complexes migrate towards the anode when subjected to an electrical field. Smaller molecules migrate faster and the distance of migration is proportional to the pore size of the polymerized acrylamide gel. Different percentages of acrylamide allow a better separation and resolution for characteristic band sizes, depending on the molecular weight of the protein. Discontinuous gels are used in all experiments, consisting of a stacking and separation gel.

Separating gels are poured first and then covered with 100 % ethanol (EtOH) to avoid drying of the gel air interface. The gel is allowed to polymerize for 30 min. The ethanol is removed and the stacking gel is poured on top, followed by the immediate insertion of a comb. The acrylamide gel is allowed to polymerize for 30 min and then wrapped in foil and stored under humidified ddH_2O conditions at 4°C.

8.3.4 Sample preparation and gel loading

Cells were usually seeded one day prior to stimulation, inhibitor treatment (Deltarasin, LDC 09577) or transfection.

Whole cell lysates are mixed with 5x SDS sample buffer and heated for 5 min at 95°C to allow the denaturation of protein by reduction with 2-mercaptoethanol (β-mercaptoethanol). Samples are spun down prior to loading. Prior to electrophoresis, the combs are removed from the gels and the sample pockets are cleaned with ddH_2O and gels are inserted into BioRad Gel chambers (TetraCell), filled with 1x running buffer and samples are loaded in their respective pocket. For size determination of separated proteins, 3 µl (Dual-Color BioRad) standard, containing different bands of known molecular weight are loaded in at least one well/gel. Empty pockets are loaded with sample buffer and electrophoresis is performed with constant voltage of 80 V until samples

leave the stacking gel, followed by an increase to 110 V for 2 h until leaving the separation gel.

8.3.5 Western Blot

One form of immuno-blotting is Western Blotting. In this technique proteins that are separated electrophoretically are transferred to a PVDF (Immobilon, Millipore, Billerica, MA, USA) membrane to enable immunological protein detection with primary and secondary antibodies. After electrophoresis blots are assembled in wet blot modules. PVDF membranes are activated for 30 sec in methanol, then left to equilibrate in 1 x transfer buffer together with the gel and two pieces of thin filter paper (Whatmann) and sponges. The blot sandwich is assembled in the following sequence: sponge, filter paper, gel, PVDF membrane, filter paper, and sponge. The transfer is carried out at 100 V for 60 min. Following transfer, the PVDF membrane is transferred to a Li-Cor® incubation box and blocked with blocking buffer (Li-Cor® Biosciences) for 1 h at RT on a shaker to saturate unspecific binding sites. The membranes are then incubated with primary antibodies diluted in 1 ml Li-Cor® blocking solution. PVDF membranes are sealed in a plastic bag and incubated overnight at 4 °C in presence of the antibodies. On the next day, the blots are washed 3x with TBS-T for 5 min and then incubated with the appropriate secondary IR-antibodies (diluted 1:5,000) diluted in 5 ml Li-Cor® blocking buffer on a shaker at RT. Finally, blots are washed 3 times, 10 min each with 0.1 % TBS-T solution and specific bands are detected with the Odyssey Imaging System (Licor, Lincoln, Nebraska USA).
Antibody Stripping was performed with NewBlot PVDF stripping solution (Licor, Lincoln, Nebraska USA) according to the manufacturer's manual. Membranes were incubated in 1x working solution for 20' at RT.

8.3.6 Primary antibodies

The following primary antibodies are used for Western Blots in the appropriate dilution in Li-Cor® blocking solution.

Table 8: List of primary antibodies used for Western Blot

antigen	host	dilution	company	order #
PDE6D	goat	1:200	SCBT	sc-50260
pan Ras	mouse	1:1,000	Calbiochem	
pErk	rabbit	1:1,000	CellSignaling	9106
tErk	rabbit	1:1,000	CellSignaling	9102
Cyclophilin B	rabbit	1:2,000	Abcam	ab16045

8.3.7 GST-pulldown

For GST-pulldown experiments, 30 µl 50 % Glutathione Sepharose 4B slurry (GE Healthcare) with a binding capacity > 5 µg GST/µl were used for each sample. To equilibrate the beads, they are washed 4x with 1 ml GST-buffer (4°C, 500 g, 5 min). After the final washing step, 100 µl liquid remain on top of the beads. In the next step, 150 µg GST-labeled 3x Raf-RBD is incubated for 30 min at 4°C on a rotating wheel. The beads are then washed 4x with 1 ml GST-buffer to remove unbound protein (4°C, 500 g, 5 min). Lysates from 10 cm dishes are washed with cold 1x PBS scraped with 1 ml GST-buffer, centrifuged and the supernatant is further processed. The lysate is incubated with the equilibrated beads for 30-40 min at 4°C on a rotating wheel. After incubation, the beads are again washed 2x with 1 ml buffer to remove unbound protein (4°C, 500 g, 5 min). After the last washing step, remaining liquid is aspirated with a cannula. 25 µl 2x SDS sample buffer is applied, vortexed and the mixture is heated for 5 min at 95°C. The samples are loaded on 15 % acrylamide gels.

8.3.8 GST-staining

8-well LabTek chambers, containing Deltarasin-treated (6 h, 5 µM) and untreated cells are removed from the incubator and washed with 1x PBS (phosphate-buffered saline). 200 µl 4 % PFA (paraformaldehyde, w/v) is added to the cells and incubated for 5 min at RT. The cells are subsequently washed twice with 500 µl 1x TBS (Tris buffered saline) and permeabilized with 200 µl 0.1 % TritonX100 in 1x TBS for 5 min at RT. In order to remove remaining detergent, all samples are washed 3x with 500 µl PBS for 5 min at RT and then blocked with blocking buffer (1x PBS with 3 % BSA) for 30 min. After blocking, the blocking solution is removed by 3 washing steps with 500 µl 1xPBS for 5 min at RT. 15-30 µg/ml 3x Raf-RBD-GST solution in blocking buffer is added and incubated for 1h. After primary staining the samples are washed 3x with 500 µl 1x PBS

for 5 min at RT and then stained with a-GST A488 antibody 1:50 for 1 h in blocking buffer, in the dark. Finally, the cells are washed 3x with 500 µl 1x PBS for 5 min at RT and stored in 1x PBS until use.

8.3.9 Immunostaining for pan Ras

Usually, 5,000 cells/well are seeded in 8-well LabTek chambers and grown over night. In CRC and lung cancer, the doxycycline induction was 72 h prior to fixation and in hPDAC cells doxycycline is incubated for 24 h. Deltarasin and Deltazinone 1 treatment starts 2 h prior to fixation. Cells are removed from the incubator and 2x washed with 1x PBS (phosphate-buffered saline). 300 µl ice-cold Methanol is added to the cells and incubated for 10 min at -20°C. The cells are subsequently washed 3x with 500 µl 1x PBS and then blocked with blocking buffer (Li-Cor®) for 1 h. After blocking, the primary antibody (pan Ras, Calbiochem) is diluted 1:200 in Li-Cor® blocking solution and incubated for 1 h at RT (200 µl/well). In order to remove remaining primary antibody, all samples are 3x washed with TBS-T for 2-5 min. Alexa488-labeled donkey anti-mouse antibody is diluted 1:1,000 in Li-Cor® buffer for 1 h (200 µl/well). Finally, the samples are 3x washed with TBS-T and stored at 4°C in the dark until use.

8.3.10 Protein labeling with Cy3.5

Using a succinimide ester of a sulfoindocyanine (Cy) dye, in a water-free environment, it is possible to label proteins specifically. Succinimide esters bind covalently to free ε-amino groups on lysine residues or alpha amino acid groups of the protein.

Cy3.5 (Fluorolink Cy 3.5 Monofunctional Dye, GE Healthcare, (PA23501)) is a monofunctional dye with a size of 1,102 kDa. Lyophilized Cy3.5 is diluted in 5 µl water-free DMF (N,N-Dimethylformamide, Sigma Aldrich). The concentration of the dye is measured in a cuvette at 584 nm (1:10,000 dilution of Cy3.5 in PBS). The concentration of Cy3.5 can be determined following the Lambert Beer law:

$$A = \varepsilon \cdot c \cdot d$$

$$A_{Cy3.5_{584}} = 150{,}000 M^{-1} cm^{-1} \cdot cm \cdot c[Cy3.5]$$

$$c = \frac{A}{\varepsilon \cdot d}$$

$$c[Cy3.5] = \frac{A_{Cy3.5_{584}}}{150{,}000 M^{-1} cm^{-1} \cdot cm}$$

$$\frac{A_{Cy3.5_{584}}}{150{,}000} = c(Cy3.5) \cdot M$$

Where d is the length of the cuvette (1 cm), c is the concentration in M, A is the absorption at a specific wavelength and ε is the extinction coefficient. 1 mg streptavidin (Sigma, Aldrich) is dissolved in 1x PBS and washed 2x with 1x PBS (1,000 g, 1-2 min) using an Amicon 30 kD cut-off vial. The concentration is determined at 280 nm (1:100 dilution in 1x PBS). The extinction coefficient of 160,000 $M^{-1}cm^{-1}$ is assumed, as streptavidin consists of four subunits with an extinction coefficient of 40,000 $M^{-1}cm^{-1}$ per domain.

$$\frac{0.001 g \cdot M \cdot cm}{160{,}000 g \cdot ml \cdot 1 cm} = c(Streptavidin) \cdot M$$

10 % Bicine (1 M, pH 9) is added. A 10-fold molar excess of the dye is calculated and slowly added to the protein solution and incubated for 18 min in the dark at RT. In order to avoid protein denaturation caused by DMF, the volume of Cy3.5/DMF must not exceed 10 % of the total volume. The reaction is terminated with 10 mM Tris buffer (0.2 M, pH 6.5) and subsequently incubated for 15 min at RT.

The excess of unbound dye molecules is removed by gel filtration (Protein Desalting Spin Columns, Thermo Scientific, (89862)), according to the manual.

Calculation of final D/P ratio:

$$D/P = \frac{1.13 \cdot A_{581}}{A_{280} - (0.24 \cdot A_{581})}$$

Typically three to four Cy3.5 molecules (Acceptor) should be bound to one protein molecule, in order to be able to quantify the experimentally obtained FRET (Grecco, 2010; Wouters, 1999).

8.3.11 PhosTag labeling with Streptavidin

Streptavidin can be labeled with Cy3.5 in order to use it as an acceptor for PhosTag-FLIM (Karajannis, 2015). Streptavidin consists of four identical subunits. Each of these allows the binding of biotin (Vitamin H). This system shows one of the strongest non-covalent binding affinities in biology (K_a ~ 10^{14}–10^{15} M^{-1}). PhosTag (Phos-tag™BTL-104Wako Pure Chemicals Industries) is a probe which allows the detection of phosphorylated tyrosines, threonines, and serines (figure 52). Originally, it was developed for western blots to detect phosphor-specific bands. Moreover it can be used as a PhosTag-Biotin-Streptavidin complex in fixed cells, where it binds to fluorescent proteins and allows the detection of FRET.

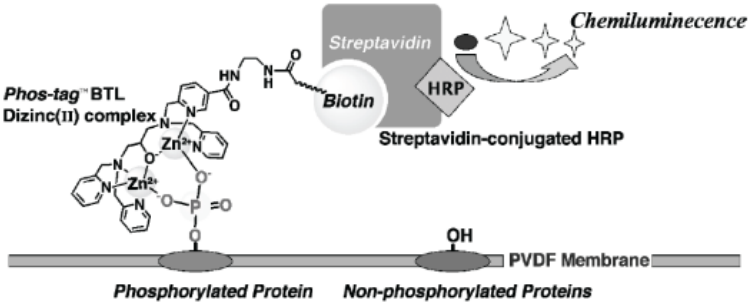

Figure 48: Schematic representation of PhosTag-Biotin bound to phosphorylated protein and Streptavidin. Figure adapted from Wako Pure Chemicals Industries.

For this, 474 µl TBS-T (Tween 0.1 %) are mixed with 20 µl $Zn(NO_3)_2$ (stock: 10 mM), 3 µl PhosTag-Biotin (figure 53) solution and 3 µl prelabeled Streptavidin-Cy3.5 (previous chapter). All ingredients are multiplied by 4, in order to achieve a total volume of 2 ml, mixed and incubated for 30 min at RT. Purification is performed with 5 ml size-exclusion columns (Zeba Spin Desalting Columns, 40 kDa MWKO, Thermo Scientific (87771)).

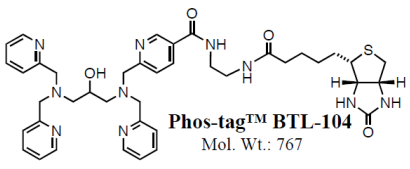

Figure 49: Chemical structure of PhosTag-Biotin

For sample preparation, a Phostag-PB-Cy3.5 ratio of 1:4 in TBS-T is used.

8.4 Studying protein states and activation using fluorescence-based techniques

Fluorescence-based approaches have strongly evolved over the past decades and became useful research tools in many disciplines. Especially in systems and molecular biology, these methods have a great impact and allow nowadays even single-molecule resolution. In 1998, the use of genetically encoded fluorophores (fluorescent proteins, FPs) was introduced and precise targeting of a certain protein was realized (Tsien, 1998). By creating such chimerical fusions, spatial and temporal profiles of proteins of interest can be observed and further used for quantitative research, answering basic questions about localization, function, and activity.

Several parts of the work presented in this thesis are based on state-of-the-art fluorescence microscopy techniques and will be discussed in more details in the following chapters.

8.4.1 Photophysics of fluorescence and FRET

Fluorescence is a random event and defined as the emission of a photon from an electron in the excited state to the ground state (figure 54). The relaxation to the ground state by radiation of a photon (fluorescence) is usually in the ns range.

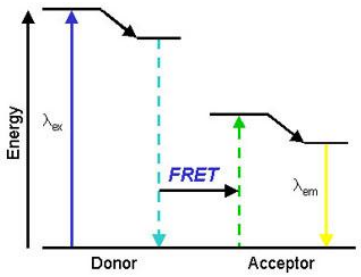

Figure 50: Jabloski diagram, which shows that a donor molecule is excited with light (dark blue), following excitation the donor molecule comes back to the ground state (light blue) and transfers energy without radiation to the acceptor fluorophore, which absorbs the energy (green) and emits light (yellow) that differs from the excitation (red-shifted) [http://www.zeiss.com/C12567BE00472A5C/GraphikTitelIntern/FRETNo_3/$File/FRET-pic03.JPG], 09.03.2015

The Jablonski plot shows that a donor molecule is excited with light (dark blue) while relaxation back to the ground state (light blue), energy is transferred without radiation to the acceptor fluorophore, which absorbs the energy (green) and

emits light (yellow) that differs from the excitation (red-shifted). The non-radiative transfer of energy is called Förster Resonance Energy Transfer (FRET) (Förster 1948) and a result of dipole-dipole coupling of nearby fluorophores. If the transition dipoles of each chromophore oscillate with the same frequency, energy can be resonantly exchanged. The rate of energy transfer k_T depends on the lifetime of the donor (τ), on the Förster radius R_0^6 (usually between 3-9 nm) and the distance r.

$$k_T = \frac{1}{\tau}\left(\frac{R_0}{r}\right)^6$$

With

$$R_0 = 9.78 \cdot 10^3 \left(\kappa^2 \cdot n^{-4} \cdot J(\lambda) \cdot Q_D\right)^{\frac{1}{6}}$$

Where κ^2 is the relative dipole-dipole orientation factor with values between 0 and 4. In the Förster equation it is assumed to be 2/3 for unrestricted isotropic motion. The dipoles have to be parallel oriented for efficient energy transfer. A perpendicular orientation allows no efficient transfer. J(λ) represents the spectral overlap integral between the donor emission and the acceptor excitation spectrum. The quantum yield of the donor Q_D is a measure for the ratio between emitted and absorbed photons and the fluorescence lifetime τ. The index of refraction is represented by n.
For FRET to occur, the emission spectrum of the donor has to overlap with the excitation spectrum of the acceptor (J(λ)). Both fluorophores have to be in close proximity and in the right orientation (κ^2).

If FRET occurs, the energy transfer efficiency E can be calculated. The energy transfer efficiency is the ratio between transferred and absorbed photons by the donor fluorophore and describes a switch-like function (figure 55).

$$E = \frac{k_T}{\tau^{-1} + k_T}$$, replacing k_T

$$E = \frac{R_0^6}{R_0^6 + r^6}$$

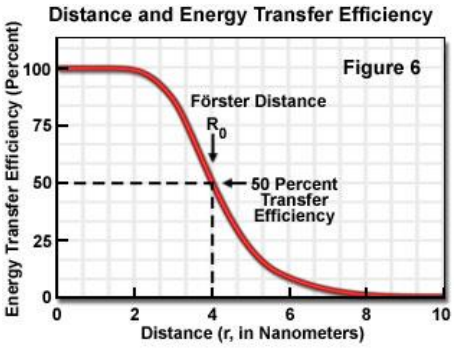

Figure 51: Energy transfer efficiency versus distance shows a switch-like curve. The Förster distance gives 50 % energy transfer efficiency. [http://micro.magnet.fsu.edu, 09.03.2015]

8.4.2 Fluorescence lifetime imaging microscopy (FLIM)

FLIM (Fluorescence Lifetime Imaging Microscopy) (Gadella, 1993; Bastiaens, 1999; Grecco, 2010) is a powerful tool to measure the fluorescence lifetime of a fluorophore and is sensitive to the molecular environment of that fluorophore. FLIM is a well-established method to quantify FRET and thus determine protein-protein interactions or protein conformational changes. In general, the concentration of the probe is not known and within reasonable limits FLIM can be independent of the local probe concentration. Only the intensity of the fluorophore depends on concentration whereas the fluorescence lifetime is mostly independent. Due to the occurrence of FRET and the consequent shortening of the donor lifetime, these measurements imply high signal specificity because only the donor, which is associated to the molecule of interest, is detected.

The donor lifetime τ_D in the excited state is reduced by radiative and non-radiative processes (k_r and k_{nr}) and additionally by the resonance energy transfer rate k_{FRET} if an acceptor is present (τ_F).

.

$$\tau_D = \frac{1}{k_r + k_{nr}} > \tau_F = \frac{1}{k_r + k_{nr} + k_{FRET}}$$

In this work, only data obtained by time-domain FLIM is presented. The time-domain information is obtained by exciting the sample with a discrete optical pulse (LED, picosecond laser) to observe the decay of the fluorescence lifetime. The decay curve can be directly acquired after excitation if the pulse of light is very short. The pulse width is kept preferably much shorter than the decay time

τ of the sample. In case of donor-only samples a single exponential decay is observed:

$$A_i \exp^{-\left(\frac{t}{\tau_D}\right)} + C_i$$

The time-dependent intensity is measured following the excitation pulse and the decay time in mono-exponential functions is calculated from the slope of the semi-logarithmic plot of the intensity versus the time (figure 56).

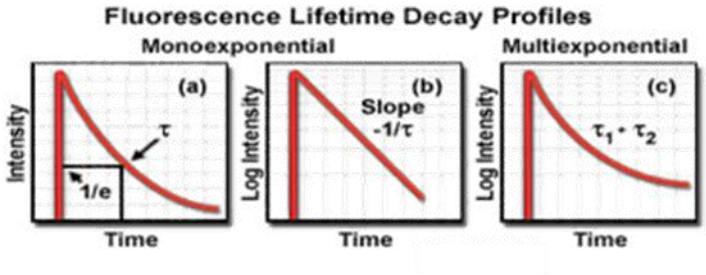

Figure 52: Mono and multi-exponential decays upon excitation; τ_2 represents a second fluorescence lifetime, i.e. donor-acceptor approaches. [http://micro.magnet.fsu.edu/, 09.03.2015]

If two fluorophores undergo FRET there are two different lifetimes present and the intensity decay becomes a double exponential function. Donor molecules interacting with the acceptors have a faster exponential decay, as represented by the second lifetime (τ_F).

$$A_i \exp^{-\left(\frac{t}{\tau_D}\right)} + B_i \exp^{-\left(\frac{t}{\tau_F}\right)} + C_i$$

The lifetime τ is the inverse of the total decay rate hence reflecting the average amount of time a fluorophore remains in the excited state following excitation. τ is determined by the slope or by fitting the data with global data analysis. The pre-exponential coefficients A and B represent the contribution of each population to the total signal. From these coefficients the bound fraction α of donor molecules bound to acceptor molecules can be calculated (Lakowicz, 2006).

$$\alpha = \frac{[DA]}{[D]+[DA]}$$

The approach assumes that two different protein states exist, present in every pixel and associated with a unique donor fluorescence lifetime in the presence (τ_F) or absence (τ_D) of FRET. The average lifetime of donor-only samples and the decreased lifetime due to FRET can be used to calculate the energy transfer efficiency.

$$E = 1 - \frac{\tau_F}{\tau_D}$$

8.4.3 FLIM sample preparation

In general, cells were seeded with an amount of $5 \cdot 10^3$-10^4 cells per well on 8-well Lab-Tek chambers (Nalge Nunc International, Rochester, NY, USA) or with an amount of $2 \cdot 10^4$ cells per well on 4-well Lab-Tek chambers and grown overnight. Higher amounts of cells resulted in confluency and lower transfection efficiency. 24 hours after seeding, transient expression of plasmid DNA was initiated after transfection (Lipofectamine 2000, Invitrogen). The cells were transfected over night with purified plasmid DNA and the transfection efficiency was determined under fluorescent light the day after.

Samples for PhosTag-FLIM are fixated with 4 % Paraformaldehyde for 5-7 minutes at room temperature after inhibitor/doxycycline treatment the cells, washed with 1x TBS (5 min, 10 min, 5 min washing steps) and subsequent permeabilized with 0.1 % Triton-X-100 in 1x TBS for 5 min and then washed at least three times with 1x TBS-T. PhosTag solution is diluted 1:4 with 1x TBS-T and incubated with the sample for 1 h in the dark. All PhosTag stainings are performed with the recommended buffer recipes for PhosTag-biotin.

8.4.4 Confocal-FRET/FLIM data

To acquire confocal TCSPC images, a LSM Upgrade Kit (PicoQuant, Berlin Germany) attached to a Fluoview 1000 (FV-1000) microscope (Olympus Deutschland GmbH, Hamburg, Germany) with a 63x/1.35 NA oil objective is used. For time-domain FLIM measurements, a 507 nm pulsed diode laser (LDH 507, PicoQuant, Berlin, Germany) is used as excitation source (25 ns pulses). Spectral filtering is performed with a narrow-band emission filter (HQ 525/15, Chroma) and a dichroic filter 530/11 HQ (AHF Analysentechnik AG, Tübingen,

Germany) filter, is used to detect the emitted photons using a Single Photon Avalanche Photodiode (SPAD, PDM Series, MPD). FLIM measurements are recorded with the SymPhoTime software (PicoQuant, Berlin, Germany). Each FLIM measurement has a minimum of total 500 photon counts for donor-only samples and in presence of acceptor ~300 photon counts per pixel are acquired.

8.4.5 Global data analysis

FLIM measurements were performed with the SymPhoTime software (PicoQuant, Berlin, Germany) and the resulting .pt3 or .ptu files were subjected to MatLab (Mathworks) based global data analysis. Using a polar plot, the intensity of each pixel, as well as the arrival time of each photon is represented as a cloud on the half circle. This is first performed for donor-only measurements. The mean value of the cloud reflects the average lifetime of the fluorophore in its excited state. The pixel information of D-A images is processed in the same way, whereas α, the bound fraction is represented as a line between the mean value of the donor-only cloud, as well as the D-A cloud (figure 58).

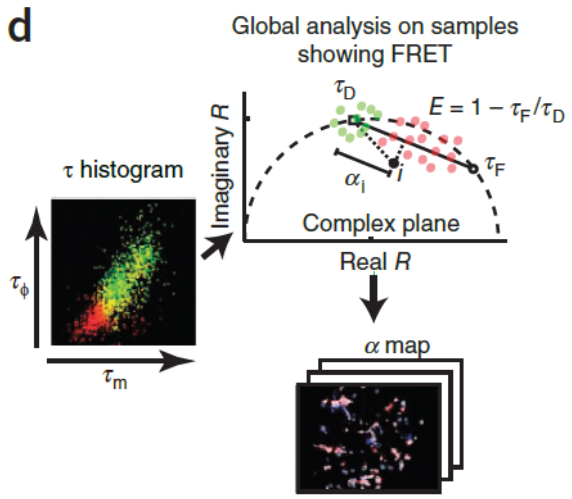

Figure 53: The spatially invariant global lifetimes τ_F and τ_D define the FRET efficiency (E), obtained by a linear fit of the Fourier coefficients (imaginary and real R). Data sets are globally analyzed and α in each pixel is calculated. Figure adapted from Grecco, 2010.

All images are processed in a stack-wise manner. First, all intensity images are corrected for background pixels, using the BG subtraction plugin (ImageJ). Second, masks are generated for each image and then multiplied with the corresponding dc, It, and alpha stacks. The resulting α maps and lifetime images

are set to the same range. The Rainbow smooth colour table was used to display the resulting differences in alpha and lt images.

8.5 Laser Scanning Confocal Microscopy (LSCM)

Confocal images of corresponding FLIM samples of live and fixed cells are obtained with an Olympus FluoView FV1000 confocal laser-scanning microscope. mCitrine is excited with the 488 nm line of a multiline Argon laser and Cy3.5 with the 561 nm line of a DPSS laser. Excitation light is focused into the sample by a 60x/1.35 NA oil objective using either the DM405/488/561/633 or dichroic mirror. Green and Yellow FPs are collected between 498-551 nm and through a SDM 560 for sequential imaging with the 561 nm laser. Live cell imaging was performed in an incubation chamber adjusted to 37 °C, while fixed cells experiments were performed at RT (~30°C).

8.6 Leica SP5

For live cell experiments in inhibitor-treated cells (KRas delocalization studies) and for pan Ras immunostainings, confocal laser scanning microscopy is performed with a Leica TCS SP5 DMI6000 microscope equipped with a HCX PL APO 63x 1.4-.6 NA Blau CS objective and an environment control chamber maintaining 37°C and 5 % CO_2. The excitation wavelength is selected by acousto-optical tunable filters (AOTF) and scanned over the sample at frequencies ranging from 200-600 Hz. The emission signal is passed through a pinhole to control confocality and detected by PTMs (photon multiplier tube), whose sensitivity can be adjusted by manipulating the applied gain voltage. Confocality is controlled by limiting pinhole-size to between 1.0 and 1.5 Airy units. Yellow fluorescent proteins (mCitrine, Alexa488) are excited with the 514 nm Argon line and the emission is filtered between 525-560 nm. In all cases, scanning is performed in line-by-line sequential mode with 2x line averaging.

9 Buffers and Recipes

9.1 PFA preparation

In order to prepare 4 %PFA in PBS, 2 g PFA powder were diluted in 45 ml H_2O. 10 µl 1 N NaOH are added to increase the pH. The whole mixture is heated up to 65°C for 10-20 min and mixed every 2 min. After complete solvation of the powder 5 ml of 10x PBS are added and the liquid is pressed through a sterile filter (pore size 45 µm). PFA is stored at 4°C or as frozen aliquots and protected from light to avoid decomposition of the polymer.

9.2 Lysogeny broth

1 % tryptone (10 g/l)

0.5 % yeast extract (5 g/l)

1 % NaCl (10 g/l)

9.3 Terrific broth (1 liter)

1.2 % tryptone (12 g/L)

2.4 % yeast Extract (24 g/L)

0.94 % (72mM) dipotassium phosphate (K_2P0_4) (9.4 g/L)

0.22 % (17mM) monopotassium phosphate (KH_2P0_4) (2.2 g/L)

0.4 % glycerol (4 g/L)

9.4 SOC medium (1 liter)

0,5 % yeast extract (5 g/l)

2 % tryptone (20 g/l)

10 mM NaCl (0.6 g/l)

2.5 mM KCl (0.2 g/l)

10 mM $MgCl_2$

10 mM $MgSO_4$

20 mM glucose

9.5 Stacking gel

0.5 M Tris buffer, pH6.8

9.6 Separation gel

1.5 M Tris buffer, pH 8.8

9.7 10x TAE

Dissolve 242 g Tris in 500 ml H_2O

Add 100 ml 0.5 M Na_2EDTA (pH 8.0) and 57.1 ml glacial acetic acid

Adjust volume to 1 liter with H_2O

Store at RT

9.8 10x PBS

Dissolve 80 g NaCl, 2 g KCl, 26.8 g Na_2HPO_4-$7H_2O$ and 2.4 g KH_2PO_4 in 800 ml H_2O

Adjust to pH 7.4 with HCl

Adjust volume to 1 liter with H_2O

Divide in aliquots and sterilize if necessary

Store at RT

9.9 1x TBS

Dissolve 6.05 g Tris (50 mM) and 8.76 g NaCl (150 mM) in 800 ml H_2O

Adjust pH to 7.5 with 1 M HCl

Adjust volume to 1 liter with H_2O

Stable for 3 months at 4°C

9.10 1x TBS-T

Dissolve 1 ml Tween 20 in 1 liter 1x TBS buffer

9.11 Lysis buffer (1x RIPA)

1 mL Tris-HCl, pH 7.5 (stock: 200 mM)

1 mL NaCl (stock: 1.5 M)

1 mL Na_2EDTA (stock: 10 mM)

1 mL EGTA (stock: 10 mM)

1 mL Igepal (stock: 10 %)

1 mL Na-deoxycholate (stock: 10 %)

1 mL Na-pyrophosphate (stock: 25 mM)

1 mL β-glycerophosphate (stock: 10 mM)

1 tab complete EDTA-free (for 10 mL) (Roche, (04693132001))

100 µL Inhibitor cocktail II (Sigma Aldrich, (P5726))

100 µL Inhibitor cocktail III (Sigma Aldrich, (P0044))

100 µL SDS (stock: 10 %)

100 µL PMSF (stock: 1 M)

H_2O up to 10 mL

9.12 BioRad 10x running buffer

Dissolve 30 g Tris (250 mM), 144 g Glycine (2 mM) and 10 g SDS in 1 liter H_2O

pH adjustment is not required

Working concentration: 1x → 100 ml stock + 900 ml H_2O

9.13 10x transfer buffer + 20 % MeOH

Dissolve 30 g Tris (250 mM), 144 g Glycine (2 mM) in 1 liter H_2O

pH adjustment is not required

Working concentration: 1x → 100 ml stock + 700 ml H_2O + 200 ml Methanol

9.14 5x SDS sample buffer (10 ml)

0.6 ml 1 M Tris-HCl pH 6.8 (60 mM)

5.0 ml 50 % Glycerol (25 %)

2.0 ml 10 % SDS (2 %)

0.5 ml β-Mercaptoethanol (14.4 mM)

1.0 ml 1 % Bromophenolblue (0.1 %)

0.9 ml ddH_2O

9.15 GST buffer

50 mM Tris (pH 7.5)

5 mM $MgCl_2$

200 mM NaCl

1 % Igepal

5 % Glycerol

9.16 10xTBS, 1 L, pH 7.5, PhosTag buffer

100 mM Tris

1 M NaCl

Distilled water ad 0.9 l

pH adjustment at 7.5 with HCl

Distilled water for preparation of the 1 L solution

9.17 1x TBS-T, PhosTag buffer

Dissolve 1 ml Tween 20 in 1 liter 1x TBS buffer (PhosTag)

9.18 2x HBS buffer 100 ml

10 ml HEPES (0.5 M) pH 7.1

9.3 ml NaCl (3 M)

750µl $NaPO_4$ (0.1 M) pH 7.1

10 Abbreviations

°C	degree Celsius
aa	amino acid(s)
A	acceptor fluorophore
ddH_2O	double distilled water
D	donor fluorophore
ET	energy transfer
EtOH	ethanol
eq	equivalent
h	hour
kDa	kilodalton
min	minute
µl	microliter
M	mole
mM	millimole
µM	micromole
nm	nanometer
nM	nanomole
RT	room temperature
V	Volt

Akt	Ser/Thr protein kinase (UniProt: Q9Y243)
Arf	ADP-ribosylation factor (UniProt: P84077)
Arl2	Arf-like protein 2 (UniProt: P36404)
Arl3	Arf-like protein 3 (UniProt: P36405)
APT	acyl protein thioesterase
ATP	adenosine triphosphate
2-BP	Bromopalmitate, palmitoylation inhibitor
BSA	bovine serum albumin
BTG2	protein for cell cycle control (UniProt: P78534)
CA	cellular automaton
CIAP	calf intestinal alkaline phosphatase

CML	chronic myeloid leukemia
CNK	connector enhancer of kinase suppressor of Ras 1
Cop-1	coat protein 1 (UniProt: P43254)
CRC	colon rectal carcinoma
Cy3.5	organic cyanine dye
Cyclin D	cyclin protein family member, involved in cell cycle progression (UniProt: P30279)
CypB	cyclophilin B (UniProt: Q3KQW3)
DMEM	Dulbecco's Modified Eagle Medium
DMSO	dimethylsulfoxide
DNA	deoxyribonucleic acid
dsDNA	double-stranded DNA
ssDNA	single-standed DNA
dNTP	deoxyribonucleoside triphosphates
Dox	doxycycline
Dpn1	restriction enzyme which cuts methylated DNA
DTT	dithiothreitol
DUSP	dual specificity phosphatase
4E-BP1	eukaryotic initiation factor 4E-binding protein
EDTA	ethylenediaminetetraacetic acid
EGF	Epidermal Growth Factor
EGFR	Epidermal Growth Factor Receptor (UniProt: P00533)
Elk-1	transcription activator protein (UniProt: P19419)
ER	endoplasmic reticulum
Erk2	extracellular-signal regulated kinase, MAPK, (UniProt: P28482)
FACS	Fluorescence Activated Cell Sorting
FCS	fetal calf serum
FLAP	Fluorescence Loss After Photobleaching
FLIM	Fluorescence Lifetime Imaging Microscopy
FRET	Förster Resonance Energy Transfer

FTI	farnesyltransferase inhibitor
Gab1	Grb2-associated-binding protein 1
GAP	GTPase-activating protein
GDP	Guanosine diphosphate
GDI	GDP dissociation inhibitor
GEF	guanine-nucleotide exchange factor
GNBB	guanine nucleotide binding protein
Grb2	growth factor receptor-bound protein 2
GSH	glutathione
GST	glutathion S-transferase
GTP	guanosine-5'-triphosphate
GTPase	hydrolase enzymes, binds and hydrolyzes GTP
HVR	hypervariable region of Ras proteins
Icmt	Protein-S-isoprenylcysteine O-methyltransferase (UniProt: O60725)
JNK	c-Jun N-terminal kinase (UniProt: P53779)
KC	mPDAC 79990, $KRas^{G12D(-/+)}$
KPC	mPDAC 79751, $KRas^{G12D(-/+)}p53^{R270H(-/+)}$
KSR	kinase suppressor of Ras 1
LB	lysogeny broth
LSM	Laser-scanning microscopy
LY294002	PI3K inhibitor
MAPK	mitogen-activated protein kinase, Erk, MAP kinase
MAPKK	Mek, MAP kinase kinase
MAPKKK	Raf, MAP kinase kinase kinase
mCitrine/mCit	monomeric variant of yellow fluorescent protein
mCherry	monomeric variant of red fluorescent protein
MDCK	Madin-Darby canine kidney cells
MDM-2	Mouse double minute 2 homolog, E3 ubiquitin-protein ligase (UniProt: Q00987)

Mek	dual specificity mitogen-activated protein kinase kinase 1, MAPKK, (UniProt: Q02750)
MeOH	methanol
MNK	MAPK-interacting ser/thr kinase
mTor	mammalian target of rapamycin (UniProt: P42345)
Myc	regulator gene, encoding a transcription factor (UniProt: 01106)
Net-1	neuroepithelial cell-transforming gene 1 protein (UniProt: Q7Z628)
NSCLC	non-small cell lung cancer
NTS	nuclear translocation signal
p14/19 Arf	Arf tumor suppressor (UniProt: P42771), p19 is the equivalent in mice
p38 MAPK	mitogen-activated protein kinase (UniProt: Q16539)
p53	tumor suppressor (UniProt: P04637)
p53 RE	p53 responsive element
p73	related to p53, involved in cell cycle (UniProt: O15350)
pan Ras	all Ras isoforms
PAT	palmitoyl transferase
PBS	phosphate buffered saline
PDAC	pancreatic ductal adenocarcinoma
PDE	phosphodiesterase
PDEδ	PDE6D (UniProt: O43924), subunit of PDE
Pdx1	pancreatic progenitor cell gene promoter
PFA	paraformaldehyde
PI3K	phosphoinositide-3 kinase
Pirh-2	ubiquitin-protein ligase
PKC	protein kinase C
PM	plasma membrane
PT	PhosTag
PTB	phosphotyrosine-binding domain

PTEN	phosphatases and tensin homolog (UniProt: P60484)
PTM	post-translational modification
PTP	protein tyrosine phosphatases
PVDF	polyvinyliden difluoride
Rab11	Ras-related protein Rab11A (UniProt: P62491)
Rac	Ras-related C3 botulinum toxin substrate 1 (UniProt: P63000)
Raf	serine/threonine-protein kinase, MAPKKK (UniProt: P15056)
Ras	small GTPase
HRas	Harvey Ras (UniProt: P01112)
NRas	neuroblastoma Ras (UniProt: P01111)
KRas	Kirsten Ras (UniProt: P01116)
RBD	Ras-binding domain of Raf
Rb	retinoblastoma protein (UniProt: P06400)
Rce1	Ras converting enzyme 1, CAAX prenyl protease 2, metalloproteinase (UniProt: Q9Y256)
RE	recycling endosome
RheB	Ras homolog enriched in brain (UniProt: Q15382)
Rho	Ras homolog gene family member A, small GTPase (UniProt: P61586)
RIPA	radioimmunoprecipitation assay buffer
RNAi	RNA interference
RPMI	Roswell Park Memorial Institute medium
RSK	p90-ribosomal-S6-kinase
RTCA	real-time cell analyzer
RTK	receptor tyrosine kinase
SDS	sodium dodecyl sulfate
SEM	standard error of mean
Ser	serine, S
SH2	Src-homology-domain 2
SH3	Src-homology-domain 3

shRNA	small hairpin RNA
Siah-1	E3 ubiquitin-protein ligase 1 (UniProt: Q8IUQ4)
siRNA	small interfering RNA
SOS	son of sevenless (UniProt: Q07899)
SRE	serum-response element
SRF	serum-response factor
TB	terrific broth
TBS	Tris-buffered saline
TCF	ternary complex factor
TCSPC	time-correlated single photon counting
TKi	tyrosine kinase inhibitor
TSC1	Hamartin, Tuberous Sclerosis Complex 1
TSC2	Tuberin, Tuberous Sclerosis Complex 2
Wip-1	protein phosphatases 1D (UniProt: O15297)
wt	wild-type

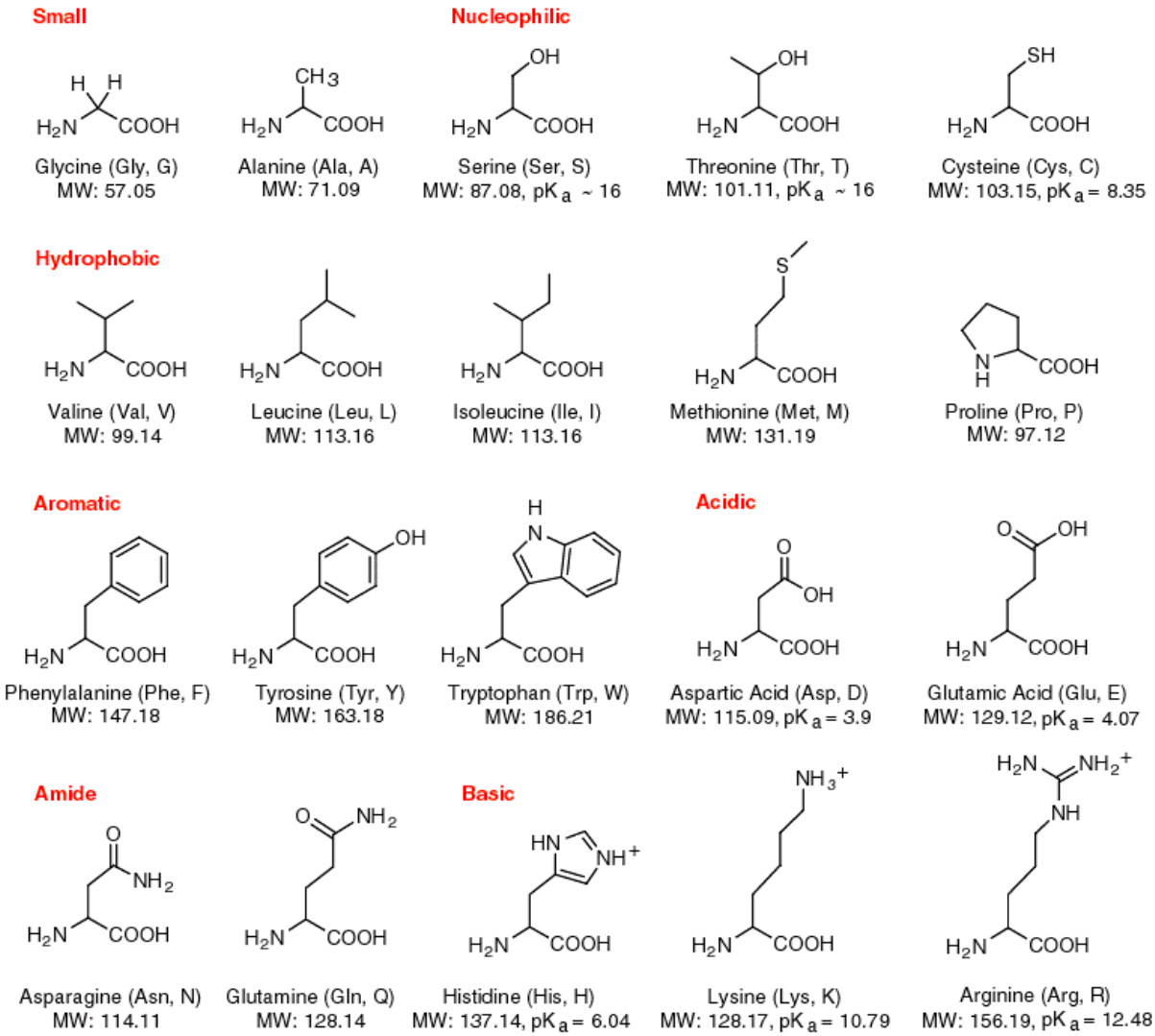

Figure 54: Representation of the 20 proteinogenic amino acids, including the full name and 3- and 1-letter code for each structure. Figure adapted from www.neb.com (24.03.2015)

11 List of figures

12 List of tables

13 Literature

Adachi, Makoto, Makoto Fukuda, and Eisuke Nishida. 1999. “Two Co-Existing Mechanisms for Nuclear Import of MAP Kinase: Passive Diffusion of a Monomer and Active Transport of a Dimer.” *The EMBO Journal* 18 (19): 5347–58.

Adjei, Alex A. 2001. “Blocking Oncogenic Ras Signaling for Cancer Therapy.” *Journal of the National Cancer Institute* 93 (14): 1062–74.

Agarwal, A., C. A. Eide, A. Harlow, A. S. Corbin, M. J. Mauro, B. J. Druker, C. L. Corless, M. C. Heinrich, and M. W. Deininger. 2008. “An Activating KRAS Mutation in Imatinib-Resistant Chronic Myeloid.” *Leukemia* 22 (12): 2269–72. doi:10.1038/leu.2008.124.

Aguirre, Andrew J., Nabeel Bardeesy, Manisha Sinha, Lyle Lopez, David A. Tuveson, James Horner, Mark S. Redston, and Ronald A. DePinho. 2003. “Activated Kras and Ink4a/Arf Deficiency Cooperate to Produce Metastatic Pancreatic Ductal Adenocarcinoma.” *Genes & Development* 17 (24): 3112–26. doi:10.1101/gad.1158703.

Allegra, Carmen J., J. Milburn Jessup, Mark R. Somerfield, Stanley R. Hamilton, Elizabeth H. Hammond, Daniel F. Hayes, Pamela K. McAllister, Roscoe F. Morton, and Richard L. Schilsky. 2009. “American Society of Clinical Oncology Provisional Clinical Opinion: Testing for KRAS Gene Mutations in Patients With Metastatic Colorectal Carcinoma to Predict Response to Anti–Epidermal Growth Factor Receptor Monoclonal Antibody Therapy.” *Journal of Clinical Oncology* 27 (12): 2091–96. doi:10.1200/JCO.2009.21.9170.

Amado, Rafael G., Michael Wolf, Marc Peeters, Eric Van Cutsem, Salvatore Siena, Daniel J. Freeman, Todd Juan, et al. 2008. “Wild-Type KRAS Is Required for Panitumumab Efficacy in Patients With Metastatic Colorectal Cancer.” *Journal of Clinical Oncology* 26 (10): 1626–34. doi:10.1200/JCO.2007.14.7116.

Amit, Ido, Ron Wides, and Yosef Yarden. 2007. “Evolvable Signaling Networks of Receptor Tyrosine Kinases: Relevance of Robustness to Malignancy and to Cancer Therapy.” *Molecular Systems Biology* 3 (1): 151. doi:10.1038/msb4100195.

Anjum, Rana, and John Blenis. 2008. “The RSK Family of Kinases: Emerging Roles in Cellular Signalling.” *Nature Reviews Molecular Cell Biology* 9 (10): 747–58.

Antonarakis, Stylianos, and Linda Van Aelst. 1998. “Mind the GAP, Rho, Rab and GDI.” *Nature Genetics* 19 (2): 106–8. doi:10.1038/450.

Appella, Ettore, and Carl W. Anderson. 2001. “Post-Translational Modifications and Activation of p53 by Genotoxic Stresses.” *European Journal of Biochemistry* 268 (10): 2764–72.

Babij, Carol, Yihong Zhang, Robert J. Kurzeja, Anke Munzli, Amro Shehabeldin, Manory Fernando, Kim Quon, et al. 2011. “STK33 Kinase Activity Is Nonessential in KRAS-Dependent Cancer Cells.” *Cancer Research* 71 (17): 5818–26.

Baehr, Wolfgang, Michael J. Devlin, and Meredithe L. Applebury. 1979. “Isolation and Characterization of cGMP Phosphodiesterase from Bovine Rod Outer Segments.” *J Biol Chem* 254 (22): 11669–77.

Barbacid, M. 1987. “Ras Genes.” *Annual Review of Biochemistry* 56 (1): 779–827. doi:10.1146/annurev.bi.56.070187.004023.

Bardeesy, Nabeel, and Ronald A. DePinho. 2002. “Pancreatic Cancer Biology and Genetics.” *Nature Reviews Cancer* 2 (12): 897–909. doi:10.1038/nrc949.

Bar-Sagi, Dafna. 2001. “A Ras by Any Other Name.” *Molecular and Cellular Biology* 21 (5): 1441–43. doi:10.1128/MCB.21.5.1441-1443.2001.

Bastiaens, Philippe IH, and Anthony Squire. 1999. “Fluorescence Lifetime Imaging Microscopy: Spatial Resolution of Biochemical Processes in the Cell.” *Trends in Cell Biology* 9 (2): 48–52.

Bates, Stewart, Andrew C. Phillips, Paula A. Clark, Francesca Stott, Gordon Peters, Robert L. Ludwig, and Karen H. Vousden. 1998. “p14ARF Links the Tumour Suppressors RB and p53.” *Nature* 395 (6698): 124–25. doi:10.1038/25867.

Batzer, A. G., D. Rotin, J. M. Urena, E. Y. Skolnik, and J. Schlessinger. 1994. “Hierarchy of Binding Sites for Grb2 and Shc on the Epidermal Growth Factor Receptor.” *Molecular and Cellular Biology* 14 (8): 5192–5201.

Bazan, V., M. Migliavacca, I. Zanna, C. Tubiolo, N. Grassi, M. A. Latteri, M. La Farina, et al. 2002. “Specific Codon 13 K-Ras Mutations Are Predictive of Clinical Outcome in Colorectal Cancer Patients, Whereas Codon 12 K-Ras Mutations Are Associated with Mucinous Histotype.” *Annals of Oncology* 13 (9): 1438–46. doi:10.1093/annonc/mdf226.

Bernards, Andre, and Jeffrey Settleman. 2004. “GAP Control: Regulating the Regulators of Small GTPases.” *Trends in Cell Biology* 14 (7): 377–85. doi:10.1016/j.tcb.2004.05.003.

Bieging, Kathryn T., Stephano Spano Mello, and Laura D. Attardi. 2014. “Unravelling Mechanisms of p53-Mediated Tumour Suppression.” *Nature Reviews Cancer* 14 (5): 359–70. doi:10.1038/nrc3711.

Blandino, Giovanni, Arnold J. Levine, and Moshe Oren. 1999. “Mutant p53 Gain of Function: Differential Effects of Different p53 Mutants on Resistance of Cultured Cells to Chemotherapy.” *Oncogene* 18 (2): 477–85.

Blum, Roy, and Yoel Kloog. 2005. “Tailoring Ras-pathway—Inhibitor Combinations for Cancer Therapy.” *Drug Resistance Updates* 8 (6): 369–80. doi:10.1016/j.drup.2005.11.002.

Bohdanowicz, Michal, and Sergio Grinstein. 2013. “Role of Phospholipids in Endocytosis, Phagocytosis, and Macropinocytosis.” *Physiological Reviews* 93 (1): 69–106. doi:10.1152/physrev.00002.2012.

Bonneau, D., and M. Longy. 2000. “Mutations of the Human PTEN Gene.” *Human Mutation* 16 (2): 109–22. doi:10.1002/1098-1004(200008)16:2<109::AID-HUMU3>3.0.CO;2-0.

Bos, Johannes L. 1989. “Ras Oncogenes in Human Cancer: A Review.” *Cancer Research* 49 (17): 4682–89.

Broermann, Petra, Klaus Junker, Burkhard H. Brandt, Achim Heinecke, Lutz Freitag, Folker Klinke, Wolfgang E. Berdel, and Michael Thomas. 2002. “Trimodality Treatment in Stage III Nonsmall Cell Lung Carcinoma.” *Cancer* 94 (7): 2055–62. doi:10.1002/cncr.10387.

Brosh, Ran, and Varda Rotter. 2009. “When Mutants Gain New Powers: News from the Mutant p53 Field.” *Nature Reviews Cancer* 9 (10): 701–13.

Brunet, Anne, DanieLe Roux, Philippe Lenormand, Stephen Dowd, Stephen Keyse, and Jacques Pouysségur. 1999. “Nuclear Translocation of p42/p44 Mitogen-Activated Protein Kinase Is Required for Growth Factor-Induced Gene Expression and Cell Cycle Entry.” *The EMBO Journal* 18 (3): 664–74.

Buchwalter, Gilles, Christian Gross, and Bohdan Wasylyk. 2004. “Ets Ternary Complex Transcription Factors.” *Gene* 324: 1–14.
Campbell, Sharon L., Roya Khosravi-Far, Kent L. Rossman, Geoffrey J. Clark, and Channing J. Der. 1998. “Increasing Complexity of Ras Signaling.” *Oncogene* 17 (11): 1395–1413.
Carón, Rubén W., Adly Yacoub, Min Li, Xiaoyu Zhu, Clint Mitchell, Young Hong, William Hawkins, et al. 2005. “Activated Forms of H-RAS and K-RAS Differentially Regulate Membrane Association of PI3K, PDK-1, and AKT and the Effect of Therapeutic Kinase Inhibitors on Cell Survival.” *Molecular Cancer Therapeutics* 4 (2): 257–70.
Chandra, Anchal, Hernán E. Grecco, Venkat Pisupati, David Perera, Liam Cassidy, Ferdinandos Skoulidis, Shehab A. Ismail, et al. 2012. “The GDI-like Solubilizing Factor PDEδ Sustains the Spatial Organization and Signalling of Ras Family Proteins.” *Nature Cell Biology* 14 (2): 148–58. doi:10.1038/ncb2394.
Ch. A, Omer, N. J. Anthony, C. A. Buser-Doepner, A. L. Burkhardt, S. J. Desolms, Ch J. Dinsmore, J. B. Gibbs, et al. 1997. “Farnesyl$\backslash$:$\backslash$, Proteintransferase Inhibitors as Agents to Inhibit Tumor Growth.” *Biofactors* 6 (3): 359–66.
Choy, Edwin, Vi K. Chiu, Joseph Silletti, Marianna Feoktistov, Takashi Morimoto, David Michaelson, Ivan E. Ivanov, and Mark R. Philips. 1999. “Endomembrane Trafficking of Ras: The CAAX Motif Targets Proteins to the ER and Golgi.” *Cell* 98 (1): 69–80. doi:10.1016/S0092-8674(00)80607-8.
Chuderland, Dana, Alexander Konson, and Rony Seger. 2008. “Identification and Characterization of a General Nuclear Translocation Signal in Signaling Proteins.” *Molecular Cell* 31 (6): 850–61.
Collins, Meredith A., Jean-Christophe Brisset, Yaqing Zhang, Filip Bednar, Josette Pierre, Kevin A. Heist, Craig J. Galban, Stefanie Galban, and Marina Pasca di Magliano. 2012. “Metastatic Pancreatic Cancer Is Dependent on Oncogenic Kras in Mice.” *PLoS ONE* 7 (12). doi:10.1371/journal.pone.0049707.
Collisson, Eric A., Anguraj Sadanandam, Peter Olson, William J. Gibb, Morgan Truitt, Shenda Gu, Janine Cooc, et al. 2011. “Subtypes of Pancreatic Ductal Adenocarcinoma and Their Differing Responses to Therapy.” *Nature Medicine* 17 (4): 500–503. doi:10.1038/nm.2344.
Costa, Mario, Matilde Marchi, Francesco Cardarelli, Anusrhee Roy, Fabio Beltram, Lamberto Maffei, and Gian Michele Ratto. 2006. “Dynamic Regulation of ERK2 Nuclear Translocation and Mobility in Living Cells.” *Journal of Cell Science* 119 (23): 4952–63.
Cox, Adrienne D., and Channing J. Der. 2002. “Ras Family Signaling: Therapeutic Targeting.” *Cancer Biology & Therapy* 1 (6): 599–606.
Crouthamel, Marykate, Manimekalai M. Thiyagarajan, Daniel S. Evanko, and Philip B. Wedegaertner. 2008. “N-Terminal Polybasic Motifs Are Required for Plasma Membrane Localization of Gαs and Gαq.” *Cellular Signalling* 20 (10): 1900–1910. doi:10.1016/j.cellsig.2008.06.019.
Davies, Helen, Graham R. Bignell, Charles Cox, Philip Stephens, Sarah Edkins, Sheila Clegg, Jon Teague, et al. 2002. “Mutations of the BRAF Gene in Human Cancer.” *Nature* 417 (6892): 949–54. doi:10.1038/nature00766.
Dekker, Frank J., Oliver Rocks, Nachiket Vartak, Sascha Menninger, Christian Hedberg, Rengarajan Balamurugan, Stefan Wetzel, et al. 2010. “Small-

Molecule Inhibition of APT1 Affects Ras Localization and Signaling." *Nature Chemical Biology* 6 (6): 449–56. doi:10.1038/nchembio.362.
De Vries, Annemieke, Elsa R. Flores, Barbara Miranda, Harn-Mei Hsieh, Conny Th M. van Oostrom, Julien Sage, and Tyler Jacks. 2002. "Targeted Point Mutations of p53 Lead to Dominant-Negative Inhibition of Wild-Type p53 Function." *Proceedings of the National Academy of Sciences* 99 (5): 2948–53.
Di Nicolantonio, Federica, Miriam Martini, Francesca Molinari, Andrea Sartore-Bianchi, Sabrina Arena, Piercarlo Saletti, Sara De Dosso, et al. 2008. "Wild-Type BRAF Is Required for Response to Panitumumab or Cetuximab in Metastatic Colorectal Cancer." *Journal of Clinical Oncology* 26 (35): 5705–12.
Dittmer, Dirk, Sibani Pati, Gerard Zambetti, Shelley Chu, Angelika K. Teresky, Mary Moore, Cathy Finlay, and Arnold J. Levine. 1993. "Gain of Function Mutations in p53." *Nature Genetics* 4 (1): 42–46.
Downward, Julian. 2003. "Targeting RAS Signalling Pathways in Cancer Therapy." *Nature Reviews Cancer* 3 (1): 11–22. doi:10.1038/nrc969.
Dreusicke, Dirk, and Georg E. Schulz. 1986. "The Glycine-Rich Loop of Adenylate Kinase Forms a Giant Anion Hole." *FEBS Letters* 208 (2): 301–4. doi:10.1016/0014-5793(86)81037-7.
Eberhard, David A., Bruce E. Johnson, Lukas C. Amler, Audrey D. Goddard, Sherry L. Heldens, Roy S. Herbst, William L. Ince, et al. 2005. "Mutations in the Epidermal Growth Factor Receptor and in KRAS Are Predictive and Prognostic Indicators in Patients With Non–Small-Cell Lung Cancer Treated With Chemotherapy Alone and in Combination With Erlotinib." *Journal of Clinical Oncology* 23 (25): 5900–5909. doi:10.1200/JCO.2005.02.857.
Eliyahu, Daniel, Avraham Raz, Peter Gruss, David Givol, and Moshe Oren. 1984. "Participation of P 53 Cellular Tumour Antigen in Transformation of Normal Embryonic Cells." *Nature* 312 (5995): 646–49.
Esser, Dirk, Bettina Bauer, Rob M. F. Wolthuis, Alfred Wittinghofer, Robbert H. Cool, and Peter Bayer. 1998. "Structure Determination of the Ras-Binding Domain of the Ral-Specific Guanine Nucleotide Exchange Factor Rlf†,‡." *Biochemistry* 37 (39): 13453–62. doi:10.1021/bi9811664.
Fedorenko, I. V., G. T. Gibney, and K. S. M. Smalley. 2013. "NRAS Mutant Melanoma: Biological Behavior and Future Strategies for Therapeutic Management." *Oncogene* 32 (25): 3009–18. doi:10.1038/onc.2012.453.
Feig, Larry A. 1999. "Tools of the Trade: Use of Dominant-Inhibitory Mutants of Ras-Family GTPases." *Nature Cell Biology* 1 (2): E25–27. doi:10.1038/10018.
Fisher, Galen H., Shari L. Wellen, David Klimstra, Joi M. Lenczowski, Jay W. Tichelaar, Martin J. Lizak, Jeffrey A. Whitsett, Alan Koretsky, and Harold E. Varmus. 2001. "Induction and Apoptotic Regression of Lung Adenocarcinomas by Regulation of a K-Ras Transgene in the Presence and Absence of Tumor Suppressor Genes." *Genes & Development* 15 (24): 3249–62. doi:10.1101/gad.947701.
Florio, Stephanie K., Rabi K. Prusti, and Joseph A. Beavo. 1996. "Solubilization of Membrane-Bound Rod Phosphodiesterase by the Rod Phosphodiesterase Recombinant Δ Subunit." *Journal of Biological Chemistry* 271 (39): 24036–47. doi:10.1074/jbc.271.39.24036.

Forbes, Simon A., Nidhi Bindal, Sally Bamford, Charlotte Cole, Chai Yin Kok, David Beare, Mingming Jia, et al. 2011. “COSMIC: Mining Complete Cancer Genomes in the Catalogue of Somatic Mutations in Cancer.” *Nucleic Acids Research* 39 (suppl 1): D945–50. doi:10.1093/nar/gkq929.

Forrester, Kathleen, Concepcion Almoguera, Kyuhyung Han, William E. Grizzle, and Manuel Perucho. 1987. “Detection of High Incidence of K-Ras Oncogenes during Human Colon Tumorigenesis.” *Nature* 327 (6120): 298–303. doi:10.1038/327298a0.

Förster, Th. 1948. “Zwischenmolekulare Energiewanderung Und Fluoreszenz.” *Annalen Der Physik* 437 (1-2): 55–75.

Fukuda, Makoto, Yukiko Gotoh, and Eisuke Nishida. 1997. “Interaction of MAP Kinase with MAP Kinase Kinase: Its Possible Role in the Control of Nucleocytoplasmic Transport of MAP Kinase.” *The EMBO Journal* 16 (8): 1901–8.

Fung, Bernard KK, Jennifer H. Young, Harvey K. Yamane, and Irene Griswold-Prenner. 1990. “Subunit Stoichiometry of Retinal Rod cGMP Phosphodiesterase.” *Biochemistry* 29 (11): 2657–64.

Gadella, Theodorus WJ, Thomas M. Jovin, and Robert M. Clegg. 1993. “Fluorescence Lifetime Imaging Microscopy (FLIM): Spatial Resolution of Microstructures on the Nanosecond Time Scale.” *Biophysical Chemistry* 48 (2): 221–39.

Gelb, Michael H. 1997. “Protein Prenylation, et Cetera--Signal Transduction in Two Dimensions.” *Science* 275 (5307): 1750–1750. doi:10.1126/science.275.5307.1750.

Gideon, P, J John, M Frech, A Lautwein, R Clark, J E Scheffler, and A Wittinghofer. 1992. “Mutational and Kinetic Analyses of the GTPase-Activating Protein (GAP)-p21 Interaction: The C-Terminal Domain of GAP Is Not Sufficient for Full Activity.” *Molecular and Cellular Biology* 12 (5): 2050–56.

Gille, Hendrik, and Julian Downward. 1999. “Multiple Ras Effector Pathways Contribute to G1Cell Cycle Progression.” *Journal of Biological Chemistry* 274 (31): 22033–40. doi:10.1074/jbc.274.31.22033.

Gillespie, P. G., and J. A. Beavo. 1989. “cGMP Is Tightly Bound to Bovine Retinal Rod Phosphodiesterase.” *Proceedings of the National Academy of Sciences* 86 (11): 4311–15.

Goodwin, J. Shawn, Kimberly R. Drake, Carl Rogers, Latasha Wright, Jennifer Lippincott-Schwartz, Mark R. Philips, and Anne K. Kenworthy. 2005. “Depalmitoylated Ras Traffics to and from the Golgi Complex via a Nonvesicular Pathway.” *The Journal of Cell Biology* 170 (2): 261–72. doi:10.1083/jcb.200502063.

Grecco, Hernán E., Pedro Roda-Navarro, Andreas Girod, Jian Hou, Thomas Frahm, Dina C. Truxius, Rainer Pepperkok, Anthony Squire, and Philippe I. H. Bastiaens. 2010. “In Situ Analysis of Tyrosine Phosphorylation Networks by FLIM on Cell Arrays.” *Nature Methods* 7 (6): 467–72. doi:10.1038/nmeth.1458.

Hancock, John F., Anthony I. Magee, Julie E. Childs, and Christopher J. Marshall. 1989. “All Ras Proteins Are Polyisoprenylated but Only Some Are Palmitoylated.” *Cell* 57 (7): 1167–77. doi:10.1016/0092-8674(89)90054-8.

Hancock, John F., Hugh Paterson, and Christopher J. Marshall. 1990. “A Polybasic Domain or Palmitoylation Is Required in Addition to the CAAX Motif

to Localize p21ras to the Plasma Membrane." *Cell* 63 (1): 133–39. doi:10.1016/0092-8674(90)90294-O.
Hanzal-Bayer, Michael, Marco Linari, and Alfred Wittinghofer. 2005. "Properties of the Interaction of Arf-like Protein 2 with PDEδ." *Journal of Molecular Biology* 350 (5): 1074–82. doi:10.1016/j.jmb.2005.05.036.
Hanzal-Bayer, Michael, Louis Renault, Pietro Roversi, Alfred Wittinghofer, and Roman C. Hillig. 2002. "The Complex of Arl2-GTP and PDEδ: From Structure to Function." *The EMBO Journal* 21 (9): 2095–2106.
Harris, Curtis C., and Monica Hollstein. 1993. "Clinical Implications of the p53 Tumor-Suppressor Gene." *New England Journal of Medicine* 329 (18): 1318–27.
Harris, Sandra L., and Arnold J. Levine. 2005. "The p53 Pathway: Positive and Negative Feedback Loops." *Oncogene* 24 (17): 2899–2908. doi:10.1038/sj.onc.1208615.
Harvey, Christopher D., Anka G. Ehrhardt, Cristina Cellurale, Haining Zhong, Ryohei Yasuda, Roger J. Davis, and Karel Svoboda. 2008. "A Genetically Encoded Fluorescent Sensor of ERK Activity." *Proceedings of the National Academy of Sciences* 105 (49): 19264–69. doi:10.1073/pnas.0804598105.
Harvey, J. J. 1964. "An Unidentified Virus Which Causes the Rapid Production of Tumours in Mice." *Nature* 204 (4963): 1104–5. doi:10.1038/2041104b0.
Hayflick, L. 1965. "The Limited in Vitro Lifetime of Human Diploid Cell Strains." *Experimental Cell Research* 37 (3): 614–36. doi:10.1016/0014-4827(65)90211-9.
Hay, Nissim, and Nahum Sonenberg. 2004. "Upstream and Downstream of mTOR." *Genes & Development* 18 (16): 1926–45. doi:10.1101/gad.1212704.
Heo, Won Do, Takanari Inoue, Wei Sun Park, Man Lyang Kim, Byung Ouk Park, Thomas J. Wandless, and Tobias Meyer. 2006. "PI(3,4,5)P3 and PI(4,5)P2 Lipids Target Proteins with Polybasic Clusters to the Plasma Membrane." *Science* 314 (5804): 1458–61. doi:10.1126/science.1134389.
Hermann, Patrick C., Stephan L. Huber, Tanja Herrler, Alexandra Aicher, Joachim W. Ellwart, Markus Guba, Christiane J. Bruns, and Christopher Heeschen. 2007. "Distinct Populations of Cancer Stem Cells Determine Tumor Growth and Metastatic Activity in Human Pancreatic Cancer." *Cell Stem Cell* 1 (3): 313–23. doi:10.1016/j.stem.2007.06.002.
Hezel, Aram F., Alec C. Kimmelman, Ben Z. Stanger, Nabeel Bardeesy, and Ronald A. DePinho. 2006. "Genetics and Biology of Pancreatic Ductal Adenocarcinoma." *Genes & Development* 20 (10): 1218–49. doi:10.1101/gad.1415606.
Hingorani, Sunil R., Emanuel F. Petricoin III, Anirban Maitra, Vinodh Rajapakse, Catrina King, Michael A. Jacobetz, Sally Ross, et al. 2003. "Preinvasive and Invasive Ductal Pancreatic Cancer and Its Early Detection in the Mouse." *Cancer Cell* 4 (6): 437–50. doi:10.1016/S1535-6108(03)00309-X.
Hingorani, Sunil R., Lifu Wang, Asha S. Multani, Chelsea Combs, Therese B. Deramaudt, Ralph H. Hruban, Anil K. Rustgi, Sandy Chang, and David A. Tuveson. 2005. "Trp53R172H and KrasG12D Cooperate to Promote Chromosomal Instability and Widely Metastatic Pancreatic Ductal Ade-

nocarcinoma in Mice." *Cancer Cell* 7 (5): 469–83. doi:10.1016/j.ccr.2005.04.023.
Hougland, James L., and Carol A. Fierke. 2009. "Getting a Handle on Protein Prenylation." *Nature Chemical Biology* 5 (4): 197–98. doi:10.1038/nchembio0409-197.
Hruban, R. H., A. D. van Mansfeld, G. J. Offerhaus, D. H. van Weering, D. C. Allison, S. N. Goodman, T. W. Kensler, K. K. Bose, J. L. Cameron, and J. L. Bos. 1993. "K-Ras Oncogene Activation in Adenocarcinoma of the Human Pancreas. A Study of 82 Carcinomas Using a Combination of Mutant-Enriched Polymerase Chain Reaction Analysis and Allele-Specific Oligonucleotide Hybridization." *The American Journal of Pathology* 143 (2): 545–54.
Huang, H., J. Daniluk, Y. Liu, J. Chu, Z. Li, B. Ji, and C. D. Logsdon. 2014. "Oncogenic K-Ras Requires Activation for Enhanced Activity." *Oncogene* 33 (4): 532–35. doi:10.1038/onc.2012.619.
Hu, Jiancheng, Edward C. Stites, Haiyang Yu, Elizabeth A. Germino, Hiruy S. Meharena, Philip JS Stork, Alexandr P. Kornev, Susan S. Taylor, and Andrey S. Shaw. 2013. "Allosteric Activation of Functionally Asymmetric RAF Kinase Dimers." *Cell* 154 (5): 1036–46.
Hupp, T. R., D. W. Meek, C. A. Midgley, and D. P. Lane. 1992. "Regulation of the Specific DNA Binding Function of p53." *Cell* 71 (5): 875–86.
Inoki, Ken, Yong Li, Tianquan Zhu, Jun Wu, and Kun-Liang Guan. 2002. "TSC2 Is Phosphorylated and Inhibited by Akt and Suppresses mTOR Signalling." *Nature Cell Biology* 4 (9): 648–57. doi:10.1038/ncb839.
Ireland, Christine M. 1989. "Activated N-Ras Oncogenes in Human Neuroblastoma." *Cancer Research* 49 (20): 5530–33.
Ismail, Shehab A., Yong-Xiang Chen, Alexandra Rusinova, Anchal Chandra, Martin Bierbaum, Lothar Gremer, Gemma Triola, Herbert Waldmann, Philippe I. H. Bastiaens, and Alfred Wittinghofer. 2011. "Arl2-GTP and Arl3-GTP Regulate a GDI-like Transport System for Farnesylated Cargo." *Nature Chemical Biology* 7 (12): 942–49. doi:10.1038/nchembio.686.
Jayaraman, Lata, and Carol Prives. 1995. "Activation of p53 Sequence-Specific DNA Bindingby Short Single Strands of DNA Requires the p53 C-Terminus." *Cell* 81 (7): 1021–29.
Jewell, Jenna L., Ryan C. Russell, and Kun-Liang Guan. 2013. "Amino Acid Signalling Upstream of mTOR." *Nature Reviews Molecular Cell Biology* 14 (3): 133–39.
Jin, Shengkan, and Arnold J. Levine. 2001. "The p53 Functional Circuit." *Journal of Cell Science* 114 (23): 4139–40.
John, Jacob, Matthias Frech, and Alfred Wittinghofer. 1988. "Biochemical Properties of Ha-Ras Encoded p21 Mutants and Mechanism of the Autophosphorylation Reaction." *Journal of Biological Chemistry* 263 (24): 11792–99.
Johnson, Leisa, Doron Greenbaum, Karen Cichowski, Kim Mercer, Elizabeth Murphy, Eric Schmitt, Roderick T. Bronson, et al. 1997. "K-Ras Is an Essential Gene in the Mouse with Partial Functional Overlap with N-Ras." *Genes & Development* 11 (19): 2468–81. doi:10.1101/gad.11.19.2468.
Jorissen, Robert N., Francesca Walker, Normand Pouliot, Thomas PJ Garrett, Colin W. Ward, and Antony W. Burgess. 2003. "Epidermal Growth Factor Receptor: Mechanisms of Activation and Signalling." *Experimental Cell Research* 284 (1): 31–53.

Kaelin, William G. 2005. “The Concept of Synthetic Lethality in the Context of Anticancer Therapy.” *Nature Reviews Cancer* 5 (9): 689–98. doi:10.1038/nrc1691.
Karajannis et al., 2015 (in preparation)
Karnoub, Antoine E., and Robert A. Weinberg. 2008. “Ras Oncogenes: Split Personalities.” *Nature Reviews Molecular Cell Biology* 9 (7): 517–31. doi:10.1038/nrm2438.
Katzel, Jed A., Michael P. Fanucchi, and Zujun Li. 2009. “Recent Advances of Novel Targeted Therapy in Non-Small Cell Lung Cancer.” *J Hematol Oncol* 2 (2): E4.
Khokhlatchev, Andrei V., Bertram Canagarajah, Julie Wilsbacher, Megan Robinson, Mark Atkinson, Elizabeth Goldsmith, and Melanie H. Cobb. 1998. “Phosphorylation of the MAP Kinase ERK2 Promotes Its Homodimerization and Nuclear Translocation.” *Cell* 93 (4): 605–15.
Kholodenko, Boris N. 2006. “CELL SIGNALLING DYNAMICS IN TIME AND SPACE.” *Nature Reviews. Molecular Cell Biology* 7 (3): 165–76. doi:10.1038/nrm1838.
Kitano, Hiroaki. 2004. “Biological Robustness.” *Nature Reviews Genetics* 5 (11): 826–37. doi:10.1038/nrg1471.
Koera, Keiko, Kenji Nakamura, Kazuki Nakao, Jun Miyoshi, Kumao Toyoshima, Toshihisa Hatta, Hiroki Otani, Atsu Aiba, and Motoya Katsuki. 1997. “K-Ras Is Essential for the Development of the Mouse Embryo.” *Oncogene* 15 (10): 1151–59.
Kolch, Walter. 2000. “Meaningful Relationships: The Regulation of the Ras/Raf/MEK/ERK Pathway by Protein Interactions.” *Biochem. J* 351: 289–305.
Kranenburg, Onno. 2005. “The KRAS Oncogene: Past, Present, and Future.” *Biochimica et Biophysica Acta (BBA) - Reviews on Cancer*, The KRAS Oncogene, 1756 (2): 81–82. doi:10.1016/j.bbcan.2005.10.001.
“K-Ras Is Essential for the Development of the Mouse Embryo.” 1997. *, Published Online: 03 September 1997; | doi:10.1038/sj.onc.1201284* 15 (10). doi:10.1038/sj.onc.1201284.
Lahav, Galit, Nitzan Rosenfeld, Alex Sigal, Naama Geva-Zatorsky, Arnold J. Levine, Michael B. Elowitz, and Uri Alon. 2004. “Dynamics of the p53-Mdm2 Feedback Loop in Individual Cells.” *Nature Genetics* 36 (2): 147–50.
Lakowicz, Joseph R., ed. 2006. *Principles of Fluorescence Spectroscopy*. Boston, MA: Springer US. http://link.springer.com/10.1007/978-0-387-46312-4.
Lane, D. P., and L. V. Crawford. 1979. “T Antigen Is Bound to a Host Protein in SY40-Transformed Cells.” http://www.nature.com/articles/278261a0.
Lavigueur, A. S., V. Maltby, D. Mock, J. Rossant, T. Pawson, and A. Bernstein. 1989. “High Incidence of Lung, Bone, and Lymphoid Tumors in Transgenic Mice Overexpressing Mutant Alleles of the p53 Oncogene.” *Molecular and Cellular Biology* 9 (9): 3982–91.
Lemmon, Mark A., and Joseph Schlessinger. 2010. “Cell Signaling by Receptor Tyrosine Kinases.” *Cell* 141 (7): 1117–34. doi:10.1016/j.cell.2010.06.011.
Lerner, EC, AD Hamilton, and SM Sebti. 1997. “Mini-Review. Inhibition of Ras Prenylation: A Signaling Target for Novel Anti-Cancer Drug Design.” *Anti-Cancer Drug Design* 12 (4): 229–38.

Liao, Jinhui, Janice C. Wolfman, and Alan Wolfman. 2003. “K-Ras Regulates the Steady-State Expression of Matrix Metalloproteinase 2 in Fibroblasts.” *Journal of Biological Chemistry* 278 (34): 31871–78. doi:10.1074/jbc.M301931200.

Lidke, Diane S., Fang Huang, Janine N. Post, Bernd Rieger, Julie Wilsbacher, James L. Thomas, Jacques Pouysségur, Thomas M. Jovin, and Philippe Lenormand. 2010. “ERK Nuclear Translocation Is Dimerization-Independent but Controlled by the Rate of Phosphorylation.” *Journal of Biological Chemistry* 285 (5): 3092–3102.

Lièvre, Astrid, Jean-Baptiste Bachet, Delphine Le Corre, Valérie Boige, Bruno Landi, Jean-François Emile, Jean-François Côté, et al. 2006. “KRAS Mutation Status Is Predictive of Response to Cetuximab Therapy in Colorectal Cancer.” *Cancer Research* 66 (8): 3992–95. doi:10.1158/0008-5472.CAN-06-0191.

Linari, Marco, Michael Hanzal-Bayer, and Jörg Becker. 1999. “The Delta Subunit of Rod Specific Cyclic GMP Phosphodiesterase, PDE Δ, Interacts with the Arf-like Protein Arl3 in a GTP Specific Manner.” *FEBS Letters* 458 (1): 55–59.

Li, Ning, Stephanie K. Florio, Mark J. Pettenati, P. Nagesh Rao, Joseph A. Beavo, and Wolfgang Baehr. 1998. “Characterization of Human and Mouse Rod cGMP Phosphodiesterase Δ Subunit (PDE6D) and Chromosomal Localization of the Human Gene.” *Genomics* 49 (1): 76–82. doi:10.1006/geno.1998.5210.

Liu, D. P., Hoseok Song, and Yang Xu. 2010. “A Common Gain of Function of p53 Cancer Mutants in Inducing Genetic Instability.” *Oncogene* 29 (7): 949–56.

Lorentzen, Anna, Ali Kinkhabwala, Oliver Rocks, Nachiket Vartak, and Philippe I. H. Bastiaens. 2010. “Regulation of Ras Localization by Acylation Enables a Mode of Intracellular Signal Propagation.” *Science Signaling* 3 (140): ra68–ra68. doi:10.1126/scisignal.20001370.

Lowe, Scott W, and Charles J Sherr. 2003. “Tumor Suppression by Ink4a–Arf: Progress and Puzzles.” *Current Opinion in Genetics & Development* 13 (1): 77–83. doi:10.1016/S0959-437X(02)00013-8.

Luo, Ji, Brendan D. Manning, and Lewis C. Cantley. 2003. “Targeting the PI3K-Akt Pathway in Human Cancer: Rationale and Promise.” *Cancer Cell* 4 (4): 257–62.

Malumbres, Marcos, and Mariano Barbacid. 2003. “RAS Oncogenes: The First 30 Years.” *Nature Reviews Cancer* 3 (6): 459–65. doi:10.1038/nrc1097.

Marte, Barbara M., Pablo Rodriguez-Viciana, Stefan Wennström, Patricia H. Warne, and Julian Downward. 1997. “R-Ras Can Activate the Phosphoinositide 3-Kinase but Not the MAP Kinase Arm of the Ras Effector Pathways.” *Current Biology* 7 (1): 63–71. doi:10.1016/S0960-9822(06)00028-5.

Martin, Dale D. O., Erwan Beauchamp, and Luc G. Berthiaume. 2011. “Post-Translational Myristoylation: Fat Matters in Cellular Life and Death.” *Biochimie*, Bioactive Lipids, Nutrition and Health, 93 (1): 18–31. doi:10.1016/j.biochi.2010.10.018.

Marusyk, Andriy, and James DeGregori. 2008. “Declining Cellular Fitness with Age Promotes Cancer Initiation by Selecting for Adaptive Oncogenic Mutations.” *Biochimica et Biophysica Acta* 1785 (1): 1–11. doi:10.1016/j.bbcan.2007.09.001.

Massarelli, Erminia, Marileila Varella-Garcia, Ximing Tang, Ana C. Xavier, Natalie C. Ozburn, Diane D. Liu, Benjamin N. Bekele, Roy S. Herbst, and Ignacio I. Wistuba. 2007. “KRAS Mutation Is an Important Predictor of Resistance to Therapy with Epidermal Growth Factor Receptor Tyrosine Kinase Inhibitors in Non–small-Cell Lung Cancer.” *Clinical Cancer Research* 13 (10): 2890–96.

McCormick, F. 1989. “Ras GTPase Activating Protein: Signal Transmitter and Signal Terminator.” *Cell* 56 (1): 5–8.

McGrath, John P., Daniel J. Capon, Douglas H. Smith, Ellson Y. Chen, Peter H. Seeburg, David V. Goeddel, and Arthur D. Levinson. 1983. “Structure and Organization of the Human Ki-Ras Proto-Oncogene and a Related Processed Pseudogene.” *Nature* 304 (5926): 501–6. doi:10.1038/304501a0.

Milenkovic, Ljiljana, and Matthew P. Scott. 2010. “Not Lost in Space: Trafficking in the Hedgehog Signaling Pathway.” *Science Signaling* 3 (117): pe14. doi:10.1126/scisignal.3117pe14.

Morales, Eva, Miquel Porta, Jesús Vioque, Tomás López, Michelle A. Mendez, José Pumarega, Núria Malats, et al. 2007. “Food and Nutrient Intakes and K-Ras Mutations in Exocrine Pancreatic Cancer.” *Journal of Epidemiology and Community Health* 61 (7): 641–49. doi:10.1136/jech.2007.060632.

Morrison, Deborah K., and Richard E. Cutler. 1997. “The Complexity of Raf-1 Regulation.” *Current Opinion in Cell Biology* 9 (2): 174–79.

Morton, Jennifer P., Paul Timpson, Saadia A. Karim, Rachel A. Ridgway, Dimitris Athineos, Brendan Doyle, Nigel B. Jamieson, et al. 2010. “Mutant p53 Drives Metastasis and Overcomes Growth Arrest/senescence in Pancreatic Cancer.” *Proceedings of the National Academy of Sciences of the United States of America* 107 (1): 246–51. doi:10.1073/pnas.0908428107.

Murphy, Leon O., Sallie Smith, Rey-Huei Chen, Diane C. Fingar, and John Blenis. 2002. “Molecular Interpretation of ERK Signal Duration by Immediate Early Gene Products.” *Nature Cell Biology* 4 (8): 556–64.

Nancy, Vanessa, Isabelle Callebaut, Ahmed El Marjou, and Jean de Gunzburg. 2002. “The Δ Subunit of Retinal Rod cGMP Phosphodiesterase Regulates the Membrane Association of Ras and Rap GTPases.” *Journal of Biological Chemistry* 277 (17): 15076–84.

Nan, Xiaolin, Eric A. Collisson, Sophia Lewis, Jing Huang, Tanja M. Tamgüney, Jan T. Liphardt, Frank McCormick, Joe W. Gray, and Steven Chu. 2013. “Single-Molecule Superresolution Imaging Allows Quantitative Analysis of RAF Multimer Formation and Signaling.” *Proceedings of the National Academy of Sciences* 110 (46): 18519–24.

Norton, J. D., F. Cook, P. C. Roberts, J. P. Clewley, and R. J. Avery. 1984. “Expression of Kirsten Murine Sarcoma Virus in Transformed Nonproducer and Revertant NIH/3T3 Cells: Evidence for Cell-Mediated Resistance to a Viral Oncogene in Phenotypic Reversion.” *Journal of Virology* 50 (2): 439–44.

Olive, Kenneth P., Michael A. Jacobetz, Christian J. Davidson, Aarthi Gopinathan, Dominick McIntyre, Davina Honess, Basetti Madhu, et al. 2009. “Inhibition of Hedgehog Signaling Enhances Delivery of Chemotherapy in a Mouse Model of Pancreatic Cancer.” *Science (New York, N.Y.)* 324 (5933): 1457–61. doi:10.1126/science.1171362.

Olive, Kenneth P., David A. Tuveson, Zachary C. Ruhe, Bob Yin, Nicholas A. Willis, Roderick T. Bronson, Denise Crowley, and Tyler Jacks. 2004. “Mutant p53 Gain of Function in Two Mouse Models of Li-Fraumeni Syndrome.” *Cell* 119 (6): 847–60. doi:10.1016/j.cell.2004.11.004.

Omer, Charles A., and Nancy E. Kohl. 1997. “CA 1 A 2 X-Competitive Inhibitors of Farnesyltransferase as Anti-Cancer Agents.” *Trends in Pharmacological Sciences* 18 (11): 437–45.

Otori, K., Y. Oda, K. Sugiyama, T. Hasebe, K. Mukai, T. Fujii, H. Tajiri, S. Yoshida, S. Fukushima, and H. Esumi. 1997. “High Frequency of K-Ras Mutations in Human Colorectal Hyperplastic Polyps.” *Gut* 40 (5): 660–63. doi:10.1136/gut.40.5.660.

Owens, D. M., and S. M. Keyse. 2007. “Differential Regulation of MAP Kinase Signalling by Dual-Specificity Protein Phosphatases.” *Oncogene* 26 (22): 3203–13.

Paduch, M., F. Jeleń, and J. Otlewski. 2001. “Structure of Small G Proteins and Their Regulators.” *Acta Biochimica Polonica* 48 (4): 829–50.

Pan, Y. H. Laurie, Edwin O. Nuzum, Laurie A. Hanson, and David G. Beer. 1990. “Ki-Ras Activation and Expression in Transformed Mouse Lung Cell Lines.” *Molecular Carcinogenesis* 3 (5): 279–86. doi:10.1002/mc.2940030508.

Papke, B., Murarka, S., Vogel, H. A., Martín-Gago, P., Truxius, D. C., Kovacevic, M., Fansa, E. K., Ismail, S., Zimmermann, G., Heinelt, K., Schultz-Fademrecht, C., Al Saabi, A., Baumann, M., Nussbaumer, P., Wittinghofer, A., Waldmann, H., Bastiaens, P. I. H. 2015 “Identification of Pyrazolopyridazinones as KRas-PDEδ Inhibitors.“ *Nature Communications* (in revision)

Parada, Luis F., Hartmut Land, Robert A. Weinberg, David Wolf, and Varda Rotter. 1984. “Cooperation between Gene Encoding p53 Tumour Antigen and.” *Nature* 312: 13.

Parada, Luis F., Clifford J. Tabin, Chiaho Shih, and Robert A. Weinberg. 1982. “Human EJ Bladder Carcinoma Oncogene Is Homologue of Harvey Sarcoma Virus Ras Gene.” *Nature* 297 (5866): 474–78. doi:10.1038/297474a0.

Pearson, Gray, Fred Robinson, Tara Beers Gibson, Bing-e Xu, Mahesh Karandikar, Kevin Berman, and Melanie H. Cobb. 2001. “Mitogen-Activated Protein (MAP) Kinase Pathways: Regulation and Physiological Functions.” *Endocrine Reviews* 22 (2): 153–83. doi:10.1210/edrv.22.2.0428.

Petitjean, A., M. I. W. Achatz, A. L. Borresen-Dale, P. Hainaut, and M. Olivier. 2007. “TP53 Mutations in Human Cancers: Functional Selection and Impact on Cancer Prognosis and Outcomes.” *Oncogene* 26 (15): 2157–65. doi:10.1038/sj.onc.1210302.

Popescu, N. C., S. C. Amsbaugh, J. A. DiPaolo, S. R. Tronick, S. A. Aaronson, and D. C. Swan. 1985. “Chromosomal Localization of Three Human Ras Genes by in Situ Molecular Hybridization.” *Somatic Cell and Molecular Genetics* 11 (2): 149–55.

Porta, M., N. Malats, L. Guarner, A. Carrato, J. Rifà, A. Salas, J. M. Corominas, M. Andreu, and F. X. Real. 1999. “Association between Coffee Drinking and K-Ras Mutations in Exocrine Pancreatic Cancer. PANKRAS II Study Group.” *Journal of Epidemiology and Community Health* 53 (11): 702–9. doi:10.1136/jech.53.11.702.

Poulin, Francis, Anne-Claude Gingras, Henrik Olsen, Simone Chevalier, and Nahum Sonenberg. 1998. “4E-BP3, a New Member of the Eukaryotic Initiation Factor 4E-Binding Protein Family.” *Journal of Biological Chemistry* 273 (22): 14002–7. doi:10.1074/jbc.273.22.14002.

Prior, Ian A., Paul D. Lewis, and Carla Mattos. 2012. “A Comprehensive Survey of Ras Mutations in Cancer.” *Cancer Research* 72 (10): 2457–67.

Privé, G. G., M. V. Milburn, L. Tong, A. M. de Vos, Z. Yamaizumi, S. Nishimura, and S. H. Kim. 1992. “X-Ray Crystal Structures of Transforming p21 Ras Mutants Suggest a Transition-State Stabilization Mechanism for GTP Hydrolysis.” *Proceedings of the National Academy of Sciences* 89 (8): 3649–53. doi:10.1073/pnas.89.8.3649.

Quatela, Steven E., Pamela J. Sung, Ian M. Ahearn, Trever G. Bivona, and Mark R. Philips. 2008. “Analysis of K-Ras Phosphorylation, Translocation, and Induction of Apoptosis.” In *Methods in Enzymology*, edited by Channing J. Der and Alan Hall William E. Balch, 439:87–102. Small GTPases in Disease, Part B. Academic Press. http://www.sciencedirect.com/science/article/pii/S0076687907004077.

Rajalingam, Krishnaraj, Ralf Schreck, Ulf R. Rapp, and Štefan Albert. 2007. “Ras Oncogenes and Their Downstream Targets.” *Biochimica et Biophysica Acta (BBA) - Molecular Cell Research*, Mitogen-Activated Protein Kinases: New Insights on Regulation, Function and Role in Human Disease, 1773 (8): 1177–95. doi:10.1016/j.bbamcr.2007.01.012.

Raman, M., W. Chen, and M. H. Cobb. 2007. “Differential Regulation and Properties of MAPKs.” *Oncogene* 26 (22): 3100–3112. doi:10.1038/sj.onc.1210392.

Riley, Todd, Eduardo Sontag, Patricia Chen, and Arnold Levine. 2008. “Transcriptional Control of Human p53-Regulated Genes.” *Nature Reviews Molecular Cell Biology* 9 (5): 402–12.

Rocks, Oliver, Marc Gerauer, Nachiket Vartak, Sebastian Koch, Zhi-Ping Huang, Markos Pechlivanis, Jürgen Kuhlmann, et al. 2010. “The Palmitoylation Machinery Is a Spatially Organizing System for Peripheral Membrane Proteins.” *Cell* 141 (3): 458–71. doi:10.1016/j.cell.2010.04.007.

Rocks, Oliver, Anna Peyker, and Philippe IH Bastiaens. 2006. “Spatio-Temporal Segregation of Ras Signals: One Ship, Three Anchors, Many Harbors.” *Current Opinion in Cell Biology*, Membranes and organelles, 18 (4): 351–57. doi:10.1016/j.ceb.2006.06.007.

Rocks, Oliver, Anna Peyker, Martin Kahms, Peter J. Verveer, Carolin Koerner, Maria Lumbierres, Jürgen Kuhlmann, Herbert Waldmann, Alfred Wittinghofer, and Philippe I. H. Bastiaens. 2005. “An Acylation Cycle Regulates Localization and Activity of Palmitoylated Ras Isoforms.” *Science* 307 (5716): 1746–52. doi:10.1126/science.1105654.

Rozenblum, Ester, Mieke Schutte, Michael Goggins, Stephan A. Hahn, Shawn Panzer, Marianna Zahurak, Steven N. Goodman, et al. 1997. “Tumor-Suppressive Pathways in Pancreatic Carcinoma.” *Cancer Research* 57 (9): 1731–34.

Samuels, Yardena, Luis A. Diaz, Oleg Schmidt-Kittler, Jordan M. Cummins, Laura DeLong, Ian Cheong, Carlo Rago, et al. 2005. “Mutant PIK3CA Promotes Cell Growth and Invasion of Human Cancer Cells.” *Cancer Cell* 7 (6): 561–73.

Sancak, Yasemin, Liron Bar-Peled, Roberto Zoncu, Andrew L. Markhard, Shigeyuki Nada, and David M. Sabatini. 2010. “Ragulator-Rag Complex Targets mTORC1 to the Lysosomal Surface and Is Necessary for Its Activation by Amino Acids.” *Cell* 141 (2): 290–303.

Sancak, Yasemin, Timothy R. Peterson, Yoav D. Shaul, Robert A. Lindquist, Carson C. Thoreen, Liron Bar-Peled, and David M. Sabatini. 2008. “The Rag GTPases Bind Raptor and Mediate Amino Acid Signaling to mTORC1.” *Science* 320 (5882): 1496–1501.

Santos, Silvia D. M., Peter J. Verveer, and Philippe I. H. Bastiaens. 2007. “Growth Factor-Induced MAPK Network Topology Shapes Erk Response Determining PC-12 Cell Fate.” *Nature Cell Biology* 9 (3): 324–30. doi:10.1038/ncb1543.

Sarbassov, Dos D, Siraj M Ali, and David M Sabatini. 2005. “Growing Roles for the mTOR Pathway.” *Current Opinion in Cell Biology*, Cell division, growth and death / Cell differentiation, 17 (6): 596–603. doi:10.1016/j.ceb.2005.09.009.

Schlessinger, Joseph. 2000. “Cell Signaling by Receptor Tyrosine Kinases.” *Cell* 103 (2): 211–25.

Schlessinger, Joseph, and Mark A. Lemmon. 2003. “SH2 and PTB Domains in Tyrosine Kinase Signaling.” *Science Signaling* 2003 (191): re12–re12. doi:10.1126/stke.2003.191.re12.

Schlessinger, J., and A. Ullrich. 1992. “Growth Factor Signaling by Receptor Tyrosine Kinases.” *Neuron* 9 (3): 383–91.

Schmick, Malte, and Philippe I. H. Bastiaens. 2014. “The Interdependence of Membrane Shape and Cellular Signal Processing.” *Cell* 156 (6): 1132–38. doi:10.1016/j.cell.2014.02.007.

Schmick, Malte, Astrid Kraemer, and Philippe I. H. Bastiaens. 2015. “Ras Moves to Stay in Place.” *Trends in Cell Biology* 0 (0). Accessed March 16. doi:10.1016/j.tcb.2015.02.004.

Schmick, Malte, Nachiket Vartak, Björn Papke, Marija Kovacevic, Dina C. Truxius, Lisaweta Rossmannek, and Philippe I. H. Bastiaens. 2014. “KRas Localizes to the Plasma Membrane by Spatial Cycles of Solubilization, Trapping and Vesicular Transport.” *Cell* 157 (2): 459–71. doi:10.1016/j.cell.2014.02.051.

Schubbert, Suzanne, Gideon Bollag, Natalya Lyubynska, Hoa Nguyen, Christian P. Kratz, Martin Zenker, Charlotte M. Niemeyer, Anders Molven, and Kevin Shannon. 2007. “Biochemical and Functional Characterization of Germ Line KRAS Mutations.” *Molecular and Cellular Biology* 27 (22): 7765–70. doi:10.1128/MCB.00965-07.

Schubbert, Suzanne, Kevin Shannon, and Gideon Bollag. 2007. “Hyperactive Ras in Developmental Disorders and Cancer.” *Nature Reviews Cancer* 7 (4): 295–308. doi:10.1038/nrc2109.

Seeburg, Peter H., Wendy W. Colby, Daniel J. Capon, David V. Goeddel, and Arthur D. Levinson. 1984. “Biological Properties of Human c-Ha-ras1 Genes Mutated at Codon 12.” http://www.nature.com/articles/312071a0.

Seger, Rony, and Edwin G. Krebs. 1995. “The MAPK Signaling Cascade.” *The FASEB Journal* 9 (9): 726–35.

Sengupta, Shomit, Timothy R. Peterson, and David M. Sabatini. 2010. “Regulation of the mTOR Complex 1 Pathway by Nutrients, Growth Factors, and Stress.” *Molecular Cell* 40 (2): 310–22. doi:10.1016/j.molcel.2010.09.026.

Shimizu, Kenji, Daniel Birnbaum, Mary Ann Ruley, Ottavio Fasano, Yolande Suard, Louise Edlund, Elizabeth Taparowsky, Mitchell Goldfarb, and Michael Wigler. 1983. “Structure of the Ki-Ras Gene of the Human Lung Carcinoma Cell Line Calu-1.” *Nature* 304 (5926): 497–500. doi:10.1038/304497a0.

Sigal, Alex, and Varda Rotter. 2000. “Oncogenic Mutations of the p53 Tumor Suppressor: The Demons of the Guardian of the Genome.” *Cancer Research* 60 (24): 6788–93.

Singh, Anurag, Patricia Greninger, Daniel Rhodes, Louise Koopman, Sheila Violette, Nabeel Bardeesy, and Jeff Settleman. 2009. “A Gene Expression Signature Associated with ‘K-Ras Addiction’ Reveals Regulators of EMT and Tumor Cell Survival.” *Cancer Cell* 15 (6): 489–500. doi:10.1016/j.ccr.2009.03.022.

Singh, Anurag, Michael F. Sweeney, Min Yu, Alexa Burger, Patricia Greninger, Cyril Benes, Daniel A. Haber, and Jeff Settleman. 2012. “TAK1 Inhibition Promotes Apoptosis in KRAS-Dependent Colon Cancers.” *Cell* 148 (4): 639–50.

Solomon, Hilla, Yosef Buganim, Ira Kogan-Sakin, Leslie Pomeraniec, Yael Assia, Shalom Madar, Ido Goldstein, et al. 2012. “Various p53 Mutant Proteins Differently Regulate the Ras Circuit to Induce a Cancer-Related Gene Signature.” *Journal of Cell Science* 125 (13): 3144–52.

Soussi, Thierry, and Christophe Béroud. 2001. “Assessing TP53 Status in Human Tumours to Evaluate Clinical Outcome.” *Nature Reviews Cancer* 1 (3): 233–39.

Suh, Young-Ah, Sean M. Post, Ana C. Elizondo-Fraire, Daniela R. Maccio, James G. Jackson, Adel K. El-Naggar, Carolyn Van Pelt, Tamara Terzian, and Guillermina Lozano. 2011. “Multiple Stress Signals Activate Mutant p53 in Vivo.” *Cancer Research* 71 (23): 7168–75.

Swarthout, John T., Sandra Lobo, Lynn Farh, Monica R. Croke, Wendy K. Greentree, Robert J. Deschenes, and Maurine E. Linder. 2005. “DHHC9 and GCP16 Constitute a Human Protein Fatty Acyltransferase with Specificity for H- and N-Ras.” *Journal of Biological Chemistry* 280 (35): 31141–48. doi:10.1074/jbc.M504113200.

Takekawa, Mutsuhiro, Masaaki Adachi, Atsuko Nakahata, Ichiro Nakayama, Fumio Itoh, Hiroyuki Tsukuda, Yoichi Taya, and Kohzoh Imai. 2000. “p53-Inducible Wip1 Phosphatase Mediates a Negative Feedback Regulation of p38 MAPK-p53 Signaling in Response to UV Radiation.” *The EMBO Journal* 19 (23): 6517–26.

Toettcher, Jared E., Orion D. Weiner, and Wendell A. Lim. 2013. “Using Optogenetics to Interrogate the Dynamic Control of Signal Transmission by the Ras/Erk Module.” *Cell* 155 (6): 1422–34.

To, Minh D., Jesus Perez-Losada, Jian-Hua Mao, and Allan Balmain. 2005. “Crosstalk between Pten and Ras Signaling Pathways in Tumor Development.” *Cell Cycle* 4 (9): 1185–88.

Tong, Liang, Abraham M. de Vos, Michael V. Milburn, Jarmila Jancarik, Shigeru Noguchi, Susumu Nishimura, Kazunobu Miura, Eiko Ohtsuka, and others. 1989. “Structural Differences between a Ras Oncogene Protein and the Normal Protein.” http://www.nature.com/nature/journal/v337/n6202/abs/337090a0.html.

Torti, Davide, and Livio Trusolino. 2011. “Oncogene Addiction as a Foundational Rationale for Targeted Anti-cancer Therapy: Promises and Perils.”

EMBO Molecular Medicine 3 (11): 623–36. doi:10.1002/emmm.201100176.
Trahey, Meg, and Frank McCormick. 1987. “A Cytoplasmic Protein Stimulates Normal N-Ras p21 GTPase, but Does Not Affect Oncogenic Mutants.” *Science* 238 (4826): 542–45.
Tsien, Roger Y. 1998. “The Green Fluorescent Protein.” *Annual Review of Biochemistry* 67 (1): 509–44.
Tuveson, D. A., and S. R. Hingorani. 2005. “Ductal Pancreatic Cancer in Humans and Mice.” *Cold Spring Harbor Symposia on Quantitative Biology* 70 (January): 65–72. doi:10.1101/sqb.2005.70.040.
Ullrich, Axel, and Joseph Schlessinger. 1990. “Signal Transduction by Receptors with Tyrosine Kinase Activity.” *Cell* 61 (2): 203–12.
Ulsh, L. S., and T. Y. Shih. 1984. “Metabolic Turnover of Human c-rasH p21 Protein of EJ Bladder Carcinoma and Its Normal Cellular and Viral Homologs.” *Molecular and Cellular Biology* 4 (8): 1647–52. doi:10.1128/MCB.4.8.1647.
Valencia, Alfonso, Pierre Chardin, Alfred Wittinghofer, and Chris Sander. 1991. “The Ras Protein Family: Evolutionary Tree and Role of Conserved Amino Acids.” *Biochemistry* 30 (19): 4637–48. doi:10.1021/bi00233a001.
Vartak, Nachiket, Bjoern Papke, Hernan E. Grecco, Lisaweta Rossmannek, Herbert Waldmann, Christian Hedberg, and Philippe IH Bastiaens. 2014. “The Autodepalmitoylating Activity of APT Maintains the Spatial Organization of Palmitoylated Membrane Proteins.” *Biophysical Journal* 106 (1): 93–105.
Vetter, I. R., and A. Wittinghofer. 2001. “The Guanine Nucleotide-Binding Switch in Three Dimensions.” *Science (New York, N.Y.)* 294 (5545): 1299–1304. doi:10.1126/science.1062023.
Vogelstein, Bert, Eric R. Fearon, Stanley R. Hamilton, Scott E. Kern, Ann C. Preisinger, Mark Leppert, Alida M.M. Smits, and Johannes L. Bos. 1988. “Genetic Alterations during Colorectal-Tumor Development.” *New England Journal of Medicine* 319 (9): 525–32. doi:10.1056/NEJM198809013190901.
Vogelstein, Bert, David Lane, and Arnold J. Levine. 2000. “Surfing the p53 Network.” *Nature* 408 (6810): 307–10.
Vojtek, Anne B., and Channing J. Der. 1998. “Increasing Complexity of the Ras Signaling Pathway.” *Journal of Biological Chemistry* 273 (32): 19925–28. doi:10.1074/jbc.273.32.19925.
Vousden, Karen H., and Xin Lu. 2002. “Live or Let Die: The Cell’s Response to p53.” *Nature Reviews Cancer* 2 (8): 594–604.
Vousden, Karen H., and Kevin M. Ryan. 2009. “p53 and Metabolism.” *Nature Reviews Cancer* 9 (10): 691–700.
Waters, Steven B., Kathleen H. Holt, Susan E. Ross, Li-Jyun Syu, Kun-Liang Guan, Alan R. Saltiel, Gary A. Koretzky, and Jeffrey E. Pessin. 1995. “Desensitization of Ras Activation by a Feedback Disassociation of the SOS-Grb2 Complex.” *Journal of Biological Chemistry* 270 (36): 20883–86.
Weinstein, I. Bernard, and Andrew K. Joe. 2006. “Mechanisms of Disease: Oncogene Addiction—a Rationale for Molecular Targeting in Cancer Therapy.” *Nature Clinical Practice Oncology* 3 (8): 448–57. doi:10.1038/ncponc0558.

Wennerberg, Krister, Kent L. Rossman, and Channing J. Der. 2005. “The Ras Superfamily at a Glance.” *Journal of Cell Science* 118 (5): 843–46. doi:10.1242/jcs.01660.

Willingham, Mark C., Ira Pastan, Thomas Y. Shih, and Edward M. Scolnick. 1980. “Localization of the Src Gene Product of the Harvey Strain of MSV to Plasma Membrane of Transformed Cells by Electron Microscopic Immunocytochemistry.” *Cell* 19 (4): 1005–14. doi:10.1016/0092-8674(80)90091-4.

Willumsen, B M, K Norris, A G Papageorge, N L Hubbert, and D R Lowy. 1984. “Harvey Murine Sarcoma Virus p21 Ras Protein: Biological and Biochemical Significance of the Cysteine Nearest the Carboxy Terminus.” *The EMBO Journal* 3 (11): 2581–85.

Wing, M. R. 2003. “PLC- : A Shared Effector Protein in Ras-, Rho-, and G -Mediated Signaling.” *Molecular Interventions* 3 (5): 273–80. doi:10.1124/mi.3.5.273.

Wolf, Ido, and Rony Seger. 2002. “The Mitogen-Activated Protein Kinase Signaling Cascade: From Bench to Bedside.” *IMAJ-RAMAT GAN-* 4 (8): 641–47.

Wullschleger, Stephan, Robbie Loewith, and Michael N. Hall. 2006. “TOR Signaling in Growth and Metabolism.” *Cell* 124 (3): 471–84. doi:10.1016/j.cell.2006.01.016.

Yan, Zhongfa, Xiaobing Deng, Mingxing Chen, Ying Xu, Mamoun Ahram, Bonnie F. Sloane, and Eileen Friedman. 1997. “Oncogenic c-Ki-Ras but Not Oncogenic c-Ha-Ras Up-Regulates CEA Expression and Disrupts Basolateral Polarity in Colon Epithelial Cells.” *Journal of Biological Chemistry* 272 (44): 27902–7. doi:10.1074/jbc.272.44.27902.

Yoon, Seunghee, and Rony Seger. 2006. “The Extracellular Signal-Regulated Kinase: Multiple Substrates Regulate Diverse Cellular Functions.” *Growth Factors* 24 (1): 21–44. doi:10.1080/02699050500284218.

Zhang, Baolin, Yaqin Zhang, Emily Shacter, and Yi Zheng. 2005. “Mechanism of the Guanine Nucleotide Exchange Reaction of Ras GTPaseEvidence for a GTP/GDP Displacement Model.” *Biochemistry* 44 (7): 2566–76. doi:10.1021/bi048755w.

Zhang, Houbin, Xiao-hui Liu, Kai Zhang, Ching-Kang Chen, Jeanne M. Frederick, Glenn D. Prestwich, and Wolfgang Baehr. 2004. “Photoreceptor cGMP Phosphodiesterase Δ Subunit (PDEδ) Functions as a Prenyl-Binding Protein.” *Journal of Biological Chemistry* 279 (1): 407–13. doi:10.1074/jbc.M306559200.

Zilfou, Jack T., and Scott W. Lowe. 2009. “Tumor Suppressive Functions of p53.” *Cold Spring Harbor Perspectives in Biology* 1 (5): a001883.

Zimmermann, Gunther, Björn Papke, Shehab Ismail, Nachiket Vartak, Anchal Chandra, Maike Hoffmann, Stephan A. Hahn, et al. 2013. “Small Molecule Inhibition of the KRAS-PDEδ Interaction Impairs Oncogenic KRAS Signalling.” *Nature* 497 (7451): 638–42. doi:10.1038/nature12205.

Zuber, Johannes, Oleg I. Tchernitsa, Bernd Hinzmann, Anne-Chantal Schmitz, Martin Grips, Martin Hellriegel, Christine Sers, André Rosenthal, and Reinhold Schäfer. 2000. “A Genome-Wide Survey of RAS Transformation Targets.” *Nature Genetics* 24 (2): 144–52. doi:10.1038/72799.

14 Acknowledgements

I am very thankful to Prof. Dr. P. I. H. Bastiaens for providing a great scientific environment and for his supervision and guidance, including constant activation and deactivation cycles.
I would like to thank Prof. Dr. F. Wehner for not just taking over the second review, but for many fruitful discussions about and around science, usually sprinkled with black humor.
I want to thank Dr. Astrid Krämer for her great support, for extremely helpful corrections and for running the lab.
I would like to express special thanks to Christian Klein, the best Master student ever.

Special thanks go to, Prof. Dr. Dieter Truxius, Dr. Romy Marx, Ronald Röhr, Felix Siedenbiedel, Dr. Jana Harizanova, and Christian Grawe for their patience in spending hours on corrections.
I would like to thank our “Master of the microscopes” Dr. Sven A. H. Müller, our great technicians Michael Reichl, Hendrike Schütz, Kirsten Michel, Manuela Grygier, Jutta Luig, Lisaweta Roßmannek, Sabine Dongard, Jana Seidel, Petra Glitz, Gaby Beetz, Anette Langerak and our lab soul Nimetka Seloska for their enormous support and understanding. Cloning-related thanks go to Dr. A. Konitsiotis.
I would like to thank Birgit’s Bistro, especially Birgit and Sandra, and the permanent employees at the MPI and the central units, including library, work security, administration, IT, tool shop and house facility management. Special thanks go to Dr. Peter Herter for his support regarding Klausenhof Meetings and PhDnet.

I am glad that I have had the opportunity to meet many fascinating and interesting people at the MPI/in the MPS, especially and without order, Dr. Andreea Scacioc, Dr. Jana Harizanova, Dr. Klaus Schuermann, Dr. Sina Koch, Dr. Jenny Keller, Dr. Marion Pesenti, Katia van Eickels, Sarah Imtiaz, Christian Klein, Katrin Prost, Kaatje Heinelt, Dr. Lisa Karajannis, Holger Vogel, Claudia Breit, Kerstin Klare, and former members from department II Thimo, Sarah W., Maja, Julia, Hernán, Pedro, Sheriff, Kondi, Rahul, Thies, Zeta, Sven F., Jenny, Jian, Franzi, Tom, Christopher, and Nash.

I am very thankful to Prof. Christian Kurts for his invitation to join his wonderful group and to focus my fascination on immunology. I would like to thank my new colleagues for the great working atmosphere, especially and without order, Marika, Ann-Kathrin, Janine, André, Cesar, Vadim, Moritz, Chrystel, Isis, Romina, Margarete, Teresa, Sonny, Sarah, Anna, Karl, Wolfgang, Meike, Kasia, Ermanila, Peter, Elmar, Andreas, Christine, Philipp, Ersin and Ismail.

My deepest thanks and love go to Chris, Friedrich, Ling-Ling, and Minki and my best friends (Felix S., Christiane S., Felix K.). I would like to thank my family and family in-law for their understanding and continuous mental support.